R. & M. No. 3738

R. & M. No. 3738

PROCUREMENT EXECUTIVE, MINISTRY OF DEFENCE

AERONAUTICAL RESEARCH COUNCIL

REPORTS AND MEMORANDA

Analysis of Flight and Tunnel Tests on the Fairey Delta 2 Research Aircraft

By R. A. FEIK

Dept. of Aeronautical Engineering,
Queen Mary College, University of London

LONDON: HER MAJESTY'S STATIONERY OFFICE

1974

PRICE £3·30 NET

Analysis of Flight and Tunnel Tests on the Fairey Delta 2 Research Aircraft

By R. A. Feik

Dept. of Aeronautical Engineering,
Queen Mary College, University of London

Reports and Memoranda No. 3738*
December, 1971

Summary

A detailed comparison of results has been made from several series of flight tests, spanning a number of years, on the Fairey Delta 2, with wind tunnel tests on 1/9 and 1/24 scale models and with reference also to simple theoretical results. The Mach number range of interest has been M = 0·6 to M = 1·8. This report considers both longitudinal and lateral characteristics together with flow field development and surface pressure measurements. In order to help explain several discrepancies observed, special interest has been focused on detailed differences in geometry between full scale aircraft and models, on aeroelastic effects and on differences in flow field development due to scale differences. It has been possible to suggest explanations for many of the discrepancies in terms of these effects. Where possible, reference has been made to other similar aircraft in order to make the conclusions as general as possible.

* Replaces A.R.C. 33 992.

LIST OF CONTENTS

1. Introduction

The Fairey Delta 2 was designed and built as a research aircraft to probe primarily the transonic and supersonic speed range. At the time of its design and manufacture very little was known in detail about the characteristics of any aircraft in this speed range and in particular of a tailless delta-wing. The delta configuration appeared to be particularly well suited to flight at high speeds because of its high sweep, low aspect ratio, thin wing section and structural strength.

The history of the Fairey Delta 2 development can be found in Refs. 1 and 2. Two aircraft were manufactured, the WG 774, first flown on 6th October, 1954, and the WG 777, which made its first flight on 15th February, 1956. In addition, a third airframe was built for structural test purposes. The WG 777 differed from the WG 774 in having slightly different equipment and basic instrumentation and this was the aircraft used in most of the flight tests to be considered here. The WG 774, which set an air speed record of 1132 m.p.h. (1826 km/h) on 10th March, 1956, was used for tests by Fairey Aviation, including sonic boom tests (Ref. 3). It has since been rebuilt with an Ogee wing as the BAC 221 (Ref. 4).

From its first flight, the Fairey Delta 2 showed 'every promise of being a very pleasant flying machine'. No artificial devices were found necessary for stability augmentation, at least in its role as a test aircraft.

As well as being concerned with establishing the behaviour of a 60 degree Delta aircraft at transonic and supersonic speeds, especially relating to anticipated problem areas such as longitudinal damping and lateral directional stability, the flight tests performed on this aircraft provided a rare opportunity for comparisons with extensive wind-tunnel tests on scale models. These comparisons were made with the object of evaluating the importance of Reynolds number, aeroelastic effects, frequency parameter and other factors which will emerge in the course of this report.

The low speed problems of high speed aircraft have received considerable attention for some time (*see* Ref. 5), including work on, for example, the Avro 707 (Ref. 6), H.P. 115 (Ref. 7), Short S.B.5 (Ref. 8), the Douglas F5D with and without ogee plan form (Ref. 9) and more recently the BAC 221 (Ref. 10). Most of these investigations include comparisons with wind-tunnel tests. However, there has been much less work done and/or published for higher speeds. In this group there is work on the Fairey Delta 2 and the English Electric P1 (Ref. 11) in this country, the Dassault Mirage family in France and of course various American research aircraft such as the X-15 (Ref. 12) and XB-70 (Ref. 13), all of which have different geometries. For one reason or another there seems to be no case where a systematic comparison has been made between flight, wind tunnel and theory aimed at bringing out general characteristics which may be applicable to other aircraft with similar design features.

The present project aims to fill this gap. The Fairey Delta 2 is particularly suitable because of its simple design, the relatively extensive flight and wind-tunnel data available and the fact that the full-scale aircraft has not undergone any serious design modifications during the test period, hence allowing the models to closely resemble it. This report is concerned mainly with a comparison of flight and wind-tunnel data, but some simple theoretical estimates are also included. A more sophisticated theory is not attempted as no existing theory is likely to be adequate to predict the complex flow fields caused by shock waves, leading-edge separations and streamwise vortices on such highly-swept aircraft.

The approach here is firstly to give fairly detailed descriptions of aircraft and models (Sections 2 and 3) with particular emphasis on points where they differ, secondly to summarise the tests performed, methods of analysis, corrections applied and estimated accuracy (Sections 4 and 5). Section 6 is concerned with a comparison of the various stability and control characteristics derived in flight and wind tunnel. The main areas of disagreement are established and an attempt made to explain the sources of the discrepancies. This involves a close look at aeroelastic distortions, slight differences in geometry, engine-inlet mass-flow and jet-efflux effects and finally wing-flow development and wing pressures.

As far as possible, flight and wind-tunnel data available on aircraft and models other than the Fairey Delta 2 will be referred to in order to strengthen the present observations and/or to broaden their scope.

2. Aircraft Description

2.1. General Layout

The aircraft has a delta wing plan form with a 60 degree swept leading edge and tapered to give an aspect ratio of 2. The thickness/chord ratio is low at 0·04 and the leading edge is blunt with a nominal radius of 0·00189 times local chord. The wing is set at +1·5 degrees to the fuselage datum. The general layout of the aircraft is shown in Fig. 1 and the leading dimensions are listed in Table 1. The moments and products of

inertia as estimated by the Fairey Co. were found to be in poor agreement with direct measurements (Ref. 14) and subsequently all flight measurements have been analysed or corrected using the measured values. Mathematically defined forms were used for aerofoils and fuselage, to enable high accuracy of contour to be achieved in the final manufactured product, and, by inference, to enable the models to be true and accurate representations of the aircraft. It might be mentioned that interchanging the wing of the WG 774 (damaged in a wheels up landing) with that originally built for structural test purposes led to no change in flight characteristics (Ref. 2). Small surface defects such as nominally flush rivet heads and detachable panels, which may significantly influence the drag, are given in detail in Ref. 15. In addition, the wings have relatively large irregularities in the form of aileron-jack fairing and undercarriage-bay fairing on the lower surface, and a fence on the suction surface (Figs. 1a, 1b). The fence is located as 0·34 semi-span and extends from 0·04 to 0·37 of local chord. The reason for the fence is not stated in any of the available reports. The influence of fences is not well understood (Refs. 16, 17) and is very dependent on Reynolds number, so that it may happen that low Reynolds number tests indicate effectiveness in controlling stall, while the fences are completely ineffective at higher Reynolds number (Ref. 17).

Other features on the aircraft are the petal airbrakes on the rear fuselage and a wind vane on the nose boom used for measuring angles of incidence and sideslip. Also present is the parachute fairing shown in Fig. 1, while for surface flow-visualisation tests a fairing to house the camera was provided on the tip of the fin. A knowledge of the presence and location of all additional features is important for a proper analysis of pressure data in Section 6.

The centre of gravity at test conditions was 163·1 ± 0·5 inches aft from the leading edge of the centre-line chord, which is 0·544 of centre-line chord or 0·317 of the mean-aerodynamic chord.

2.2. Controls and Control Flexibility

Primary control is by full-span trailing-edge controls, split into separate elevators and ailerons, and by conventional rudder. All the surfaces are operated by irreversible hydraulic jacks. Feel for all three controls is provided by simple spring systems. The jacks operating the elevators and the rudder are located in the rear fuselage and operate the surfaces via torque tubes, while the aileron jacks are situated beneath the outer wing, forward and slightly inboard of the mid portion of the ailerons, and operate the ailerons directly. Control surface gaps on the aircraft are sealed as far as possible with felt strips.

The flexibility of the elevators and ailerons under loading was measured experimentally on the ground by uniformly loading the surfaces with lead shot bags. Due to experimental difficulties (Ref. 15) only 25 per cent of maximum flight load values were achieved. The assumptions implicit in this approach are,

(a) The distorted elevator can be represented by an undistorted control at an appropriate mean angle.

(b) The loads on the surfaces in flight are uniformly distributed.

(c) Calibrations may be extrapolated linearly to the considerably higher flight loading conditions.

These are only working assumptions and none is strictly correct. In fact, a quick comparison of flight measurements of elevator pressures, from which elevator loads in flight were derived, indicates a substantially higher loading outboard than near the fuselage. The uncertainties involved make it difficult to put a figure on the accuracy of corrections for, say, elevator angle to trim. However, in view of the scatter in the flight data, this is not thought to be too important.

The effective stiffnesses measured, including jack linkages, were 2000 lbf ft/degree* for the elevator, and 40 000 lbf ft/degree for the aileron. Unfortunately no stiffness tests were performed on the rudder. The low elevator stiffness arises because of the jack location in the fuselage and the load application through flexible linkages. This accounts for about two-thirds of the measured distortions. The aileron jack load, on the other hand, was applied nearer the aileron mid-span and the flexibility of the linkages is negligible (Ref. 15). Although the effective stiffnesses may be in considerable error due to the factors already mentioned, it will be shown later that corrections to flight derivatives, such as C_{L_α} and C_{m_α}, are fairly insensitive to large variations in the stiffness (*see* Section 6.6).

Some manufacturer's estimates for aeroelastic effects are included in Ref. 18, but it is unclear how these were derived or what they take into account (whether elevator, aileron or wing distortions). In any case the estimates quoted were relatively small and made little headway in resolving the large differences found in the data.

---

* Since throughout all wind-tunnel and flight tests discussed in this report 'British' units were used, these have been retained and not converted to Metric System.

2.3. Aileron Rigged-Up Angle

In order to be able to trim the aircraft in as wide a range of turns as possible, the ailerons were rigged up at 3·2 degrees relative to the wing chord with the aircraft on the ground. However, in flight this angle changed from the ground setting and varied with flight conditions as shown in Fig. 2. One of the suggestions made in Ref. 15 is that the change may be due to some distortion of the outer wing structure porting the hydraulic jack valves and thus moving the ailerons. This seems a likely explanation as similar movement of the rudder was found during lateral flight tests (Ref. 19). The magnitude of the change is relatively independent of Mach number up to M = 1·6, for steady level flight with $C_L = C_W$ (above M = 1·6 the effect increases, perhaps due to a changing load distribution near the wing tip). Some results for normal acceleration, n, other than one are also included in Fig. 2. They show considerable scatter and are generally inconclusive although at 40 000 ft the results for M greater than 1 and n greater than 1 are, in general, higher than the $n = 1$ values. This is consistent with the wing-tip distortion hypothesis.

Another suggestion, involving some sort of differential temperature effect in the control circuit, seems less likely since a greater Mach number dependence would be expected in this case, if one assumes that the recovery temperature is the main parameter involved.

2.4. Powerplant

Propulsive force is provided by a Rolls Royce Avon RA 28R turbojet with test bed ratings of engine and jet-pipe equal to 9530 lbf without reheat and 11 820 lbf with reheat. The thrust axis is inclined at +1 degree to the fuselage datum. The jet pipe nozzle has movable eyelids which are fully open for reheat operation and closed to reduce the nozzle area for non-reheat running. The exit nozzle is choked under almost all test conditions. Neither the jet pipe nor the eyelids are represented in the models and are an obvious source of discrepancies.

The engine inlets, located at the wing roots, were designed with a wedge shaped upper forward lip and rounded lower one which lay behind the oblique shock generated by the upper lip. Thus inlet 'buzz' was avoided by preventing the shock from entering the inlet while losses associated with a strong normal shock ahead of the inlet were also avoided. A fuselage boundary layer bypass is also present. 'The entry area was chosen to give full mass flow at the most critical point, which in this case occurs in the transonic range; this results in a moderate amount of spillage in the supersonic design range.' 'Although certain difficulties were experienced, mainly due to separation at the corners of the ducts, the intake at present is substantially as originally designed and has operated without sign of instability throughout the transonic range and up to the highest Mach numbers the aircraft is capable of.' The above remarks come from Ref. 1, which also gives further design details. They are included to highlight certain features such as spillage and separation which may not be exactly reproduced in the models. This is relevant in view of the observed C_{m_0} differences in particular.

Differences in engine mass flow and jet exit conditions between aircraft and models will be looked at in more detail in Section 3.4.

2.5. Boundary-Layer Transition

An investigation relating to the position of boundary layer transition on the fin in flight is reported in Ref. 20. This established that between M = 1·0 and M = 1·5, transition to turbulence on the fin occurred at least within 3 per cent local chord of the fin leading edge. The method used examined the sublimation patterns of a thin layer of azobenzene crystals in petroleum ether to indicate whether the boundary layer was laminar or turbulent. The results presumably also apply to transition on the wings, although the tests there were unsuccessful because of leaky wing tanks removing the azobenzene layer in the vicinity of the wing leading edge.

At angles of incidence other than zero, the transition position moves forward, especially on the upper surface (Ref. 21), and it would seem fair to assume that in flight transition occurs at or very close to the leading edge on the wing so that the boundary layer is entirely turbulent. Further comments related to the boundary layer are made in Section 3.3.

3. Models

Two models of the Fairey Delta 2 were built for wind tunnel testing purposes. The first was built to 1/24 scale while a second, more accurate model was built later to 1/9 scale. Each model will be described in turn.

3.1. 1/24 Scale Model

3.1.1. General arrangement. The 1/24 scale model was constructed according to early drawings of the aircraft which showed the air intake about 10 per cent smaller than the final version. Full details of the model are given in Ref. 22, but some of its features are emphasised here.

The model (Fig. 3a) has a slightly different nose shape from full scale, having a fuselage which is slightly longer and deeper, in order to accommodate the sting balance, and it is not boattailed to the extent which applies on the aircraft.

Air was allowed to flow through the wing root intakes and exhaust out of the annulus formed by the model base and sting. The jet pipe and exhaust nozzle were not represented. Boundary-layer-bleed ducts inboard of the intake were also represented but the diverted air neither followed the same path nor did it exhaust at the same point as on the aircraft. Auxiliary air intakes and exhausts, various vents, aerials, incidence vane, thermometer and other small excrescences were omitted as on the 1/9 scale model. Other major features such as wing fences and fairings were represented.

3.1.2. Control surfaces. The elevators, ailerons and rudder were represented by cutting grooves in the wing and fin surfaces along the control hinge lines and deflecting the surfaces behind the grooves about the resulting spring centres. To represent the aircraft, ailerons were rigged up to 3 degrees relative to the wind chordal plane, and all derivatives on this model, including those due to aileron deflection, were measured with this as zero setting.

Control-surface flexibility was considered but corrections for deflection under load were estimated to be small and hence neglected.

3.1.3. Boundary layer transition. Transition to turbulence was fixed by distributed roughness applied between 1·25 and 1·75 inches aft of the nose, while on the wings and fin roughness was applied between 0 and 10 per cent of local chord. The roughness took the form of carborundum grains stippled on a base of silver paint.

3.2. 1/9 Scale Model

3.2.1. General arrangement. The 1/9 scale model is described in detail in Ref. 23 and was in general a more accurate representation of the aircraft than the 1/24 model. Even so, some distortion of the fuselage boattail remained because of the necessity to accommodate the sting balance and exhaust the duct flow (Fig. 3b). The jet pipe and exhaust nozzle were not represented. Neither was the fuselage boundary-layer diverter-system at the engine intakes represented on the 1/9 model, whereas some attempt was made to represent this on the 1/24 model.

3.2.2. Control surfaces. The ailerons, elevators and rudder were attached to the model by interchangeable hinge plates, changes of control angle being made by changing the hinge plate. The ailerons were set at 2·9 degrees trailing edge up in order to reproduce what was thought to be the aircraft datum, and all but the aileron derivatives were measured with this as reference. For aileron derivatives, the aileron angles were measured relative to the wing chordal plane as zero setting.

It appears that the control surfaces were less stiff than on the 1/24 model and underwent significant distortion under load. Thus the aileron angle changed by 24 per cent as α_F changed from -2 degrees to $+6$ degrees (Ref. 24). The elevator, however, was much stiffer, the equivalent change being 3·7 per cent. Because of this flexibility, corrections have been made on control derivatives in the 1/9 model tests, and some of these will be pointed out later. The corrections are normally small and even if they are entirely neglected, the major discrepancies between flight and wind-tunnel results are still clearly apparent and unaltered.

3.2.3. Boundary-layer transition. Transition on the wings and fin of the 1/9 model was fixed by bands of ballotini attached to the surface by a suitable adhesive, such as a thin film of araldite, starting from 5 per cent local chord. The fuselage had bands at 1 inch and 6 inches aft of the nose probe while bands were also attached to the inside and outside of the intakes at $\frac{1}{4}$ inch from the lip. The size of particle and the band width varied slightly in different series of tests. For example, Ref. 23 reports a grain size of 0·005 inches or above and a band width of 0·1 inches. It was confirmed in this case that transition was indeed fixed for Reynolds number based on $\bar{c}$ greater than 5×10^6 which included the test conditions. Ref. 25, on the other hand, used a smaller grade particle (0·003 to 0·0035 inches) but a greater band width of 0·125 inches. Here also, acenaphthene tests confirmed that transition was fixed under the test conditions, i.e. Reynolds number of $6{\cdot}8 \times 10^6$ or higher.

3.3. Boundary-Layer Development in Flight and Wind Tunnel

Although the geometric dimensions of the 1/24 and 1/9 models are scaled as closely as possible to the aircraft, it was not possible to achieve flight Reynolds numbers in the wind tunnel. A typical flight Reynolds number

based on $\bar{c}$ for M = 1·35 at 40 000 ft is 4·3 × 10^7 compared with tunnel Reynolds numbers of 7 × 10^6 for the 1/9 scale model and 2 × 10^6 for the 1/24 model. More details are given in Section 4. The lower Reynolds numbers in the tunnels lead to boundary layers which are thicker on the models than is appropriate to the geometric scaling. To give some idea of the differences involved an estimate can be made of relative boundary-layer thicknesses and in particular the ratio of the boundary-layer thickness at the wing fence to the height of the wing fence.

As a very rough estimate, assume an incompressible, two-dimensional, turbulent boundary-layer in zero pressure gradient starting at the wing leading-edge. It has already been shown that transition to turbulence occurs close to the leading edge in both models and on the aircraft. The boundary-layer displacement thickness is then given by (*see* e.g. Ref. 26)

$$\frac{\delta^*}{x} = \frac{0{\cdot}046}{\mathrm{Re}_x^{1/5}},$$

while the boundary-layer thickness, δ, can be assumed to be about 8 δ^*. This formula can be used to calculate the boundary-layer thickness at 0·34 semi-span and 0·37 local chord, which corresponds to the trailing-edge position at the wing fence. At M = 1·35 and 10 000 ft the Reynolds number in flight is about 1·2 × 10^8 giving δ^* equal to 0·101 ins. The 1/9 model tests were performed at a Reynolds number of 7 × 10^6 approximately, which results in a δ^* of 0·020 ins. while the Reynolds number for the 1/24 model was about 2 × 10^6 giving δ^* equal to 0·010 ins. Thus the flight δ^* is approximately five times the δ^* of the 1/9 model instead of being nine times as thick, as would be necessary to conform to the geometric scaling. Similarly the figure for the 1/24 model is about 10 instead of 24.

The ratios of the boundary-layer thicknesses, δ, to the fence height at the position calculated are approximately 0·14 in flight, 0·24 on the 1/9 model and 0·31 on the 1/24 model.

The relative thickness of the boundary layer on the models is thus considerably greater than in flight and the effects on flow development around the fences and fairings especially are bound to be altered because of the diffusive influence of the boundary layer.

Compressibility and/or pressure gradient should not change these general observations since their effects would be similar on model and aircraft alike.

3.4. Engine Mass Flow and Jet Exit Conditions

3.4.1. Mass flow. The provision of air intake and exit ducts means that air flows through the models due to the ram effect of the wind-tunnel stream. It is, however, not possible to simulate correctly the mass flow at all test conditions.

The mass flow through the model duct was evaluated by pitot and static surveys during preliminary test runs, while the actual engine mass flow was measured by means of previous calibrations together with in-flight measurements (*see* Ref. 27 for calibrations). A summary of all air mass-flow parameter measurements, $Q\sqrt{T_0}/P_0S$, is presented in Fig. 4. Also shown on the figure is an estimate of the maximum boundary-layer bleed mass-flow on the aircraft. The figure shows that the air mass-flow through the 1/9 model is less than the full scale value except in the range of Mach numbers from 1·0 to 1·3. The 1/24 model air mass flow values are always below full scale.

The difference between the engine mass flow plus bleed flow, and the model duct flows represents spillage at the model inlets and could have significant aerodynamic implications.

The flow through the turbine-nozzle guide-vanes is choked for most engine conditions (Ref. 27) so that engine mass-flow parameter is the same under reheat or non-reheat operation and, as expected, is approximately constant with Mach number at maximum r.p.m., which is the condition for most of the flight tests. The final nozzle design is such that the jet exit is also choked under most test conditions (Ref. 27). On the other hand, it appears from the mass-flow characteristics of the models that the duct flow is not choked except perhaps around the range M = 1 to 1·3 on the 1/9 scale model.

3.4.2. Jet exit condition. Because of the possible influence of the jet exit flow on the base and afterbody of the aircraft and models, it is desirable to know not only the mass flow but also the jet velocity and particularly the jet to ambient pressure ratio at exit (p_j/p_a).

Consider first the models. For unchoked flow, exit pressure equals the ambient pressure, i.e. $p_j/p_a = 1$, and there is no effect due to jet over or under expansion. For choked flow at the exit, M = 1 and $p_j/p_0 = 0{\cdot}528$, where p_0 is the total pressure and is the same for duct flow and external flow. The pressure ratio p_j/p_a now depends on the external Mach number and some appropriate results are given in Table 2.

Table 2 shows a considerable underexpansion at higher Mach numbers for a choked exit. However, the mass flow parameter indicates that the flow is unchoked for Mach numbers above 1·3. The exit jet is cold in all cases.

Turning now to the actual aircraft, where the exit nozzle is almost always choked, the pressure ratios can be inferred from Ref. 27 and are shown in Table 3 for different Mach numbers and altitudes.

The figures in Table 3 apply for maximum engine r.p.m., i.e. 8000. The temperatures of the exhaust jet are extremely high, being about 800 °K at 8000 r.p.m. and 40 000 ft without reheat, and higher still with reheat (Ref. 27). The jet temperature does not vary greatly over the Mach number range of interest. The influence of the jet temperature has been emphasised in Ref. 28, for example, which shows that for sonic jets exhausting into surrounding transonic flow fields, the specific-heat ratio of the jet at exit, as well as the jet-pressure ratio, is important when considering the interference on the external stream.

In summary, it seems that the exit jet on the aircraft is sonic, highly underexpanded, and very hot. Further, there are important differences in geometry between models and aircraft around the rear fuselage. The practical significance of these factors will be considered further in Sections 6.

4. Flight Tests

This section is concerned with a summary of the flight tests performed on the Fairey Delta 2. The emphasis is on the flight test techniques used and the methods of analysis together with their assumptions and expected accuracy, and their limitations. Table 4 contains a summary of the major flight references together with the range of conditions (e.g. Re, M, C_L, η, etc.) covered in each, and the quantities measured.

4.1. Longitudinal Stability and Control Tests

Longitudinal flight tests have been reported in Refs. 15, 29, 18 and 30. Ref. 30 was only concerned with low-speed drag of the approach configuration and is of no direct interest here.

4.1.1. Steady manoeuvres. The results of Ref. 15 were obtained in steady level flight, during turns or, in order to reduce C_L, in 'push-over' manoeuvres.

At subsonic speeds up to M = 1, tests were performed with reheat off and speed both stabilised and non-stabilised. Both turns and 'push-overs' were used.

At supersonic speeds all results were obtained in turns and reheat was left on to prevent too rapid a deceleration. Hence the eyelids were in the open position throughout most of the tests. The speed was not stable because of the limited throttling available but the rate of deceleration was at most $\Delta M = 0{\cdot}1$ in 20 seconds and usually much better, while variations in M of $\pm 0{\cdot}025$ at a particular point were accepted except at M = 0·94 and 0·97, where $\Delta M = \pm 0{\cdot}015$ was required. Some tests performed in accelerating flight gave results with no detectable difference from those in decelerating flight. The results of Ref. 15 were corrected for elevator distortions under load using the flexibility results reported in Section 2.2. Incidences obtained from incidence-vane readings were corrected for boom distortion and upwash effect using the calibrations of Ref. 31. Drag was obtained from measurements of acceleration along the flight path, gross thrust and intake momentum drag, the latter two being obtained from previous engine calibrations. Some indication of the accuracy of the measurements is given by the scatter. Thus the scatter of the C_L *vs.* α_F curves in Ref. 15 is such that the slope cannot be determined to better than 5 per cent at best and is usually worse than this.

A more usual method of obtaining some of the longitudinal characteristics, by movement of the centre-of-gravity position, was not used since it was decided to limit the amount of flying necessary by using only one centre-of-gravity position. It was believed that tests at other centre-of-gravity positions would yield little information that could not be obtained from the dynamic tests.

4.1.2. Short period oscillation. The analysis reported in Ref. 18 uses the basic method of Ref. 32 to obtain various longitudinal stability derivatives. The accuracy of the method is good as long as the motion is not too severely damped. Ref. 33 states that an accuracy of better than 10 per cent can be expected from such an analysis provided the damping factor is less than 0·2. At 40 000 ft the damping factor was about 0·21 for Mach numbers between 0·70 and 0·95 while for M greater than one ξ was less than 0·14. At 10 000 ft, ξ was less than 0·2 for M greater than 0·94. Hence the method should give accurate results for all supersonic Mach numbers at either 40 000 or 10 000 ft. The accuracy is expected to be bad only for M less than 0·95 at 10 000 ft.

In general the period of the short period oscillations decreased with increasing M, with a minimum value during tests of 0·6 seconds at 10 000 ft and 0·7 seconds at 40 000 ft. The rigid body modes of vibration were measured by Fairey as part of the flight clearance programme. The principal symmetric mode of vibration was

found to be a wing 'flapping' with fundamental frequency of 9·6 cycles/sec, which is about six times greater than the highest short-period frequency. There is thus a substantial separation between rigid-body and short-period frequencies and no interaction is expected.

The test procedure was first to trim the aircraft and then strike the elevator control sharply. The stick was returned to the trim position by artificial feel springs. In practice accurate longitudinal trimming was virtually impossible for transonic and supersonic speeds. This was because at transonic speeds the nose-down trim change makes the aircraft statically unstable while at supersonic speeds the velocity was either increasing or decreasing depending on whether the reheat was on or off. Difficulties in trimming laterally also often led to some roll divergence during the longitudinal oscillation. It is presumed that reheat was off during most tests (i.e. eyelids closed). This is not made clear in Ref. 18 but Ref. 19, reporting similar tests with lateral Dutch roll oscillations, states that in that case reheat was off, otherwise too much of the pilot's attention has to be focused on the engine instruments.

Several sources of systematic error have been considered in Ref. 18. In particular, coupling between lateral and longitudinal oscillations has been ruled out as unimportant as has engine gyroscopic coupling. On the other hand, there was some uncertainty about the possible effects of elevator oscillations small enough to be undetected by the instrumentation. This would be especially important at 10 000 ft. The magnitude and sign of the error would depend on the phase angle between the elevator motion and the normal acceleration ($\phi_{\eta n}$). The analysis of Ref. 18 assumes a maximum undetected elevator oscillation of $\pm 0{\cdot}04$ degrees. This leads to possible errors in C_{L_α} and C_{m_α} of 10 per cent and 20 per cent respectively for M = 1·2 at 10 000 ft provided $\phi_{\eta n}$ is -150 degrees. In fact, from the elevator motion that can be detected at 10 000 ft, $\phi_{\eta n}$ appears to be about 0 degrees which would result in errors of 5 per cent and 10 per cent respectively, but in the opposite direction to those for $\phi_{\eta n} = -150$ degrees. The possible errors are greater for lower M but decrease with increasing M. At 40 000 ft the effect of undetected elevator oscillations is negligible according to Ref. 18. The subject will be considered further in Sections 6.2.2 and 6.3.5 when C_{L_α} and C_{m_α} are examined in detail.

The frequency parameter ($2\pi f\bar{c}/V$) reached a maximum of about 0·15 at M = 1·15 and 10 000 ft altitude during the flight tests. For the tests at 40 000 ft it was generally below 0·11. A physical idea of the importance of unsteady effects may be gained by comparing the $\frac{1}{2}$-period of the oscillatory motion with a characteristic aerodynamic time such as the time taken for a change in vortex pattern (caused by an incidence change say) to travel one span downstream. The ratio of the half-period to this characteristic time at M = 1·15 and 10 000 ft is about 8·5, suggesting that the oscillations are slow enough to give ample time for aerodynamic adjustment. Thus it seems reasonable to neglect any unsteady aerodynamic effects when comparing the flight results with the steady wind-tunnel measurements.

Ref. 18 claims that at 40 000 ft, the measurements of C_{L_α}, H_M and C_{m_α} have an error of less than ± 5 per cent while m_0 is accurate to within $\pm 0{\cdot}03$. No figure is put on the 10 000 ft results because of the possible errors due to undetected elevator oscillations. Corrections for elevator distortion under load have not been made in Ref. 18 and these will be considered in Section 6.6.

Finally, it might be mentioned that no attempt has been reported to determine any control derivatives through analysis of the initial response to control pulses. Perhaps this was due to inadequate instrumentation available at the time to measure such quantities as $\Delta\dot{p}$, $\Delta\dot{q}$, etc. Elsewhere in the flight tests (e.g. Ref. 29), $\Delta\dot{p}$, $\Delta\dot{q}$ have been estimated using measured values of $\Delta\eta$, $\Delta\xi$ and wind-tunnel or estimated values of C_{m_η}, C_{l_ξ}.

4.1.3. Elevator and aileron hinge moment derivatives. The method used to measure the hinge-moment derivatives was an analysis of the motion following an elevator or aileron pulse-input. Unsteady aerodynamic loads are neglected (Ref. 34) and use is made of a relation derived between control jack loads and aerodynamic and inertia loads on the controls.

The initial response to an elevator pulse, $\Delta\eta$, allows the calculation of b_{2E} and b_{3A} when the increments in jack loads are measured. (Ref. 29.) The initial response to an aileron pulse, $\Delta\xi$, likewise gives b_{2A} and b_{3E}. Finally, the short-period oscillation following an elevator pulse produces jack loads in both elevator and aileron and enables b_{1E} and b_{1A} to be determined.

The assumptions involved in the calculations are given in Ref. 29. Control angles were corrected for distortions due to both aerodynamic and inertia loads using the flexibility measurements previously reported (Section 2.2).

The inertia terms are usually relatively small, contributing about 5 per cent of the total jack load in the calculations involving initial response to elevator pulse, and about 15 per cent elsewhere. Thus great accuracy (e.g. exact knowledge of moments of inertia) is not necessary in evaluating them.

At subsonic speeds, reliable results for b_{1A} and b_{1E} were difficult to obtain by the short-period analysis because of increased damping and increased residual control motion following the pulse. An alternative steady technique

involving the measurements in turns was used. Absolute rather than incremental jack loads were required with this method. Unfortunately zero drift in the strain gauges measuring jack loads, as well as other reasons given in Ref. 29, restricted the accuracy of this otherwise simple method.

Because of the many assumptions and difficulties involved in the test techniques, it is not really possible to estimate the errors, but some indication is given by the scatter. A large amount of scatter is present in the results for b_{1E}, b_{2E} and b_{1A} (especially at subsonic and transonic Mach numbers and at 10 000 ft) but the scatter is much less for b_{2A} and the cross derivatives. Nevertheless, all derivatives are sufficiently well defined to indicate general trends and to allow comparisons with wind-tunnel data.

4.2. Lateral Flight Tests

These are reported in Refs. 19, 35 and 29. The aileron hinge-moments given in Ref. 29 have been discussed in the previous section.

4.2.1. Steady manoeuvres. Tests were performed at subsonic speeds to obtain the derivatives l_v, y_v and l_ξ (Ref. 35). The aileron power, l_ξ, was obtained in level flight by balancing aileron aerodynamic rolling moments against moments produced by loaded canisters attached to the wing tips. Once l_ξ was known the sideslip derivatives l_v and y_v were obtained from steady sideslips, using wind tunnel values for l_ζ, y_ζ and y_ξ. The values used were those given in Ref. 36 resulting from tests on the 1/24 model.

Inaccuracies were introduced by the use of these tunnel derivatives and by the fact that steady sideslips were very difficult to maintain without some oscillation in roll and yaw. Comparisons with other flight or wind-tunnel data are also complicated by the unknown influence of the bulky wing-tip canisters, which make estimates of errors difficult.

Because of these difficulties and also because of the narrow Mach number range covered, these results are not a primary source of flight data.

4.2.2. Dutch roll oscillations. The main flight results for the aircraft lateral characteristics are reported in Ref. 19. These were obtained by vector analysis of the damped Dutch roll oscillations which were induced by a rudder pulse. The initial response to a pulse is a combination of roll subsidence, spiral mode and Dutch roll. The roll subsidence is quickly damped out and the remaining Dutch roll and spiral modes can be separated out.

The derivatives obtained in this way were the sideslip derivatives n_v, l_v and y_v, and the damping derivatives n_r and l_p. Estimates were used for the relatively unimportant cross derivatives n_p and l_r, and y_p was assumed to be zero. Further, records showed the presence of inadvertent rudder movements, whose contribution was calculated using theoretical estimates for the rudder derivatives n_ζ, l_ζ and y_ζ.

The rudder movement was attributed to aeroelastic distortion of the fin under sideslip load. Although the fin distortions were thought to be very minor, they succeeded in porting the valves of the rudder jack, which is situated at the base of the fin, and thus operated the jack. A similar process capable of explaining the observed change in aileron uprigged angle has been mentioned in Section 2.3.

The flight tests were mainly in initially steady level flight, although a few results were obtained in '2g' level turns at 40 000 ft. As with the short period technique, it was possible to trim the aircraft longitudinally and laterally at Mach numbers of 0·9 or less and then fly 'hands off'. After a sharp kick, the rudder pedals were returned to the trim position by the spring feel. At transonic and supersonic speeds trimming was much more difficult and 'hands off' flying was not possible. However, any records showing measurable aileron movements during the free oscillation were discarded. At supersonic speeds all tests were performed with reheat off (eyelids closed) and the aircraft decelerating, otherwise too much of the pilots' attention needed to be concentrated on the engine instrumentation.

The Dutch roll is less highly damped than the short period oscillations, with damping factor, ξ, less than or equal to 0·1 for practically all conditions. The frequency parameter at 10 000 ft lies between 0·05 and 0·06 as Mach number goes from 0·4 to 1·1, while at 40 000 ft the frequency parameter varies from 0·030 to 0·035 for M from 0·7 to 1·6. The low lateral damping combined with very effective controls made lateral trimming difficult especially at transonic M. On the other hand, the low damping factor allows for a more accurate analysis while the longer period, i.e. lower frequency parameter, makes possible unsteady effects even less important than with the short period analysis.

The period of the Dutch roll oscillations was at least 1·5 seconds at 40 000 ft and about half that at 10 000 ft. The principal antisymmetric mode of rigid body vibration, involving mainly the fin, had a fundamental frequency of 10·5 cycles/sec. As in the short period case the separation is substantial, with rigid body frequencies at least seven to eight times greater than those of the Dutch roll oscillation.

In addition to the vector analysis, approximate formulae, derived in Ref. 37, for n_v and l_v were used for cross check purposes. The agreement with the vector analysis was very good in general for n_v, with the approximate method giving slightly higher values, while for l_v the approximate method gives $|l_v|$ about 20 per cent low. The vector method is generally considered to be the most accurate method for extracting lateral derivatives (Ref. 33).

The instrumentation, described in Ref. 19, was the best available at the time although improvements have since been made. The wind vane mounted on the nose boom was found to be unreliable as an indicator of sideslip angle, β, and, in fact, lateral accelerometer readings enabled β to be deduced much more reliably.

Apart from instrumentation and recording errors which result in scattering of the data, systematic errors can arise through errors in the assumed derivatives and, in particular, through errors in the inertia characteristics. The latter have been corrected for, using the measured data of Ref. 14. An assessment of errors induced by inaccuracies in the assumed derivatives is made in Ref. 19, which concludes that in many cases quite large errors have very minor effects on the extracted derivatives. Thus n_v and l_v are estimated to be correct to within ± 5 per cent. On the other hand, y_v is very dependent on the value assumed for y_ζ. Further, a quick check on the values used for y_ζ shows them to be as small as a third the wind-tunnel measured values at supersonic speeds. This would lead to calculated values of $|y_v|$ being too large by quite substantial amounts. In general, however, the random scatter of the flight results is so large that it over-rides any systematic errors in all of the sideslip derivatives.

Finally, it is possible that aeroelastic distortions of the rudder may have an important influence on the flight results. In this respect it is unfortunate that the flexibility of the rudder has not been measured, nor have any rudder hinge moments, so that a quantitative assessment cannot be made. An attempt to evaluate the possible effect of rudder flexibility will be made in Section 6.8.2.

4.3. Flow Visualisation and Surface Pressures

Tests, reported in Ref. 20, to investigate the position of boundary-layer transition have been mentioned in Section 2.5.

An investigation of wing flow-patterns by photographing tufts attached to the wing surface is the subject of Ref. 38. The tests were performed at 40 000 ft in steady turns at M between 0·4 and 1·3. The flight test techniques are largely as described in Section 4.1.1 and the difficulties of stabilising speed at transonic and supersonic Mach numbers have already been indicated. Only films covering a Mach number range of $\pm 0{\cdot}01$ and a C_L variation of ± 5 per cent were analysed. The duration of the record was normally at least 5 seconds but lengths of 1 to 2 seconds were included in rapidly varying flight conditions. From these records it was possible to determine something of the flowfield development over the wing, including the vortex position and areas of separation near the tip. Interpretation of the records was possible because of the knowledge of the general flowfield characteristics obtained through numerous wind-tunnel studies (e.g. Refs. 39 and 40).

Measurements of surface pressures in flight are reported in Refs. 41 and 42. Ref. 41 is a detailed investigation of pressures near the leading edge at 50 per cent semi-span. The region studied was from 0 to 3·7 per cent of local chord over a fairly wide Mach number and C_L range obtained in turns and pull-ups. While the main purpose of the original tests was to measure leading-edge suction in supersonic flight, valuable data presented shows leading-edge-pressure trends as C_L or M change and establishes their non-linear character. A comparison with wind-tunnel results is also possible and this will be done in Section 6.9.3.

The surface pressures of Ref. 42 cover the entire wing, including elevator and aileron surfaces. Although Ref. 42 has yet to be published, much of the basic data has been made available to the writer, while some of it in the range up to M = 1·25 has been included in Ref. 38 and correlated with the tuft visualisation studies. The range of conditions covered is summarised in Table 4 and the data obtained are chordwise pressures on both upper and lower surfaces at four spanwise locations, viz. 20 per cent, 38·5 per cent, 58 per cent and 85 per cent of semi-span.

Finally, some pressures on the rear fuselage are given in Ref. 15. These were mainly measured for drag comparison purposes and will be considered further in Section 6.9.4.

4.4. Powerplant Calibrations

Two references (27 and 43) are specifically concerned with measurements of performance and calibrations of the Avon RA28 engine used in the Fairey Delta 2. An accurate knowledge of engine net thrust in flight is essential for drag measurements, while differences in engine flow between wind tunnel and flight could have

major effects on other characteristics through changes in flow around the intakes and jet exit. Although Refs. 27 and 43 are not directly relevant to the present investigation, the engine mass and momentum flows cited in Section 3.4 have been derived from them.

4.5. Miscellaneous

The following reports, involving tests on aspects of the Fairey Delta 2, are mentioned for completeness and in general have only an indirect bearing on the present investigation.

Calibration tests on the wind vane mounted on the aircraft nose boom are reported in Ref. 31, while Ref. 14 reports direct measurements of the aircraft inertia characteristics.

Results of measurements on nose-aerodynamic heating are given in Ref. 44, and measurements of structural strains in the wing panels arising out of fluctuations in the turbulent boundary-layer are reported in Ref. 45.

Finally, the Fairey Delta 2 has also been involved in tests in the development of a ventilated propelling nozzle (Ref. 46) and in the study of sonic-boom effects (Refs. 3, 47).

5. Model Tests

The main references, the quantities measured, and the range of conditions and altitudes covered are summarised in Table 5. A brief description follows of the test procedures and corrections made to measurements.

5.1. Tests on 1/24 Scale Model

This model was tested over the Mach number range M = 0·85 to 1·25 in the 8 ft × 6 ft tunnel at Farnborough (Ref. 36) and at supersonic M in the 3 ft × 3 ft supersonic tunnel at Bedford (Ref. 22). The model was sting mounted, with an annular space between the fuselage and sting forming the exit duct through which the intake air was exhausted.

5.1.1. Transonic tests. Ref. 36 reports results for lift, drag, longitudinal trim characteristics, sideslip derivatives and aileron and rudder derivatives. The drag results were corrected for drag due to the internal duct flow, which is a substantial part of the measured drag. However, there is some doubt as to the accuracy of the corrections. Corrections were also made for tunnel-flow angularity and for deflection of the balance and support system under load. But no corrections were made for blockage or wall-constraint effects which were not known at the time. Also errors due to control-surface distortions under load were estimated to be small. Intake mass flow was obtained in preliminary test by pitot and static-pressure surveys at the exit.

5.1.2. Supersonic tests. The same range of results is covered as in Ref. 36, except that Ref. 22 only reports incremental drag measurements due to various externals such as airbrake and ventral tank. Total drag was not presented since it was not possible to correct for drag due to internal duct flow. Tunnel-flow corrections were considered to be within the experimental scatter but corrections were made for balance-system deflections. Blockage corrections did not apply while control-surface deflections were small. Intake mass flow was measured as in Section 5.1.1.

5.2. Tests on 1/9 Scale Model

This model was subjected to an extensive series of tests in the 9 ft × 8 ft A.R.A. transonic wind tunnel (Refs. 24, 25) and at subsonic and supersonic speeds in the 8 ft × 8 ft wind tunnel at Bedford (Refs. 23, 38, 48 and 49). While Refs. 48 and 49 have yet to be issued in report form, many of the basic results have been made available to the writer or else quoted in part in some of the other references. Tests were performed with the model sting mounted similar to the 1/24 model, but, because of the larger model scale, less boattail distortion was necessary in order to accommodate the sting.

5.2.1. Subsonic and supersonic tests. The 8 ft × 8 ft tunnel tests reported in Ref. 23 include lift, drag, longitudinal derivatives, sideslip derivatives, rudder derivatives and aileron derivatives. Aileron and elevator hinge moments are dealt with by Ref. 48. Ref. 23 was especially concerned with drag measurements and took considerable care with corrections. Preliminary tests on exit-duct flow using pitot and static-pressure surveys enabled the mass flow to be calculated and also made possible corrections, where necessary, to normal force, axial force and pitching moment due to change in momentum of the stream tube ingested by the intakes. Drag results were also corrected for base pressure effects. Tunnel-flow deflection was checked and corrected for where

necessary and the deflection of the balance and support system allowed for. Corrections to control derivatives for control-surface distortion under load have been discussed in Section 3.2.2. At subsonic Mach numbers additional corrections were made for tunnel blockage and wall-constraint effects, for axial buoyancy effect of the empty tunnel streamwise pressure-gradient and for the forward effects of the sting. The latter two corrections are small and relevant only to drag measurements. It is assumed that other results from the 8 ft × 8 ft tunnel (Refs. 38, 48 and 49) have had similar corrections applied where relevant.

Ref. 49 deals with model wing-surface pressure measurements. Only the basic data are as yet available. These take the form of *Cp vs. x/c* at four spanwise locations (viz. 20 per cent, 38·5 per cent, 58 per cent and 85 per cent of semi-span). These can be compared with similar flight measurements although, on the model, no pressures were measured on the control surfaces.

Flow-visualisation studies on the model are described in Ref. 38. The technique involved the photographing of nylon tufts glued to the wing surface. The spacing of the tufts was greater than on the aircraft so that some detail was lost. Also, the elevator angle was set at −2·5 degrees for most of the tests so that the model was not, in general, trimmed. However, Ref. 38 asserts that changing the elevator setting from −2·5 degrees to −10 degrees at either M = 0·9 or M = 1·5 only affected a few tufts in the vicinity of the outboard end of the elevator, so that most results are unaffected and can be compared with flight.

5.2.2. Transonic tests. The transonic results of Ref. 25 covered lift, drag and other longitudinal characteristics, sideslip derivatives, aileron derivatives and rudder derivatives, while Ref. 24 measured elevator and aileron hinge moments as well as wing pressures. The hinge moments were measured by special resistance strain gauges mounted along the hinge lines of elevator and aileron but only the elevator angle was measured during the tests, so that hinge moment derivatives with respect to aileron angle are not available. Wing pressures were measured chordwise at 20 per cent, 38·5 per cent, 58 per cent and 85 per cent semi-span as in the other tunnel.

Corrections, where applicable, were made for tunnel-flow non-uniformities, and for deflection of balance and support systems. Control-surface distortions have been discussed in Section 3.2. Drag measurements were corrected for internal duct flow but no mention is made of base or boattail pressure corrections in Ref. 25. No corrections were made in the 9 ft × 8 ft tunnel for blockage since this was presumed to be small.

There is no reason to doubt the accuracy of wind-tunnel measurements or the adequacy of the corrections, so that major differences between tunnel and flight are indeed a true reflection of factors such as geometry, scale, aeroelasticity, etc.

5.3. Free Flight and Wing-Flow Model Tests

Free flight model tests are reported in Ref. 50. Their chief advantage is the ability to achieve high Reynolds numbers. Valuable data relating to zero-lift drag were provided by these tests. Several other longitudinal characteristics such as C_{L_T}, $\Delta\eta/\Delta C_L$, C_{L_α}, C_{m_α} and $m_q + m_{\dot{w}}$ were also measured, together with aileron effectiveness and damping in roll. However, because of lack of geometrical similarity with full scale aircraft (including the absence of air intakes, different fuselage shape, etc.) and the different centre of gravity location (especially important with damping in pitch), the results cannot be used for detailed comparisons.

Wing flow tests for lift, pitching moment and damping in pitch have also been performed over the range M = 0·8 to 1·1 with Reynolds number 0·8 × 10^6 and are reported in Refs. 51 and 52. Some comparisons with flight and tunnel tests have been made in Ref. 18, showing reasonable agreement in general at 38 000 ft, and these results are not considered further here.

6. Results and Analysis

6.1. Introduction

The main section of this report is concerned with the presentation and critical evaluation of the available wind-tunnel and flight data. The emphasis will be on results for which both wind-tunnel and flight data are available. Results where direct comparisons are not possible will be considered only in so far as they may shed light on areas of discrepancy or draw attention to important behavioural characteristics of the aircraft. In some cases, where particular results are not directly presented, they have been derived or interpolated from curves which have been presented (e.g. wind tunnel $\Delta\eta/\Delta C_{L_T}$) or else calculated from the available data (e.g. flight C_{m_0}). As far as possible, results will be discussed and analysed as they are given.

Table 6 is a summary of quantities measured in flight and/or wind tunnel, and the references where they are reported. A glance at Table 6 shows that flight/tunnel comparisons are possible with lift, longitudinal trim and elevator effectiveness ($\Delta\eta/nC_w$). The elevator derivatives C_{L_η}, C_{m_η} are, however, not directly measured in flight

but derived from other measurements. The hinge-moment derivatives are all measured in flight but those due to aileron angle change have not been measured in the wind tunnel. Pitching moment at zero lift is directly measured in the tunnel but flight values are derived. Drag has already been the subject of extensive comparisons (Ref. 23) but no comparisons can be made with the unsteady damping derivatives $m_{\dot{\theta}}$, l_p and n_r since only flight values are available. The only lateral derivatives for which both wind-tunnel and flight data over the entire Mach-number range exist are the sideslip derivatives.

The results will be considered in the order shown in Table 6. The aim will be to bring out the main features and isolate areas of discrepancy. After presentation of the hinge-moment data it will be possible to estimate the effects of elevator flexibility and this will be done before proceeding to consider C_{m_0}, drag and sideslip derivatives.

Once the gross longitudinal and lateral characteristics have been established, attention will be directed to the flowfield visualisation and pressure measurements. In this way it is hoped to shed light on discrepancies which remain to be explained.

In some cases test results are compared with theoretical estimates. These estimates are mainly the ones given in Ref. 23, based on simple linear theory, often directly taken from Royal Aeronautical Society Data Sheets and similar sources. Details are given in Ref. 23.

6.2.1. Lift. Wind-tunnel tests show (Fig. 5) that the general nature of the C_L *vs.* α_F curves at constant elevator angle depends on what the Mach number is. At subsonic M (say M = 0·60) the curve, shown in Fig. 5, is clearly non-linear, the slope increasing up to α_F about 6 degrees, then decreasing and subsequently recovering. This is in agreement with the observations of Refs. 39 and 40, among others, and for a delta wing with blunt leading edge, can be explained roughly as follows.

As α_F increases the flow separates at the leading edge, starting at the wing tip, and the formation of a rolled up vortex commences. Since the leading edge is rounded, the apex of the vortex moves towards the wing root and the core moves inboard as α_F further increases. The added suction under the vortex causes the extra lift at this stage. At higher angles still, there are losses due to the secondary separation outboard of the vortex core, together with the lifting of the vortex core from the trailing edge. This tends to check the non-linear increase of lift. As the vortex apex continues to move towards the root, the character of the C_L versus α_F curve reflects a balance between increased lift under the vortex and loss of lift further outboard and at the trailing edge.

At supersonic M (e.g. M = 1·35) the non-linearity is far less marked but a small increase in slope at small incidences is discernible up to M = 1·4. For larger incidences ($\alpha_F > 6$ degrees), the slope starts decreasing gradually. For supersonic Mach numbers greater than 1·4 the curves are essentially linear up to α_F about 6 degrees after which the slopes start to decrease gradually.

There is some evidence that increasing the elevator angle suppresses the non-linearities at small incidences for both subsonic and supersonic Mach numbers. Thus Ref. 36 presents almost linear C_{L_T} *vs.* α_F curves for the 1/24 model, while the flight results in Ref. 15, although subject to considerable scatter, show little sign of non-linearities.

6.2.2. Lift-curve slope. A more quantitative picture, from wind-tunnel tests, of the non-linearities in the lift curves is given in Fig. 6, which plots $(C_{L_\alpha})_{\eta M}$ *vs.* M for C_L going from 0·05 to 0·30. Over this range of C_L, the lift curve slope varies by about 30 per cent at M = 0·70 but remains within ± 4 per cent of a mean value at M = 1·35. For larger incidences, C_{L_α} would start to drop at both subsonic and supersonic M.

The lift-curve-slope is not much dependent on elevator angle setting. Figure 6 shows that going from $\eta = 0$ to $-4{\cdot}8$ at M = 0·7 increases C_{L_α} by about 5 per cent for a given C_L. This increase is probably due to the fact that at a given C_L, α_F is larger for $\eta = -4{\cdot}8$ than for $\eta = 0$ and hence there is a slightly larger non-linear lift contribution. At supersonic speeds there is no consistent trend with η.

A comparison of flight and wind-tunnel lift-curve-slopes appropriate to steady level flight conditions is shown in Fig. 7. Flight data at both 40 000 ft and 10 000 ft are given.

At 40 000 ft flight and tunnel appear to be in very good agreement, falling within a ± 5 per cent band except around M = 1. A simple theoretical estimate is also shown but falls well below the other data for M less than 1·3, while the agreement is good for higher M. The good agreement above M = 1·3 is perhaps due to the fact that incidences are small and is also consistent with the smaller non-linear effects at these higher M. If the linear theory is compared with wind-tunnel values of lift-curve-slope appropriate to small angles of incidence, where non-linear effects are not yet important, then much better agreement is obtained (Fig. 8) at subsonic speeds. However, over the range M = 1·0 to 1·25 the theoretical estimates are still about 10 to 15 per cent low.

At 10 000 ft, only flight data for M = 1 or more is included. This is because at lower M, the analysis of the short period oscillations is hindered by excessive damping (*see* Section 4.1.2). The 10 000 ft results for C_{L_α} shown on Fig. 7 are about 20 per cent below the 40 000 ft results. None of the flight results have been corrected

for aeroelasticity at this stage, but this will be considered in Section 6.6.1. Non-linear effects may be expected to be small on the basis of wind-tunnel tests at supersonic speeds. It may also be worth mentioning that wind-tunnel tests on the 1/9 and 1/24 scale models showed no significant difference in C_{L_α} although the Reynolds numbers differed by a factor of about 4. The influence of possible undetected elevator oscillations cannot be estimated quantitatively since their amplitude is unknown. Further, the uncertainty in $\phi_{\eta n}$ at 10 000 ft makes it impossible to know even the sign of the possible error involved. If $\phi_{\eta n}$ is taken as 0 degrees, a value obtained from only half a cycle record, then the maximum error of 5 per cent at M = 1·2 (Ref. 18) would lower the 10 000 ft results even further. Only by assuming $\phi_{\eta n}$ to be -150 degrees (which is the 40 000 ft flight result) will a correction of suitable sign and magnitude result. Further, the effect of undetected elevator oscillations would be considerably larger at lower M. Thus for $\phi_{\eta n} = -150$ degrees at M = 0·7 the error in C_{L_α} would be 20 per cent and at M = 1·0 a maximum error of 17 per cent would be expected (Ref. 18). This is inconsistent with the trends measured in flight which indicate a better agreement at M = 1·0 and below than at M = 1·2 between C_{L_α} at 40 000 ft and 10 000 ft (Fig. 7).

For the present, the differences in C_{L_α} between the 40 000 ft and 10 000 ft flight results will be accepted but will be referred to again in subsequent sections.

Trimmed lift-curve-slope data, $dC_{L_T}/d\alpha$, are shown in Fig. 9. The agreement between flight and tunnel is good except between M = 1·05 and 1·15. Linear theory gives results about 20 per cent low for M less than 0·9 but is in good agreement for M above 1·3. Between M = 0·9 and 1·3 the difference between theory and experiment gradually diminishes. The low values given by theory below M = 1·3 presumably reflect the presence of substantial non-linear lift due to the development of the leading edge vortex. Contrary to the differences in C_{L_α} between 10 000 ft and 40 000 ft noted above, there appears to be no equivalent difference in $dC_{L_T}/d\alpha$. In fact the C_{L_T} *vs.* α_F curves at 10 000 ft and 40 000 ft run parallel to each other within the scatter of the data, although the 10 000 ft curves are perhaps slightly displaced to the left of the 40 000 ft curves, notably at M = 1·1 and 1·15 (Ref. 15). It is significant that $dC_{L_T}/d\alpha$ has been corrected for elevator distortion under load whereas C_{L_α} has not.

6.3.1. Pitching moment. Typical C_m *vs.* C_L curves, as obtained from wind-tunnel tests, are presented in Fig. 10. At supersonic speeds above M = 1·3 the curve is practically linear over the range tested. At subsonic speeds, M = 0·9 say, the slope at first very gradually increases with C_L, then encounters a sharp pitch-up (at C_L = 0·4 here), where the slope of the curve can change sign over a small range of C_L, and this is followed by a recovery.

These non-linear characteristics are typical of delta wings with blunt leading edges and have been explained along the same lines as the non-linear lifting characteristics in Section 6.2.1. The pitch-up appears to commence at roughly the same incidence as that at which the lift-curve-slope starts to decrease. For different constant elevator settings the curves of C_m *vs.* C_L run roughly parallel to one another, but the pitch-up occurs at a given α_F rather than a given C_L. The difference can be seen clearly in Fig. 10 where pitch-up occurs at α_F about 7 degrees for both $\eta = 0$ and $\eta = -4{\cdot}8$ degrees, even though C_L is 0·4 and 0·3 respectively. Thus curves of C_m *vs.* α_F would be more closely parallel up to pitch-up.

Some comparison of C_m *vs.* C_L curves for 1/9 and 1/24 scale models is shown in Fig. 10a. At M = 1·1 agreement is good though C_{m_0} seems to be slightly smaller for the 1/9 model. At M = 0·9, C_{m_0} is smaller for the 1/9 model and the pitch-up appears to be more severe. The slope of the curves and the position at pitch-up do not differ significantly. C_{m_0} differences increase with increase in elevator setting and can be attributed to differences in rear-fuselage geometry, as will be seen later.

6.3.2. Angle of incidence in trimmed flight. Figs. 11a, 11b show wind-tunnel and flight values of α_F to trim for various normal accelerations. The flight values are those reported in Ref. 15 and are taken directly from the curves presented there. Although flight tests at 10 000 ft were only made up to M = 1·15, values of α_F at higher M, in Fig. 11b, were obtained using the 40 000 ft curves. This has been possible since the C_{L_T} *vs.* α_F curves vary very little with altitude, except perhaps for a slight displacement towards the left for lower altitudes (10 000 and 20 000 ft) at M = 1·1 and 1·15 (Ref. 15). Also, some results at 20 000 ft available up to M = 1·4 show very good agreement with the 40 000 ft results above M = 1·15. Wind-tunnel values of α_F appropriate to trimmed flight at 40 000 ft or 10 000 ft have been interpolated, or in some cases extrapolated, from the available wind-tunnel data. No subsonic-wind-tunnel values are included since interpolation there is very inaccurate because of non-linearities in the pitching-moment curves and because of the large intervals in elevator angles tested. Within the accuracy of interpolation, there is no observable difference between 1/9 and 1/24 scale models.

The flight results are rather erratic between M = 0·95 and 1·15 with relatively large changes in α_F over a small Mach number range. At 40 000 ft in steady level flight ($n = 1$), α_F increases by about 0·5 degrees as M goes from 1·05 to 1·10. At $n = 2$, α_F decreases smoothly while at $n = 3$ there is a relatively sudden decrease in α_F

between M = 1·05 and M = 1·10. At 10 000 ft, where α_F is smaller for a given n than at 40 000 ft, the changes are even more marked. For instance at $n = 1$, α_F increases by about one degree for M going from 1·05 to 1·10. These characteristics reflect a sideways shift of the entire C_{L_T} *vs.* α_F curve as M goes from 1·05 to 1·10. The cause of this is presumably a sudden change of aerodynamic load distribution.

The wind-tunnel results appear to have a much smoother transition through the transonic Mach number range, so that for supersonic speeds the trim angle of incidence is about 0·5 degrees less than the flight value. Hence the change in loading at M about 1·05 suggested by the flight data is not nearly as marked in the wind-tunnel data. This may be due to differences in Reynolds number, differences in boundary layer, etc. and will be kept in mind when examining pressure distributions in more detail.

6.3.3. Elevator angle to trim. The elevator angle to trim is sensitive to many influences and good agreement between flight and wind-tunnel is not often achieved (*see* for example Refs. 7 and 9).

Present data for elevator angle to trim in steady level flight, as obtained from flight and wind-tunnel tests, are summarised in Figs. 12a and 12b, appropriate to 40 000 ft and 10 000 ft respectively. The flight data are taken directly from the curves of Ref. 15. A sharp drop in elevator angle, due to compressibility effects as M = 1 is approached, is followed by an even sharper rise at about M = 0·90 to 0·95 for both the 40 000 ft and 10 000 ft results. The curves flatten off for M going from 1·10 to 1·20 and the elevator angle gradually decreases thereafter. The sharp rise in elevator angle occurs at a significantly different Mach number from that at which α_F was seen to rise, i.e. at M = 1·05 to 1·10 (Fig. 10). Thus the shift of the C_L *vs.* α_F curve and the change of the pitching stability do not occur entirely simultaneously.

All the flight data have been corrected for elevator distortion under load. With this in mind, it is interesting to compare flight elevator angles to trim at a given C_{L_T} and M for flight at 40 000 ft and 10 000 ft (Fig. 13). It appears that the η_T *vs.* C_{L_T} curve at 10 000 ft is displaced to the left of the 40 000 ft curve by amounts equivalent to about 1 to 2 degrees of elevator angle, even though the slopes of the curves are similar. This displacement is apparently due to a change in C_{m_0}. It has been suggested that this may be caused by differences in up-rigged aileron angles at 40 000 and 10 000 ft. However, no consistent differences have been observed (Fig. 2) nor does the magnitude of any such effect seem sufficient since the scatter in up-rigged angle is only about $\pm 0{\cdot}5$ degrees. More data at 10 000 ft would have been welcome. If neither elevator flexibility nor changes in up-rigged angle can explain the differences in flight elevator angle to trim, it would seem necessary to look closely at the flow-field for non-linear effects or Reynolds number effects.

Wind-tunnel values of elevator angle to trim, shown in Figs. 12a and 12b, have been interpolated or extrapolated from C_m *vs.* C_L curves at different η. At subsonic speeds, only a few isolated points are included because of the difficulties of interpolation. However, it appears that at 40 000 ft agreement between flight and tunnel is good for M less than 0·9, but for conditions appropriate to 10 000 ft tunnel angles are somewhat lower than flight.

At supersonic speeds, Fig. 12a, for 40 000 ft, shows that wind-tunnel elevator angle starts to rise between 0·95 and 1·0, a fractionally higher M than in flight. The flight value thus rises to 1·4 degrees above the tunnel value at M = 1·0 and remains about 1 degree above the 1/9 model value up to M = 1·6. The 1/24 model values for 40 000 ft are about 0·5 degrees to 1·0 degrees below the 1/9 values for M greater than 1·3, becoming progressively worse as M rises to 1·8. Figure 12b, for 10 000 ft, shows similar trends except that the difference between flight and tunnel is now as high as 2 degrees while 1/9 and 1/24 models give results in much better agreement, except perhaps at M = 1·8. The lack of agreement between 1/9 and 1/24 model at 40 000 ft can be traced to differences in C_{m_0} which are especially important for larger elevator angles. More will be said on this in the next section.

The differences between flight and wind-tunnel elevator angles to trim in steady level flight at supersonic speeds remain to be explained. At 10 000 ft the discrepancies are worse than at 40 000 ft and in both cases a larger nose down C_{m_0} in flight is implied. Aeroelastic effects do not seem to be the answer since flight results have been corrected for elevator flexibility and the slope of the η_T *vs.* C_{L_T} curves do not differ markedly at 40 000 and 10 000 ft. As for aileron angle differences, the larger measured aileron angle in flight would result in larger nose up C_{m_0} in flight compared to tunnel, rather than the converse.

Hence it is possible that the differences in elevator angle to trim are due to differences in flowfield caused by scale effects, as has already been postulated in Section 6.3.2. This will be further amplified in Section 6.9 when examining the flowfields and wing-pressure-distributions. For the present, it might be added that the trends are not inconsistent with Reynolds number effect. Thus the higher flight Reynolds numbers lead to elevator angles greater (in a negative sense) than those measured in the tunnel, while 10 000 ft results are greater than 40 000 ft results at a given C_{L_T}, in keeping with the higher Reynolds numbers.

6.3.4. Elevator 'power'. The main concern of the previous Section 6.3.3 was with elevator angle to trim in steady level flight ($n = 1$). More generally steady flight with normal accelerations are of interest

especially in relation to the slope of the η_T *vs.* C_{L_T} curve, which is here referred to as the elevator power, $(\Delta\eta/nC_W)_{\text{Trim}}$.

To begin with, data for η_T in steady flight with normal acceleration is given in Figs. 14a and 14b for 40 000 ft and 10 000 ft respectively. The sources of data are the same as in Section 6.3.3 but the accuracy of the flight 10 000 ft data is not very good since in many cases large extrapolations are involved. Nevertheless, general trends are not affected.

Figure 15 summarises all the available data for $(\Delta\eta/nC_w)_{\text{Trim}}$. The flight data, corrected for elevator flexibility, is obtained from the slope of the linear portion of the η_T *vs.* C_{L_T} curve, i.e. $|\eta_T|$ less than 5 degrees, and is the same at 10 000 ft as at 40 000 ft as far as can be checked, so that aeroelastic effects are not thought to be important. Agreement between flight and tunnel data at subsonic M is reasonable, although interpolations from tunnel data are not very accurate here. The rise in the value of $(\Delta\eta/nC_w)_{\text{Trim}}$, indicating loss of elevator effectiveness, starts at about M = 0·95 in all cases. Tunnel data at supersonic speeds shows $(\Delta\eta/nC_w)_{\text{Trim}}$ to be a function of C_{L_T} and/or η and this non-linearity is especially marked with the 1/24 model. The differences in elevator effectiveness between flight and models are reflected in the η_T curves of Figs. 14a and 14b, e.g. in Fig. 14a, the lower elevator effectiveness of the 1/9 model means that $|\eta_T|$ is higher than the flight value at $n = 3$ (M > 1·4) even though it is lower at $n = 1$. The lack of agreement between 1/9 and 1/24 models and the non-linearities are most pronounced at M above 1·3. Reynolds number does not seem to be a predominant factor here because the differences between flight and models show no consistent trends with Reynolds number, nor is there any marked change in flight results going from 40 000 ft to 10 000 ft despite the difference in Reynolds number.

Geometrical differences between the 1/9 and 1/24 scale models around the rear fuselage have been pointed out previously and these may well explain the large differences in $\Delta\eta/nC_w$ between the two models. Thus, with η increasing from zero at supersonic M, shocks and expansions forming at the hinges interact with the rear-fuselage region. The contribution of the induced pressure distribution to the pitching moment will differ with differing boat-tail geometries. These points will be amplified as we proceed.

In summary, the elevator angle to trim at various normal accelerations reflects differences in both C_{m_0} and elevator effectiveness $(\Delta\eta/nC_w)_{\text{Trim}}$. C_{m_0} shows trends consistent with Reynolds number changes while $(\Delta\eta/nC_w)_{\text{Trim}}$ seems more strongly influenced by geometrical differences.

6.3.5. Manoeuvre margin and related parameters. H_M, C_{m_α} and dC_m/dC_L bear the following relationship in a pull-up

$$\frac{dC_m}{dC_L} = \frac{C_{m_\alpha}}{C_{L_\alpha}} = -\left(H_M - \frac{1}{\mu_1}\left(z_q\frac{dC_m}{dC_L} + m_q\right)\right)$$

where $\mu_1 = 2m/\rho S\bar{c}$ is approximately 230 at 40 000 ft and 77 at 10 000 ft for the Fairey Delta 2.

The term involving the rotational derivatives z_q and m_q is usually small. An estimate for the effects of q using slender wing theory gives a maximum contribution of 5 per cent at 40 000 ft and 15 per cent at 10 000 ft (*see* e.g. Ref. 53). These contributions are such as to reduce the absolute value of dC_m/dC_L if included. It is likely that the q contributions would in fact be smaller for a 60 degree Delta wing than that given by slender wing theory. Thus for the present it will be assumed that $dC_m/dC_L = -H_M$ to sufficient accuracy. This is further justified by the fact that the discrepancies to be noted are only worsened if q effects are included.

Flight measurements of H_M from short-period oscillations have used the equation

$$H_M = \frac{4i_B}{\mu_1 C_{L_\alpha}}(R^2 + J^2)$$

Calculations of C_{L_α}, in the same tests, depend on R, J, q/n and ϕ and thus H_M is also a function of all these. On the other hand $C_{m_\alpha} = -C_{L_\alpha}H_M = (4i_B/\mu_1)(R^2 + J^2)$ depends mainly on J since R^2 is much smaller than J^2. Thus it is to be expected that C_{m_α} will be more accurate than either C_{L_α} or H_M. Examination of data given in Ref. 18 supports this. C_{m_α} shows a consistent trend with altitude, with the absolute value decreasing as altitude changes from 38 000 ft, through 21 000 ft, 15 000 ft to 10 000 ft. This simply reflects the trends in measured period (J) which are clear and subject to relatively little scatter. Trends in C_{L_α}, on the other hand, are much less clearly defined although values at 10 000 ft are clearly less than at 40 000 ft.

All flight data to be considered in this section are uncorrected for any aeroelastic effects.

Before comparing flight and tunnel results, some general features of the tunnel C_m *vs.* C_L (or α_F) curves discussed in Section 6.3.1 are summarised in Fig. 16 in the form of C_{m_α} at various C_L. At subsonic speeds the non-linear nature of the curves leads to an increase of C_{m_α} as C_L goes from 0 to 0·2 by as much as 80 per cent.

At supersonic speeds the curves become linear and a scatter of ± 5 per cent in C_{m_α} is apparent at M = 1·35. Changes in η shift the entire C_m *vs.* C_L curve but do not normally alter the slope appreciably as is clear from camparisons of $\eta = 0$ and $\eta = -4{\cdot}8$ data (also *see* Fig. 10). Tunnel results on the 1/24 model generally agree well with the 1/9 scale model, but are perhaps slightly high at M = 1·4, the agreement becoming excellent at higher M.

A theoretical estimate (from Ref. 23) is included in Fig. 16. At subsonic speeds linear theory agrees with tunnel data for $C_L = 0$ but for M between 1·0 and 1·6 the theory is up to 20 per cent below the tunnel results. Above M = 1·6 theory and experiment are again close. These features are similar to those found in the C_{L_α} results (Section 6.2.2).

Flight tunnel comparisons of C_{m_α} at C_L's appropriate to flight at 40 000 ft and 10 000 ft are made in Fig. 17.

At 40 000 ft, flight and wind tunnel appear to be in reasonable accord for subsonic M, but the flight results are around 15 per cent low for M above 1·05. The 10 000 ft flight values are even worse, being as little as half the tunnel values for the supersonic range covered, while at subsonic M they are about 15 per cent below tunnel values.

One obvious reason for these discrepancies is the absence of any corrections for elevator flexibility to the flight data. These will be considered in Section 6.6.2, but in themselves are not completely successful in reconciling the differences, especially at 10 000 ft and supersonic speeds. There also seems to be a consistent trend with Reynolds number in Fig. 17, i.e. the higher the Reynolds number, the lower the value of C_{m_α}, especially at supersonic speeds. So it is desirable to keep in mind the influence of scale effects on flow development especially regarding aerodynamic-centre position. The possible effect of Reynolds number on C_{m_0} (or elevator angle to trim) has been mentioned already in Section 6.3.2 and this entire aspect is being left to Section 6.9. There is finally the possibility of further aeroelastic distortions such as at the wing tips.

Flight and tunnel results for dC_m/dC_L appropriate to level flight at 40 000 and 10 000 ft are summarised in Fig. 18. Flight values are simply $C_{m_\alpha}/C_{L_\alpha}$ and so errors in C_{L_α} compound those in C_{m_α}. This is especially important for subsonic speeds at 10 000 ft where C_{L_α} values used may involve large errors. Nevertheless, these are included in Fig. 18 mainly for use later when correcting for elevator distortions.

Despite the greater inaccuracies involved in dC_m/dC_L, all the comments relating to C_{m_α} apply equally well here. dC_m/dC_L is of course directly related to aerodynamic-centre position if q effects are neglected.

6.4.1. Elevator derivatives—Introduction. The elevator trimming 'power' considered in Section 6.3.4 was a quantity obtained directly from flight tests. The flight quantities to be considered in this section are secondary in the sense that they have not been directly measured but are derived from other measured quantities. This was due to limitations on test techniques (e.g. limited centre-of-gravity movement) and/or on the accuracy of instrumentation available at the time of the tests. Thus flight/tunnel discrepancies merely reflect lack of agreement in the more directly measured quantities.

Wind-tunnel data are direct, even though often obtained by linear interpolation from lift and pitching-moment curves.

The results to be presented in this section will be used for later estimates of the effects of elevator distortion.

6.4.2. Lift due to elevator—C_{L_η}. Wind-tunnel data at supersonic M indicate that C_{L_η} is a strong function of elevator angle, η, but relatively insensitive to incidence (Fig. 19). The values of C_{L_η} shown are averages over the ranges of η quoted and although the accuracy of these averaging processes is not always high, it is nevertheless clear that results from the 1/24 and 1/9 scale models do not agree. C_{L_η} is a stronger function of η on the 1/24 model than on the 1/9 model and there are large changes in C_{L_η} depending on whether C_{L_η} is the average from $\eta = 0$ to -4 degrees or from -4 to -10 degrees.

These characteristics are very similar to those noted about $(\Delta\eta/nC_w)_{\text{Trim}}$ in Section 6.3.4 and are thought to be largely due to the interaction of elevator with the rear fuselages which are different on the two models.

Figure 20 presents a summary of test results over the entire Mach number range. A large drop in C_{L_η} at supersonic speeds is apparent. There is a fair degree of scatter and agreement between various tunnels is not as good as may be desired. In general it seems that C_{L_η} is much more sensitive to precise tunnel conditions, geometry etc. than is, say, C_{L_α}.

An estimate for the effects of elevator flexibility on the 1/9 model (Ref. 23) raises C_{L_η} by up to 10 per cent, the largest corrections being at transonic speeds.

The flight results given in Fig. 20 have been inferred from the difference between trimmed and untrimmed lift-curve-slope using the equation

$$(C_{L_\eta})_\alpha = [dC_{L_T}/d\alpha - (C_{L_\alpha})_\eta]/(\Delta\eta/nC_w)(dC_{L_T}/d\alpha).$$

This is an inaccurate process because $dC_{L_T}/d\alpha$ and $(C_{L_\alpha})_\eta$ do not differ by much, but the results thus obtained are at least of the right order of magnitude.

Finally, a simple theoretical estimate from Ref. 23 is also included in Fig. 20 and agrees remarkably well with wind-tunnel data at subsonic speeds and for Mach numbers greater than about 1·2.

6.4.3. Pitching moment due to elevator—$(C_{m_\eta})_{C_L}$, $(C_{m_\eta})_\alpha$. Data for these two related derivatives are given in Figs. 21 and 22. The relation between them is as follows:

$$(C_{m_\eta})_\alpha = (C_{m_\eta})_{C_L} + C_{L_\eta} C_{m_\alpha}/C_{L_\alpha}.$$

Wind-tunnel values given are averages over specified ranges of η. Comments made in Section 6.4.2 regarding dependence on η and α, and comparisons between 1/9 and 1/24 model results hold equally well here (Fig. 21). Data on non-linearity with η at subsonic speeds are not available. Corrections for elevator flexibility would raise the 1/9 model results slightly, but overall accuracy due to scatter etc. hardly warrants this here.

Figure 22 shows some wind-tunnel data for $(C_{m_\eta})_\alpha$ compared with $(C_{m_\eta})_{C_L}$. The difference, which equals $C_{L_\eta} \times (dC_m/dC_L)$ is as much as 30 per cent. Flight results for $(C_{m_\eta})_{C_L}$, corrected for elevator flexibility, will be presented in Section 6.6.4.

Theoretical estimates, derived in Ref. 23, agree roughly with measured values of $(C_{m_\eta})_\alpha$ for M above 1·25 but are around 40 per cent low at subsonic speeds (Fig. 22). This is surprising in view of the good agreement with C_{L_η} and implies a poor estimate of the centre of pressure at subsonic speeds.

6.5.1. Hinge moment derivatives—Introduction. These derivatives are of importance here not only for the light they shed on differences between flight and wind tunnel, but also because a knowledge of the elevator hinge-moment derivatives makes it possible to estimate corrections due to elevator distortions under load (Section 6.6).

The following definitions hold:

$$\Delta C_{H_E} = b_{1E}\Delta\alpha + b_{2E}\Delta\eta + b_{3E}\Delta\zeta$$

and

$$\Delta C_{H_A} = b_{1A}\Delta\alpha + b_{2A}\Delta\zeta + b_{3A}\Delta\eta$$

Flight measurements exist at both 40 000 ft and 10 000 ft for all the above derivatives including the cross derivatives b_{3E}, b_{3A}. Tunnel data are available for the 1/9 model only and do not include the derivatives b_{3E} or b_{2A}.

6.5.2. Elevator derivatives. Plots of tunnel results given in Ref. 24 indicate that b_{1E} and b_{2E} are in general not strongly dependent on elevator angle or incidence at supersonic Mach numbers. Under some conditions there is a slight dependence on α_F (e.g. M = 1·02, $\eta = -5$ degrees). At subsonic speeds, especially M = 0·90 and 0·94, b_{1E} and b_{2E} appear to be more dependent on η.

Flight data are subject to quite large scatter but no significant difference is discernable between 40 000 ft and 10 000 ft. The bands of flight results for b_{1E} and b_{2E} are shown in Figs. 23 and 24 respectively, together with the appropriate wind-tunnel data. All flight data have been corrected for elevator distortion under load.

Figure 23 shows that tunnel values for b_{1E} appropriate to flight at 40 000 ft lie well within the flight data band except for M above about 1·1 where they lie towards the upper edge. Tunnel results for supersonic M at 10 000 ft (not shown) would, if anything, be slightly lower where non-linearities of b_{1E} with α_F are present.

For b_{2E}, Fig. 24 shows the tunnel values at supersonic speeds to be towards the lower edge of the band. If anything, $|b_{2E}|$ is a slightly decreasing function of $|\eta|$ at supersonic M so that tunnel values appropriate to 10 000 ft would lie closer to the middle of the band.

Hence, as far as can be judged from the available data, wind-tunnel and flight values of elevator hinge-moments show no major discrepancies.

Flight measurements for the cross derivative b_{3E} (Ref. 19) indicate that b_{3E} can reach values as high as 0·6 to 0·7 at Mach numbers close to 1, but decrease rapidly away from the transonic range. It is to be expected that aileron movements influence forces on the elevator at transonic speeds, but the magnitude of the effect is perhaps surprising.

6.5.3. Aileron derivatives. In contrast to the elevator derivatives, the curves of Ref. 24 indicate that the aileron derivatives, b_{1A} and b_{3A}, are strongly non-linear with both α_F and η. For instance Fig. 25, taken from

Ref. 18, shows that the slope of the C_{H_A} *vs.* α_F curve changes rapidly at α_F around 2 to 3 degrees for M = 1·02 depending on elevator setting. $|b_{1A}|$ is thus much smaller at α_F less than 2 or 3 degrees. Further, flight values of b_{1A} are obtained from an analysis of short period oscillations during which α_F varies by around ± 1 degree, implying that the resulting value of b_{1A} is often an average value over a range where large non-linearities are present. Similar non-linearities in b_{1A} are present at higher Mach numbers.

Results for b_{3A} in Ref. 24 shows changes with elevator angle at constant α_F, as well as changes with α_F at constant elevator setting.

Flight and tunnel data for b_{1A} and b_{3A} for level flight at 40 000 ft and 10 000 ft are given in Figs. 26 and 27. Figure 26 shows that the values of b_{1A} for supersonic speeds at 10 000 ft are well below the values at 40 000 ft, even accounting for the large scatter in the results. This is consistent with the non-linearities observed above. Tunnel values appropriate to 40 000 ft, however, lie well above the flight data for M above 1·1. Possibly this is partly because flight results are in fact an average over a ± 1 degree range of incidence.

Some idea of the relatively sudden change of b_{1A} at a specific α_F, which wind-tunnel measurements indicate, is also shown in Fig. 26. In particular, at M = 1·2 and 1·3, this occurs at α_F approximately 1 degree and the values shown are for $\eta = -5$ degrees, although similar behaviour occurs at other elevator settings. The magnitude of the change is clearly in keeping with the changes between 10 000 ft and 40 000 ft measured in flight.

Similar changes with altitude are also present in flight measurements of the derivative b_{2A} (Ref. 29) but these are not shown here since no tunnel data is available for comparison.

The cross derivative b_{3A}, on the other hand, shows no significant tendency to change with altitude and the tunnel results seem to fall within the flight scatter band (Fig. 27). The insensitivity to altitude is possibly because the non-linearities with incidence and elevator setting, which have been remarked on, tend to cancel each other out.

The aileron-jack system is very stiff, while pressure data presented in Section 6.9.4 do not point to substantial twisting of the wing tip. Further, the fact that the non-linearities occur in both flight and tunnel all suggests an aerodynamic explanation for differences between the 10 000 ft and 40 000 ft results and also for the differences between tunnel and flight shown in Fig. 26 for b_{1A}. This is probably associated with leading-edge separation, which commences at the tips, and the subsequent formation of the rolled up vortices which lie right across the ailerons.

The elevator hinge-moment derivatives, which are relatively free from the influence of these vortices show a much more linear behaviour. A comparison of b_{2E}, which is practically independent of η between $\eta = 0$ and -10 degrees supersonic speeds (Ref. 24) and C_{m_η} which shows a much stronger dependence on η reinforces the suggestion in Section 6.4.2, attributing non-linearities in C_{m_η}, C_{L_η} and $(\Delta\eta/nC_w)_{\text{Trim}}$ with η to interaction of the elevator with the rear fuselage, rather than to changes of load distribution on the elevators themselves.

6.6.1. Corrections for elevator flexibility—Introduction. Using the data presented for the elevator lifting and pitching-moment derivatives, C_{L_η} and C_{m_η}, together with the hinge moment derivatives b_{1E} and b_{2E}, it is possible to make estimates for the effect of elevator distortions under load on C_{L_α} and C_{m_α}. The latter were measured in flight by analysing the short period oscillations but no corrections were made for elevator flexibility.

Following these estimates, corrected values of $(C_{m_\eta})_{C_L}$ will be presented, and this together with other corrected trim data will enable a calculation, free from the effects of elevator flexibility, to be made for C_{m_0}. This can then be compared with direct wind-tunnel data.

6.6.2. Corrections to C_{L_α}. Referring to the sketch below, the following simple analysis is used:

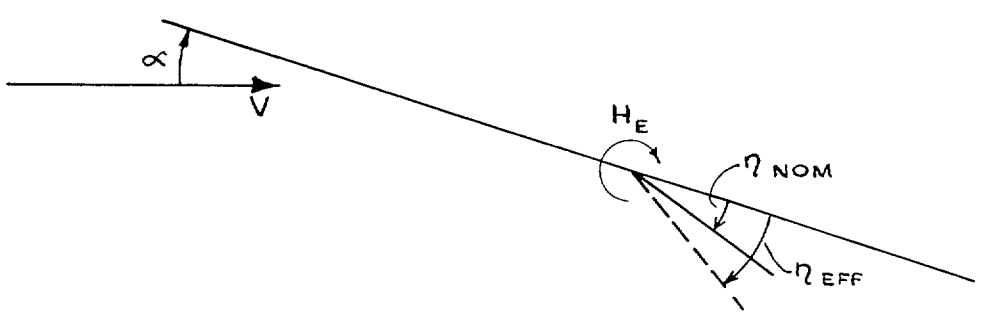

Assuming η_{NOM} = constant, then

$$\Delta C_L = C_{L_\alpha}\Delta\alpha + C_{L_\eta}\Delta\eta_{\text{EFF}} \tag{1}$$

Also

$$\eta_{\text{NOM}} - \eta_{\text{EFF}} = -H_E/2000 \tag{2}$$

where H_E is elevator hinge-moment, and elevator stiffness is

$$2000 \text{ lb ft/degree} = 35 \text{ ft lb/radian.}$$

From (1) and (2) it follows that

$$\Delta\eta_{\text{EFF}} = \Delta H_E/35 = (H_{E_\alpha}\Delta\alpha + H_{E_\eta}\Delta\eta_{\text{EFF}})/35 \tag{3}$$

Combining (1) and (3) then gives

$$(\Delta C_L/\Delta\alpha)_{\eta_{\text{NOM}}=\text{const}} = C_{L_\alpha} + C_{H_{E\alpha}}C_{L_\eta}/(35/\tfrac{1}{2}\rho V^2 S_E c_E - C_{H_{E\eta}})$$

$$= C_{L_\alpha} + b_{1E}C_{L_\eta}/(70/\rho V^2 S_E c_E - b_{2E}).$$

C_{L_α} is the quantity required while $(\Delta C_L/\Delta\alpha)$ at $\eta_{\text{NOM}} = \text{const.}$ is the quantity which was measured.

The correction term $b_{1E}C_{L_\eta}/(70/\rho V^2 S_E c_E - b_{2E})$ has been evaluated using tunnel values of C_{L_η} (Section 6.4.2) and flight measurements of b_{1E} and b_{2E}. The corrected values of C_{L_α} are shown in Fig. 7. At 40 000 ft the corrections are relatively small and the good agreement between tunnel and flight is not upset. At 10 000 ft the corrections raise the measured C_{L_α} by about 8 per cent at supersonic speeds, but this is still insufficient to bridge the gap, so that the flight results at 10 000 ft remain some 10 to 15 per cent below the rest. If an effective elevator stiffness of say 1500 ft lb/degree were assumed, the magnitude of the correction would be changed very little (from 8 per cent to 9 per cent at 10 000 ft).

6.6.3. Corrections to C_{m_α}. These can be estimated in a manner analogous to that above. Thus:

$$(\Delta C_m/\Delta\alpha)_{\eta_{\text{NOM}}=\text{const}} = C_{m_\alpha} + b_{1E}C_{m_\eta}/(70/\rho V^2 S_E c_E - b_{2E}).$$

Tunnel values have been used for C_{m_η} (Section 6.4.3). The corrected values of C_{m_α} are shown in Fig. 17.

Considering first the 40 000 ft results, corrections for M below 0·95 are small and agreement with wind tunnel remains good. At supersonic speeds, corrections are much larger and raise C_{m_α} by 10 to 15 per cent. This brings flight results into much better agreement with tunnel, although flight results are still perceptibly lower. The maximum difference is now about 10 per cent at M = 1·35.

Turning to the 10 000 ft results, Fig. 17 indicates substantial corrections throughout the Mach number range. Because of the intrinsic accuracy of C_{m_α} measurements (Section 6.3.5), subsonic values at 10 000 ft are also included. The corrections at subsonic speeds are about 20 per cent and seem notably to improve agreement of flight with tunnel values. At supersonic speeds the measured C_{m_α} is increased by as much as 50 per cent, but, as with C_{L_α}, this is still insufficient to bridge the gap. However, flight values are brought up to 75 per cent of tunnel results. Using a stiffness value of 1500 ft lb/degree makes only marginal differences in the corrections.

Figure 18 presents corrected values of $dC_m/dC_L (= C_{m_\alpha}/C_{L_\alpha})$, to be used in Section 6.6.4. The flight data simply reflect the corrected values of C_{m_α} and C_{L_α} in Figs. 7 and 17. For subsonic flight at 10 000 ft accurate C_{L_α} are not available, but for purposes of calculation, the 40 000 ft results are used, and the resulting dC_m/dC_L is in surprisingly good agreement with tunnel data.

So, after elevator flexibility corrections, some differences between flight and tunnel values of C_{m_α} and dC_m/dC_L, as well as C_{L_α}, remain at supersonic speeds, notably at 10 000 ft. Also remaining are the differences between flight measurements at 10 000 ft and 40 000 ft. Leaving aside the possible effects of undetected elevator oscillations (Section 4.1.2), and assuming the results at 10 000 ft are accurate, these differences require further explanation. Since tunnel tests show that the C_L *vs.* α_F and C_m *vs.* α_F curves are both linear at supersonic speeds for fixed Reynolds number, these differences are unlikely to be caused by non-linearities due to different incidences. The influence of Reynolds number changes on flow development, especially at low incidences, and possible wing-tip distortions will be considered further in Section 6.9.

6.6.4. Corrections to $(C_{m_\eta})_{C_L}$. Values of this derivative, free from the effects of elevator flexibility, can be calculated using the corrected data for dC_m/dC_L (given in Section 6.6.3) and $(\Delta\eta/nC_w)_{\text{Trim}}$, by means of the equation

$$(C_{m_\eta})_{C_L} = -(dC_m/dC_L)/(\Delta\eta/nC_w)_{\text{Trim}},$$

which is correct provided the effects of pitching velocity, q, are small. Estimates show this to be the case here. The value of $(\Delta\eta/nC_w)_{\text{Trim}}$ is taken to be the same at 10 000 ft or 40 000 ft within flight test accuracy (Ref. 15), so flight values of $(C_{m_\eta})_{C_L}$ reflect the dC_m/dC_L curves in these calculations. The results are given in Fig. 28 with wind-tunnel data from Fig. 21. The tunnel data is averaged over $\eta = 0$ to $-4{\cdot}8$ degrees. Unfortunately, due to insufficient tunnel data at subsonic and low supersonic M, it is not possible to check non-linearities of $(C_{m_\eta})_{C_L}$ with η, although non-linearities with η have been noted at higher supersonic M (Section 6.4). The differences between the flight results at 40 000 ft and 10 000 ft suggest marked non-linearities with C_L at subsonic M, arising through the dC_m/dC_L term (Fig. 18), but tunnel results (Fig. 21) do not show $(C_{m_\eta})_{C_L}$ to be a strong function of C_L here. The discrepancies at subsonic M may be due to inaccuracies in the value of $(\Delta\eta/nC_w)_{\text{Trim}}$ used and could perhaps be resolved by means of more direct flight measurements of $(C_{m_\eta})_{C_L}$ and additional tunnel data over a range of η. The supersonic results in general reflect the differences between tunnel and flight dC_m/dC_L (Fig. 18).

6.6.5. Calculation of C_{m_0} and comparison with tunnel. All the necessary data, corrected for elevator flexibility, is now at hand to calculate C_{m_0}. Assuming linear characteristics and neglecting the effects of q, the following equation for C_{m_0} is easily derived:

$$C_{m_0} = (C_{m_\eta})_{C_L}(-\eta_T) - (dC_m/dC_L)C_{L_T}.$$

This formula simply represents a linear projection back to the C_m axis (the $(dC_m/dC_L)C_{L_T}$ term) together with a projection along the C_m axis to the reference elevator angle (the $(C_{m_\eta})_{C_L}(-\eta_T)$ term). Thus greatest inaccuracies would be expected to occur where the distance projected back is greatest and/or where non-linearities are most pronounced. Thus, at a given M, errors should be less at 10 000 ft than at 40 000 ft because of smaller distances projected. Also errors should decrease as M increases both because of the decrease in C_{L_T} and because of the more linear C_m *vs.* C_L curves.

Flight and tunnel data, together with some estimates, are presented in Fig. 29. Tunnel results for both 1/9 and 1/24 scale models have been read off the C_m *vs.* C_L curves where available and the theoretical estimates are from Ref. 23.

Wind-tunnel results include C_{m_0} at $\eta = 0$, $-4{\cdot}8$ and $-9{\cdot}8$ degrees on the 1/9 model and at $\eta = 0$, -4 and -10 degrees on the 1/24 model. Tests on a given model give consistent results from tunnel to tunnel but there are some discrepancies in C_{m_0} between 1/9 and 1/24 model, especially at larger elevator angles. At $\eta = 0$, the 1/24 model results are very slightly higher than the 1/9 model data for M above 1·4, but are more substantially higher for M below 1·2. For larger elevator settings, C_{m_0} on the 1/24 model becomes progressively greater than on the 1/9 model, at least at supersonic speeds where comparisons are most readily made. These trends reflect the point previously noted, *viz.*, the shift of the C_m *vs.* C_L curves with changes in η differ for the different models, and seem to be due to interaction of the elevators with the afterbody. To avoid this complicating factor, flight and tunnel results will be compared only for $\eta = 0$ as reference, with the 1/9 model results as a basis.

At subsonic speeds below M about 0·9, the 40 000 ft flight values of C_{m_0} lie above the 1/9 model data while the 10 000 ft values are significantly below the tunnel data. The differences are due to the $(C_{m_\eta})_{C_L}(-\eta_T)$ term since the contributions of $(dC_m/dC_L)C_{L_T}$ are very similar in tunnel and flight. On further inspection, it becomes apparent that the differences are mainly due to the differences in η_T. The low value of $(C_{m_\eta})_{C_L}$ at 10 000 ft has a very minor effect. Differences in C_{m_0} at 40 000 ft are equivalent to elevator-angle difference of 0·6 to 0·7 degrees at M = 0·7 and about 0·3 to 0·4 degrees at M = 0·9. At 40 000 ft, these differences are consistent with a larger aileron rigged-up angle in flight, at least in direction (Section 2.3). At 10 000 ft differences in C_{m_0} are equivalent to 0·6 to 0·7 degrees of elevator angle at M = 0·7, increasing to almost 1 degree at M = 0·9, and are inconsistent in direction with the difference in aileron setting. Thus it appears that these discrepancies point to differences in aerodynamic loading distribution at the smaller angles of 10 000 ft flight, i.e. differences compared with 40 000 ft flight and with tunnel results. The total loading is of course the same since the projection back is from level trimmed flight conditions.

Between M = 0·9 and M = 1·0 there is a rapid decrease in flight C_{m_0}, consistent with the increase in elevator angle to trim which commences at M = 0·95. In the tunnel, the drop in C_{m_0} commences later (M = 1·0) and this too reflects the later commencement of increase of elevator angle to trim in the tunnel.

At supersonic speeds, the calculated flight values of C_{m_0} are significantly lower than the wind-tunnel values for both 40 000 ft and 10 000 ft flight, and this is despite the larger aileron settings in flight. At 40 000 ft and M above 1·1, C_{m_0} differences reflect η_T since both dC_m/dC_L and $(C_{m_\eta})_{C_L}$ agree reasonably in flight and tunnel. The elevator angles to trim differ by up to 1·3 degrees. At 10 000 ft there are larger discrepancies in dC_m/dC_L and $(C_{m_\eta})_{C_L}$ between flight and tunnel but these tend to cancel one another, so that once again C_{m_0} values are

a direct reflection of η_T's which in this case differ by over 2 degrees. The differences in aerodynamic loading distribution thus implied are much greater at supersonic speeds than at subsonic speeds. At the same time incidences are smaller and the vortex flow system is in an earlier and perhaps more critical state of development.

The main nose-up contribution to C_{m_0} at $\eta = 0$ comes from the rigged-up ailerons. Fuselage incidence is slightly negative at $C_L = 0$ so that the fuselage in isolation would contribute a small nose-down moment of the order of 0·001 per degree incidence. The main nose-down contribution comes from the wing-elevator surface (excepting the aileron). Thus the low C_{m_0} in flight implies that the centre of pressure of the wing-elevator is further back compared with that in the tunnel, especially when it is remembered that the aileron settings in flight are such as to produce a larger C_{m_0}. A comparison of all available tunnel and flight data for C_{m_0} indicates a trend towards lower C_{m_0} with higher Reynolds number.

The theoretical estimates included in Fig. 29 (taken from Ref. 23) give values of C_{m_0} substantially below the tunnel values (equivalent to about 1 degree in elevator angle).

This section has served to summarise trim differences in terms of C_{m_0} difference at $\eta = 0$. The lack of agreement between different measurements and/or calculations of C_{m_0} emphasises the important effects which relatively small differences in flow development may have. As well as wing flow development, differences with the Fairey Delta 2 at the nozzle exit, on the boattail, or at the intakes could make major contributions to C_{m_0}. This is quite plausible in view of the different engine mass and momentum flows under most test conditions.

C_{m_0} at elevator settings other than zero adds the questions of elevator fuselage interaction and boattail geometrical differences to those already discussed.

6.6.6. Non-linearities in longitudinal characteristics. By way of summary, two main areas where non-linearities are pronounced have been brought out in the preceding discussion. In the first place, due to the way in which the flow over the wing develops, derivatives such as C_{L_α} and C_{m_α} (Figs. 6 and 16) are seen to be functions of C_L (or α_F), most markedly at subsonic and transonic M. The aileron hinge-moment derivatives, on the other hand, display strong non-linearities with α_F at supersonic speeds (Figs. 25, 26). Because of these non-linearities it is important to make sure that flight and tunnel tests refer to similar configurations when making comparisons. In this respect, lack of tunnel data over a range of η, sufficiently closely spaced, has made some results at subsonic M difficult to interpolate or inaccurate, e.g. α_F and η_T in Figs. 11 and 12. Another aspect of the non-linear flow development relevant to flight/tunnel comparisons arises as a result of the changes in loading distribution going from subsonic to supersonic M. Because of scale differences these changes do not appear to develop in exactly the same manner in flight and on the models, leaving differences in trim configuration at supersonic M such as those apparent in Figs. 11 and 12, and in C_{m_0} (Fig. 29). This perhaps also helps to explain the low C_{L_α} (Fig. 7) and C_{m_α} (Fig. 17) in supersonic flight, especially at 10 000 ft, even though the curves of C_m or C_L *vs.* α_F appear to be linear according to model tests. Wing flow visualisation pictures and surface pressures will be studied with a view to bringing out differences in the way in which the flow develops over the aircraft and models.

The second area where non-linearities have been apparent is in the elevator characteristics. Tunnel tests have clearly brought these out at supersonic M where $(\Delta\eta/nC_w)_{\text{Trim}}$, C_{L_η} and C_{m_η} are seen to be strong functions of η (Figs. 15, 19 and 21). This is thought to be due to interactions between the shocks and expansions produced by the deflected elevator and the rear fuselage. One effect of these non-linearities is to produce substantial differences in C_{m_0} at supersonic speeds for elevator settings other than zero (Fig. 29). When comparing the various sources of data, an attempt has been made to distinguish this effect from the differences in C_{m_0} due to other causes such as differences in wing flow-pattern. At lower M, the lack of data over a range of η, referred to previously, prevents a detailed analysis of possible non-linearities with η.

6.7. Drag—Summary

Ref. 23 reports extensive tunnel tests on the 1/9 scale model and a comprehensive comparison with flight tests and estimates. No further analysis is attempted here and only a brief summary of results follows.

The tunnel tests included measurement of contributions to the drag from various components, (e.g. fuselage, fin, canopy, wings, etc.). One of the major conclusions was that theoretical estimates of drag variation with Reynolds number were inconsistent with measurements, especially at supersonic speeds. This was attributed partly to wing-fuselage interference flow and partly to a flow interference between the parachute fairing and the rear fuselage. These effects complicate the extrapolation of drag results from tunnel to full scale. However, it was possible to take this into account empirically and comparisons between tunnel and flight results were made doing this.

In addition to corrections for Reynolds number, the tunnel data was also corrected for contributions of the intake bleed system, drag of the external surfaces of the aircraft jet-pipe and nozzle, boattail drag differences and drag due to various excrescences omitted from the model. Many of these corrections involve a degree of uncertainty. Nevertheless, with all corrections made, tunnel measurements were found to be within 8 per cent of flight measurements for minimum drag. This contrasts with theoretical estimates of minimum drag for the model, which were up to 16 per cent below the measurements.

Flight and tunnel results were also in fair agreement for lift-dependent drag at most supersonic speeds for both trimmed and fixed-elevator configurations.

All details are given in Ref. 23.

6.8.1. Sideslip derivatives—Introduction. The sideslip derivatives n_v, y_v and l_v are the only lateral derivatives of particular interest to this report since they are the only ones for which both tunnel and flight data are available.

In general, all the wind-tunnel tests have shown yawing moment, sideforce and rolling moment to be linear functions of sideslip angle β, for small β and most of the derivatives have been obtained for β going from -2 to $+2$ degrees, although linearity usually in fact extends over a wider range than this. The behaviour of the derivatives with changes in incidence and/or elevator angle have been studied in the tunnels both with 1/9 and 1/24 scale models and the non-linearities revealed will be considered in the relevant sections.

6.8.2. Yawing moment due to sideslip—n_v. This particular derivative has proved to be very difficult to match in tunnel and flight, especially at supersonic speeds. For example, work on the Lightning P1 gives flight n_v around 25 per cent below tunnel measurements for M greater than 1, even after aeroelastic corrections. Similarly low flight n_v, by about 25 per cent, have been reported for the McDonnell F 101 for M above 1·2 (Ref. 54), while the X-15 (Ref. 12) has high flight n_v for M between 1·2 and 1·8 by about 10 per cent, but this is followed by a drop to 20–25 per cent below tunnel values for M above 1·8. Aeroelastic causes were suggested in Ref. 12. Further, wind-tunnel work on the XB-70 (Ref. 13), without the canard surface, showed a substantial reduction in n_v (35 per cent at M = 1·2) with increase in Reynolds number from $9{\cdot}4 \times 10^6$ to $2{\cdot}1 \times 10^7$. No single cause seems to have emerged to explain all these discrepancies, and a number of possibilities, all of which may make some contribution, will be explored with respect to the Fairey Delta 2.

A study of wind-tunnel data brings out several important characteristics of n_v. At subsonic speeds n_v does not seem to vary with incidence for α_F up to 8 degrees or more. For supersonic speeds up to M = 1·20, n_v increases above a certain α_F, depending on M, but for supersonic speeds above M = 1·3 a drop of n_v is noticed above a certain incidence depending on M and elevator setting (Fig. 30). Thus for M = 1·35, n_v with elevator set at 0 degrees drops significantly above $\alpha_F = 4$ degrees, while with $\eta = -4{\cdot}8$ degrees no drop occurs up to $\alpha_F = 10$ degrees. For M = 1·50, on the other hand, drops occur for both $\eta = 0$ and $\eta = -4{\cdot}8$ commencing at quite low incidences.

This drop in n_v with increase of incidence is due to loss of fin effectiveness, as is apparent in Fig. 30, which shows that, without the fin, n_v remains roughly constant over the entire incidence range tested. A similar loss of fin effectiveness is also present in y_v to be considered later. It is not possible to pinpoint the cause of this loss of effectiveness but Ref. 23 has suggested that it may be due to body vortices interacting with the fin. The interaction of a streamwise vortex with a vertical fin would mainly produce a rolling moment in the same sense as the vortex rotation, while a comparatively small force towards the vortex would also result (Ref. 55). This could give a reduction in n_v as observed, provided the vortex were on the windward side of the vertical fin. However, corresponding reductions in l_v do not seem to be present (Section 6.8.4), thus casting some doubt on this explanation. Nevertheless, body vortices have been noted in wind-tunnel tests on the Lightning P1A (Ref. 56) for wing incidences greater than 5 degrees and a similar effect may well be present on the Fairey Delta 2 although no data are available. Another possible effect which may lead to a loss of fin effectiveness is the relative change of the angle of sweep of the fin leading edge as incidence is increased. Thus a change of sweep of a delta wing from 60 to 70 degrees leads to a theoretical reduction of lift-curve-slope by about 25 to 30 per cent. If the effective sweep of the fin is increased relative to the impinging stream this would result in a reduction of n_v.

As well as the influence of incidence on n_v there is a very substantial non-linear dependence of n_v on elevator setting for supersonic speeds (Fig. 30). This appears to be caused by an interaction between the fin and a shock produced near the elevator hinge line. The shock would produce changes in Mach number and dynamic pressure over most of the fin since the hinge line is approximately level with the fin root. At M = 1·35, Fig. 30 shows that an absolute increase in elevator angle leads to a reduction of n_v at $\alpha_F = 0$. At M = 1·80, on the other hand, the effect is to increase n_v, while at M = 1·50 n_v at first increases and then decreases. Simple two-

dimensional shock expansion theory gives qualitative agreement with these observations, but the much more complex real problem makes quantitative agreement very difficult to achieve.

The non-linear behaviour of n_v with α_F and η changes in the wind tunnel can be used to explain some of the trends noted in the flight measurements of n_v. For instance, flight measurements at 40 000 ft give values for n_v at $n = 2$ which are below the $n = 1$ values for M less than 1·45 but greater for higher M. Tunnel results give very similar trends although the cross-over point occurs at M = 1·65 rather than 1·45. At 10 000 ft, only a limited amount of flight data for M below 1·05 are available. These show n_v to be slightly below the 40 000 ft data but well within the scatter band. Tunnel data for 10 000 ft differs only slightly from 40 000 ft data. Thus it appears that differences between $n = 1$ and $n = 2$ flight and/or between 10 000 ft and 40 000 ft are consistent with non-linear trends appearing in tunnel measurements.

Notwithstanding similar trends, the actual values of n_v show large differences between tunnel and flight especially at supersonic speeds. Tunnel and flight results are shown in Fig. 31. The model data is for trimmed level flight except where otherwise stated. The 1/9 and 1/24 model data are in reasonable agreement for M up to 1·25 but above M = 1·4 the 1/24 model data is 10 to 15 per cent below the 1/9 data. The influence of elevator setting is important especially at about −10 degrees where the trend of n_v with M is quite different from that at lower elevator settings. The bar on tunnel results at M = 1·4 indicates the possible errors of measurement.

The most prominent feature of Fig. 31 is the low values of flight compared to tunnel values for Mach numbers above 1·05. Despite the relatively large scatter band, the flight values drop to as little as half those of the tunnel and there is no sign of improved agreement for higher Mach numbers. This contrasts somewhat with some of the longitudinal characteristics (C_{m_α}, η_T, C_{m_0}) which show maximum discrepancies at M about 1·35 and thereafter improve. It is difficult to pinpoint any one specific reason for the differences in n_v but a number of possibilities have been evaluated.

First, consider the effect of non-linearities with incidence and elevator angle. In the range under consideration, the slightly larger flight angles and incidence would give smaller flight n_v while the larger elevator angles to trim would have the opposite effect. The changes, small as they are, would tend to cancel each other and can thus be disregarded.

Differences in Reynolds number may be expected to alter the flow pattern over the fin (which in the tunnel tests on the 1/9 model contributed 3 to 4 times more than the body to n_v) and/or to influence possible body vortices. Results on the XB-70 (Ref. 13) in fact showed a large decrease in n_v with increasing Reynolds number. The trends in the present case are not consistent with Reynolds number changes, the 1/9 model n_v being greater than the 1/24 values at supersonic speeds in general, while the flight results are smaller. This inconsistency argues against the importance of Reynolds number differences, but at this stage they still cannot be put aside. A further evaluation of them will be made in the next section (6.8.3). Unfortunately, no flow or pressure measurements have been made on the fin.

Important differences between models and full scale aircraft exist around the base of the fuselage. The 1/24 model differs from the 1/9 model in having a relatively larger base area such that inviscid slender body theory would predict a larger n_v all else being equal. The opposite is the case, at least above M = 1·3, so that a different kind of interaction between the base exit flow and the flow over the rear fuselage, involving shock movements, becomes a stronger possibility. The difference between flight and tunnel may also be explained in this way. The aircraft differs from the models in having eyelids at the nozzle exit and these were closed during the lateral tests, so that a substantial extra area was present at the base. The hot under-expanded exit jet has a jet/ambient pressure ratio which increases with M and is around 3·5 at M = 1·6. Thus after exit the jet will expand rapidly and induce compression and/or shock waves near the rear fuselage of the aircraft. The higher the pressure ratio the greater the effect is likely to be, and this is consistent with the increasing discrepancies as M increases. Quantitative data for the effect of such a process on the lateral derivatives seems very scarce, but Ref. 33 reports tests on a rocket-powered aircraft where n_v is reduced to below half the tunnel values at supersonic speeds, by the effects of jet expansion.

It is interesting to recall the low flight values of C_{m_α} previously described (Section 6.6.3) and ascribe this to interaction of the expanding jet with the rear fuselage. However, the contribution of the boattail is relatively much smaller in the longitudinal case. Further, the expansion ratios are less at 10 000 ft than at 40 000 ft, so the destabilising effect should be less. This is contrary to observations, suggesting other processes at work, such as differences in wing flow development.

A final possibility for explaining the low n_v in flight is the effects of rudder flexibility. In view of the significant effects of elevator flexibility on C_{m_α}, a similar estimate should be made for the rudder. Unfortunately, no reliable quantitative estimates can be made since no measurements have been made for rudder flexibility or hinge-moment derivatives. Yawing moments due to rudder are available from tunnel tests.

As with the elevator, the rudder jack is housed in the fuselage near the root while the force is transmitted presumably through a torque tube. Thus a degree of flexibility comparable to that of the elevator may be

expected. The difference between rigid rudder and flexible rudder n_v is

$$n_\zeta b_{1R}/(G + b_{2R})$$

if the same reasoning as in Section 6.6.2 is used. G is a measure of rudder flexibility and b_{1R}, b_{2R} are rudder hinge-moment derivatives. Also n_ζ, taken from tunnel measurements, is considerably larger than C_{m_η}, so that rudder flexibility should have a proportionately larger effect on n_v than was calculated with C_{m_α}. For a rough estimate of the magnitude of the above term, assume G to be the same as for the elevator while for b_{1R} and b_{2R} the aileron hinge moment derivatives can be used. The resulting corrections are summarised in Table 7. Clearly the corrections are large for M above 0·9 and establish the importance of properly accounting for rudder flexibility. The trend is not entirely consistent with the observed discrepancies since the magnitudes decrease with M at supersonic speeds. Further, the corrections are still insufficient to bridge the gap.

It appears then that the major part of the discrepancies in n_v at supersonic speeds can be accounted for by allowing for rudder flexibility and by taking into account the interaction of the expanding jet with the rear fuselage and/or nozzle. The differences in Reynolds number, and also non-linearities with α_F and η, seem to be less important.

6.8.3. Side force due to sideslip—y_v. A study of wind-tunnel measurements establishes the main characteristics of y_v with respect to changes in incidence and elevator angle.

In general y_v changes less with incidence than did n_v. For M between 1·05 and 1·20 $|y_v|$ increases slightly as α_F increases, similar to n_v. Without the fin, the tunnel values of y_v are more or less constant so changes are attributable to the presence of the fin, again similar to n_v in this range. For M above 1·3 y_v stays relatively constant for α_F up to around 8 degrees. However this represents a balance between decreases in fin effectiveness and increases in $|y_v|$ for the wing-body.

The behaviour of y_v with changes in elevator angle is closely similar to that of n_v although the magnitude of the changes are smaller. For example, at $\alpha_F = 0$ and M = 1·35 a change of elevator setting from 0 to $-14·8$ degrees decreases $|y_v|$ by 18 per cent compared to a 50 per cent decrease in n_v. The ratio $|n_v/y_v|$ thus decreases somewhat indicating a forward movement of lateral aerodynamic centre with increasing elevator setting. At M = 1·80, on the other hand, $|n_v/y_v|$ increases with increasing elevator setting implying a backward movement of aerodynamic centre. These effects are attributed to changing pressure fields induced by the shock generated by the elevator.

On the whole the non-linearities in y_v are similar to and consistent with those in n_v.

A summary of flight and tunnel data for y_v is presented in Fig. 32. The results are for trimmed level flight at 40 000 ft except where otherwise indicated. The scatter of the flight data is large, especially at supersonic speeds and reflects the difficulties involved in measuring the derivative. However, within the scatter band, there is r o difference between flight and tunnel data at supersonic speeds, in contrast to the very large differences found in n_v. The effects of changing altitude or normal acceleration are insignificant (where data is available) relative to the large scatter. At subsonic speeds flight $|y_v|$ appears to be somewhat lower than tunnel data with a maximum difference of about 25 per cent at M = 0·9, but the main concern here is with supersonic speeds.

There is reasonable agreement between 1/24 and 1/9 models and most of the differences, where present, can be attributed to differences in elevator angle setting.

The reasons put forward in Section 6.8.2 to explain the low values of n_v in supersonic flight can now be re-examined in terms of their influence on y_v, keeping in mind the relatively good agreement between flight and tunnel values of y_v. Thus the difference between the flight and tunnel values of the ratio n_v/y_v is equivalent to a forward shift of lateral aerodynamic centre by around 2 feet in flight at M = 1·4. Even taking the most favourable limits of the scatter band, the shift is still 1·3 feet. It is inconceivable this could be caused solely by differences in flow field over the fin due to Reynolds number differences. For instance, differences in dC_m/dC_L, after elevator flexibility corrections, are at most equivalent to a shift in wing aerodynamic centre of 6 inches.

On the other hand, rudder flexibility corrections to y_v should be of the same absolute magnitude as the corrections to n_v since rudder derivatives y_ζ and n_ζ are of roughly the same magnitude, from tunnel tests. So, a correction to n_v large enough to bring the wind tunnel and flight into agreement would raise the lower limit of the flight scatter band for $|y_v|$ well above the tunnel value. Alternatively, a correction small enough to allow tunnel y_v to remain within the scatter band would be too small to reconcile n_v. The previous conclusion, in Section 6.8.3, that rudder flexibility corrections were insufficient to account for the differences is thus reinforced.

Finally, consider the effect of the expanding exit jet. In this case, a large change in n_v and a relatively small change in y_v are quite compatible, because of the large contribution to yawing moment of small forces near the fuselage base.

Thus a consideration of flight and tunnel values of y_v, in conjunction with the earlier discussion on n_v, supports the idea of an important influence of the expanding exit jet. The effect of rudder flexibility may also need to be accounted for, while Reynolds number changes seem to be of relatively minor importance.

6.8.4. Rolling moment due to sideslip—l_v. Tunnel tests show that the contribution of the wing-body combination, without fin, is more or less independent of elevator setting and, in general, $|l_v|$ increases smoothly with incidence for small α_F. The rate of increase is less as M increases and at M = 1·8 on the 1/9 model Ref. 23 shows an actual decrease for small positive α_F followed by an increase. For larger incidences, the behaviour of the wing-body l_v becomes erratic especially at transonic speeds. This reflects the developing influence of the leading edge vortices. The effect of the vortices is especially clear at subsonic Mach numbers where a sudden decrease in $|l_v|$ commencing around $\alpha_F = 6$ degrees at M = 0·6, followed by a recovery at higher incidences, is similar to the behaviour shown by the pitching moment curve as incidence increases (Section 6.3.1).

The contribution to l_v made by the fin decreases with increasing incidence due largely to the geometric fact that the fin moves downward with respect to the stability-axes system as incidence increases. There may also be a loss of fin effectiveness corresponding to that noted in n_v and y_v, but in general the fin contribution changes fairly smoothly and any erratic behaviour of the l_v curve for the complete model is usually due to the wing-body contribution. The fin does, however, bring with it a dependence on elevator angle. This is very similar to that already noted with y_v and n_v. At M = 1·35, a change from $\eta = 0$ to $\eta = -14{\cdot}8$ degrees leads to a decrease in $|l_v|$ by 15 per cent at $\alpha_F = 0$.

Figure 33 compares flight and tunnel data for level trimmed flight at 40 000 ft except where otherwise indicated. The scatter of the flight data is quite large especially at supersonic speeds. The agreement with tunnel is good for Mach numbers below 1·1 while for Mach numbers above 1·1, tunnel $|l_v|$ is, if anything, slightly high being right at the edge of the flight scatter band. This may reflect differences in wing loading and as such would be consistent with differences in C_{m_α} noted in supersonic flight.

Agreement between 1/9 and 1/24 model data for l_v is good. Some 1/24 model data is included in Fig. 33 for different incidences, and demonstrates the very strong dependence of l_v on incidence, especially at subsonic speeds.

6.9.1. Flow visualisation and pressure measurement—Introduction. In previous sections dealing with trim and aerodynamic centre position, it has been suggested that part of the discrepancy between tunnel and flight results at supersonic M is due to differences in flow field development over the wings. In particular, Reynolds number differences make it necessary to artificially trip the boundary layer near the leading edges of the models thus leading to relatively thick boundary layers on the models (Section 3.3). Some of the available flow and pressure data have been chosen to illustrate the differences found between tunnel and flight and to indicate how they could influence some gross parameters. The main interest will be with the supersonic results, with particular emphasis on those aspects which seem most relevant to the observed discrepancies. Detailed and comprehensive presentation of flight and tunnel comparisons of wing flow visualisation and pressure distributions is left to the cited references, *viz.* Refs. 38, 41, and 42 for flight results, and Refs. 24, 38, 49, and 50 for results on the 1/9 scale model.

In addition to the wing, there are a few pressure measurements available, in both flight and tunnel, on the rear fuselage. These are of special interest in view of the comments made in Sections 6.8.2 and 6.8.3 regarding the large differences in n_v at supersonic speeds.

6.9.2. Flow visualisation. A study of the flow pattern over the Fairey Delta wing, using surface tufts, in both flight and wind tunnel has been reported in Ref. 38.

The flight tests, covering up to M = 1·35, confirmed the existence of a leading edge vortex, accompanied by a secondary separation outboard, under most flight conditions. At subsonic speeds the vortex develops from a leading edge separation. At supersonic speeds a region of supersonic expansion near the leading edge is usually present for lower incidences. This is terminated by a shock which, under the right conditions, leads to flow separation and vortex formation. The extent of the supersonic expansion increased with increasing Mach number.

In the wind tunnel, tuft flow visualisation studies on the 1/9 model showed the same general features as in flight. However, detailed flow patterns were more difficult to interpret because of the wider spacing between the rows of tufts. An important difference noticed was that the inward movement of the leading edge vortex, as incidence increased, developed more quickly in the tunnel than in flight. This is the sort of difference in flow development which could explain the differences in C_{m_α} observed earlier.

Another result arising out of the tuft flow visualisation studies was that a reasonable correlation was found between buffet onset and the existence of a significant area of secondary separation near the wing tips.

6.9.3. Chordwise pressure distributions. Consider first the pressure development close to the wing leading edge. Detailed flight measurements at the 58 per cent semi-span station over the first 5 per cent of the chord have been reported in Ref. 41 and a typical set of results is shown in Fig. 34. The loading develops in a markedly non-linear fashion so that $\Delta C_p/C_L$ is a function of both Mach number and lift coefficient, contrary to the predictions of supersonic wing theory for a subsonic leading edge (Ref. 57). Experimental $\Delta C_p/C_L$ tends to zero at the leading edge and has a maximum at about 1 to 2 per cent of chord. Theory predicts that $\Delta C_p/C_L$ should tend to infinity at the leading edge and then decrease monotonically. Flight results also show that, near the leading edge, higher M or higher overall C_L actually leads to lower $\Delta C_p/C_L$. It might be remarked that the C_L value used in calculating $\Delta C_p/C_L$ is appropriate to zero elevator and aileron settings, suitable corrections having been applied to account for their contributions.

Some wind-tunnel results at M = 1·3 are also shown for comparison in Fig. 34. A correction of 0·014 has been applied to C_L for the effect of uprigged aileron angle. In general the data for the 1/9 model are much less detailed because of the relatively greater spacing between pressure taps on the model than in flight. However, the non-linearity with C_L is also apparent with the tunnel results. It also seems, after some interpolation, that $\Delta C_p/C_L$ for a given M and C_L is somewhat higher in the tunnel than in flight. To examine this more closely plots of C_p *vs.* x/c for tunnel and flight can be compared at a given M and incidence. Two such plots, for M = 1·175 and M = 1·3 are shown in Figs. 34a and 34b. The tunnel results have been interpolated, where necessary, to the flight incidence and/or Mach number. The results confirm a higher loading on the models as compared with flight, over the first 5 per cent or so of chord. The differences are as much as 25 per cent and are typical for subsonic and supersonic speeds. The reasons for these differences are unclear but may be associated with differences in the relative thicknesses and state of the boundary layer near the leading edge (Sections 2.5, 3.1.3, 3.2.3, 3.3). This could be particularly important in view of the presence of separation and vortex formation, which, it has been suggested (Ref. 39), may well progress in accordance with criteria connected with the pressure reached at the leading edge. This is also consistent with differences in movement inboard of the leading edge vortices in flight and tunnel (Section 6.9.2).

Consider now the chordwise pressure distributions over the wing at 20 , 38·5, 58 and 85 per cent semi-span. As an aid to illustrate some of the main features of the pressure curves, a typical set is shown in Figs. 35a–d from flight and tunnel at closely corresponding Mach number and incidence. Some interpolation is often necessary when comparing flight and tunnel, since tests have usually been performed at different incidences, elevator settings and aileron angle. At subsonic Mach number, in particular, any change in elevator angle has an influence on pressures over the entire wing so matching of angles is very important. However, the main concern here is with supersonic speeds and the following comments result largely from comparisons of supersonic pressure distributions.

Looking at Figs. 35a–d, the greater irregularity of the flight curves is very apparent. This partly reflects the close spacing of the pressure taps in flight compared to the model so that small scale changes are not recorded on the model. Nevertheless, the model pressure distributions are markedly smoother and a great deal of interpolation would be required to force an irregular shape onto the data points. The smoother pressure distributions on the models can partly be attributed to the greater diffusive effects of the relatively thick model boundary layer (Section 3.3). In addition, the model surfaces are smooth while the aircraft has many small-scale surface irregularities, such as nominally flush rivet heads and detachable panels, which could produce small scale fluctuations in surface pressure on the aircraft.

Many of the larger scale irregularities in the flight pressure curves can be correlated with the presence of the wing fences and fairings on the aircraft wing which distort the flow patterns in their vicinity. Figures 1a and 1b show the location of the fence on the upper surface, and the undercarriage and aileron jack fairings on the lower surface.

The chordwise pressure curve for the upper wing surface at 38·5 per cent semi-span (Fig. 35c) shows the sort of perturbed distribution, between x/c = 0·05 and x/c = 0·35, which is quite consistent with the presence of the fence in that region. The wind-tunnel curve gives no hint of the large compression dips apparent in flight, but downstream of x/c = 0·35 the flight and tunnel curves are in good agreement. For the lower surface (Fig. 35c), the presence of the undercarriage fairing appears to be reflected in the pressure distribution, between x/c = 0·10 and x/c = 0·45, in both flight and tunnel. Again, the tunnel curve is clearly smoother than the flight result. It also appears from Fig. 35c that the loading on the forward part of the wing, i.e. forward of x/c = 0·30 at the 38·5 per cent station, is greater on the model. This is true also at the 58 and 85 per cent semi-span stations and is typical of all the available pressure data. Further downstream, away from the leading edge, reasonably good agreement of pressures in flight and tunnel is also typical. All these trends are also evident in Fig. 35a for the 85 per cent semi-span station near the tip where separation first appears.

The flight pressure curves for the upper surface at 58 per cent semi-span, shown in Fig. 35b, display erratic dips and rises near the leading edge which cannot be easily associated with surface irregularities in the near vicinity but seem to suggest the presence of compression and/or expansion waves. In fact for M about 1·2 and α_F about 3·5 degrees, Ref. 38 indicates an area of supersonic expansion at the leading edge, terminated by a shock and the formation of a vortex. The apex of the vortex could be close to 58 per cent semi-span for the conditions in Fig. 35b. The lower surface flight pressure distribution in Fig. 35b is also very irregular near the leading edge, while, farther back, the presence of the aileron jack fairing is probably reflected in the pressure development beyond $x/c = 0{\cdot}45$. The tunnel pressure curves are much smoother and the observations made on Figs. 35a and 35c apply in general.

Finally, Fig. 35d gives the pressure curves for the station closest to the fuselage, i.e. at 20 per cent semi-span. Unfortunately, no tunnel results are available forward of 30 per cent of the local chord, which covers the intake fairing. The presence of the intake, the wing-body junction, plus the fence on the upper surface and the undercarriage fairing on the lower surface, all in close proximity, lead to relatively complex flow patterns and this is reflected in the waviness of the pressure profiles, especially on the lower surface. Tunnel and flight are in reasonable agreement over the region $x/c = 0{\cdot}30$ to $x/c = 0{\cdot}70$. Forward of $x/c = 0{\cdot}30$, i.e. close to or on the intake fairing, the flight pressure results show large and rapid changes, probably due to shock waves. It is here that flight and tunnel may differ considerably especially as the intake mass flows are not generally the same (Section 3.4.1). Differences here would also have a relatively important effect on the moments about the centre of gravity (e.g. C_{m_0}), because of the relatively large moment arm. Whether important differences actually occur cannot be established in the absence of tunnel data.

Tunnel pressure results are also entirely lacking close to the control surface hinge lines and on the control surfaces, no doubt due to experimental difficulties. Thus, flight/tunnel comparisons are not possible in these regions, though they would clearly be of value.

6.9.4. Boattail pressures. A few measurements of pressure on the rear fuselage of the aircraft and the model were made for comparison purposes, mainly with a view to correlating drag measurements in flight and tunnel by allowing for the influence of the expanding jet, which is likely to cause separation upstream of the jet exit on the aircraft.

Available data, shown in Fig. 36, show a rapid increase in pressure towards the base of the fuselage consistent with separation and an associated shock wave near the base of the fuselage. The pressure on the model (1/9 scale) without any flow through the duct rises less steeply, as the base is approached, than with duct flow while the pressure on the aircraft, which has a highly expanding jet, shows the steepest rise. In addition, the pressure on the aircraft shows a local rise at about 4 inches (model scale), but this is probably due to the presence of the airbrakes and associated jack system, which is absent from the model. The different pressures near the rear fuselage combined with differences in geometry there (e.g. presence of jet pipe and nozzle on the aircraft, different boattail geometries on 1/9 and 1/24 model) make contributions to drag which have been examined in Ref. 23.

These few pressure results are particularly important here for the light they shed on the possible influence of the exit jet on the sideslip derivative, n_v, where large discrepancies have been shown to exist between tunnel and flight at supersonic speeds. The presence of the shock near the base on the model and aircraft, the movement of the shock as the aircraft yaws and the presence of eyelids and jet pipe on the aircraft, together with other lesser geometrical differences between models and aircraft, all add up to confirm the importance of carefully studying the effect of the expanding jet on n_v. In the absence of more quantitative data, this report must be satisfied with having established a probable explanation, consistent with the trends at supersonic speeds on the Fairey Delta 2 and on other aircraft with similar expanding jet features.

6.9.5. Integrated wing pressures. Where comparable flight and wind-tunnel pressure distributions are available, they have been integrated in order to give an indication of the total force, moment about the centre of gravity, and position of centre of pressure. In this way, some of the gross effects of the detailed differences discussed in Section 6.9.3 are brought out.

The pressure distributions have been integrated from 0 to 40 per cent chord at the 85 per cent semi-span station, from 0 to 60 per cent chord at the 58 per cent station, from 0 to 70 per cent at the 38·5 per cent station and from 30 to 70 per cent of local chord at the 20 per cent semi-span station. Thus detailed differences in pressure near the leading edge are included in the integrations except for the 20 per cent semi-span station, but contributions from or near the control surfaces are excluded in all cases. Mainly supersonic results are considered because differences in elevator angle have a major effect on the pressure distributions at subsonic speeds and in general the elevator settings are different for flight and tunnel data.

The results presented are the following integrals, plotted against α_F :

$$I_1 = \int \Delta Cp \, d\left(\frac{x}{c}\right)$$

and

$$I_2 = \int \frac{x}{c} \cdot \Delta Cp \, d\left(\frac{x}{c}\right)$$

where c is the local chord and x is measured from the centre of gravity in I_2. The ratio I_2/I_1 makes it possible to calculate the centre of pressure for a particular chordwise distribution. The results chosen for presentation here are those at M about 1·3 (Figs. 37a, b, c) and at M = 1·5 (Figs. 38a, b, c). These Mach numbers are chosen because at M = 1·3 the differences in C_{m_α} and C_{m_0} between flight and tunnel are most pronounced, while at higher M the trend is for differences to diminish so that at M = 1·5 the discrepancies are much smaller. This should hopefully be reflected in the pressure data. The incidences for trimmed level flight in both tunnel and flight at 40 000 ft and 10 000 ft are marked for reference on the figures.

Looking first at the results for M = 1·3, Fig. 37a shows I_1 *vs.* incidence. Consistent with the higher α_F to trim in supersonic flight (Section 6.3.2), the loading on the aircraft in flight is less than that on the model for a given incidence, especially at the 85 per cent station, although the agreement at the 20 per cent station is as good as may be expected because of the limited chordwise extent of integration. In fact, good agreement is obtained for all integrated values at the 20 per cent station and these results will not be considered further in the ensuing discussion.

Several points should be made about the development of loading as α_F increases. At low incidences, i.e. α_F less than about 1·3 degrees in Fig. 37a, no flight results are available; however, extrapolation of results from higher incidences implies that the way in which the loading develops at low α_F is somewhat different in flight and tunnel. As α_F increases above about 2 degrees, the loading at 85 per cent and 58 per cent semi-span develop more or less in parallel, although the flight curves are well below the equivalent wind-tunnel curves. The similar slopes, especially at 85 per cent span, imply that there is no major aeroelastic distortion occurring, i.e. twisting of the wing tips. Above about α_F = 6 degrees, the loading at 85 per cent semi-span barely increases, indicating perhaps the establishment of a dominant flow pattern such as that associated with a streamwise vortex. However, at 58 per cent and 38·5 per cent semi-span, the loading continues to increase with incidence and the flight curves actually cross those from the tunnel.

Figure 37b shows the developing moment about the centre of gravity at M = 1·3. At the 85 per cent semi-span station the moment curve reflects the load curve of Fig. 37a, with the flight values showing a smaller nose down moment at a given α_F. At 58 per cent and 38·5 per cent semi-span, there is on the other hand rather good agreement between flight and tunnel. This is because those parts of the pressure distribution which give rise to the loading differences of Fig. 37a either contribute very little to the moment due to their small moment arm about the centre of gravity (58 per cent station), or else differences on opposing sides of the centre of gravity cancel out (38·5 per cent station).

The centre of pressure locations given in Fig. 37c suggest that, at low incidences especially, the model centre of pressure is significantly forward of the equivalent flight location. The forward movement at low incidences is particularly evident on the model, while differences tend to become less marked at higher incidences. Hence differences would be greater at conditions appropriate to 10 000 ft than at 40 000 ft. One of the effects of the more forward position of the model wing centre of pressure would be to require a smaller elevator angle to trim than in flight. Alternatively, C_{m_0} at fixed η would be larger (nose up) on the model. This has already been noted in Section 6.6.5. The aerodynamic centre position, or dC_m/dC_L depends both on the centre of pressure position and the rate at which it moves as incidence increases. From the available data it is not possible to make precise quantitative statements about dC_m/dC_L but the differences in centre of pressure position and rapid changes in position on the model at lower incidences (Fig. 37c) suggest that the measured differences in dC_m, dC_L and C_{m_α} may well be due to differences in flow field development.

The results in Figs. 38a, b and c for M about 1·5 give rise to broadly similar observations but the magnitude of the differences between flight and tunnel are smaller, as was indeed expected. The largest differences in loading and centre of pressure location now occur at 38·5 per cent semi-span.

In order to check the accuracy of the integrations and the effect of possible errors in the measured pressures at the leading edge (x/c = 0), the widest possible range of leading edge pressures was used. The effect on the calculations at 38·5 per cent semi-span is indicated in Figs. 38a, b and c. The loading and the moment are only

minutely altered while the shift of centre of pressure is 5 per cent at most. These are typical values and are not large enough to affect the conclusions drawn.

It seems then that differences in flow development, due to Reynolds number differences, are an important feature, especially at low incidences and go some way towards explaining discrepancies between tunnel and flight tests at supersonic speeds. A fuller investigation would need to consider the area around the inlets, the control surfaces and fuselage as well as the wing.

At subsonic speeds, no direct comparisons between flight and tunnel pressure distributions have been made here because of differences in elevator angles. Ref. 38 has, however, noted differences in vortex development even though gross quantities such as C_{L_α}, C_{m_α} appear to agree reasonably well at subsonic speeds in flight and tunnel. This may be because, at the larger angles of incidence appropriate to subsonic flight (Fig. 11), flow differences are not as important as at low incidences where vortices are just beginning to develop. Alternatively, such differences as do occur may cancel each other out.

7. Conclusions

This report has been concerned with a detailed analysis of flight and tunnel tests on the Fairey Delta 2 and comparisons between the two. This has been done with reference to some simple theoretical estimates and to tests on other relevant aircraft where possible. The main emphasis has been on the supersonic flight regime up to M = 1·65 where relatively little comparable work exists.

Flight tests have been done at 40 000 ft over the Mach number range from about 0·7 to 1·65, and at 10 000 ft at M from 0·6 to 1·20. Tunnel tests over a Mach number range from 0·6 to 2·0 were performed on two models, one of 1/24 scale and the other of 1/9 scale.

A detailed description of the aircraft and models has been included with a view to bringing out small geometrical differences which may affect the comparison of results. In addition, attention has been paid to the boundary layer transition and growth, which do not scale on aircraft and models, and also to differences in engine mass and momentum flux, engine inlet conditions and jet exhaust effects.

The flight test techniques included analysis of steady manoeuvres, short period oscillations and Dutch roll oscillations. Possible errors involved and estimates of accuracy of the flight measurements have been summarised. The flight test techniques did not involve centre of gravity movement, nor was any attempt made to analyse initial response to control pulses in order to obtain control derivatives.

Tunnel tests on sting mounted models were able to determine all static derivatives of interest, but no dynamic derivatives were obtained. Various corrections made to the tunnel measurements and estimates of the accuracy of the measurements have been indicated where appropriate.

The main section of this report presented and analysed all flight and tunnel results where any comparisons were possible. This included lift, longitudinal trim, elevator derivatives, aileron and elevator hinge-moment derivatives and lateral sideslip derivatives. Previous comprehensive work on drag analysis has been referred to. At subsonic speeds, in general, flight and tunnel tests were in reasonable agreement and gave little cause for special concern. Thus most of the following remarks apply specifically to supersonic speeds where several important discrepancies were found between flight and tunnel tests. The main results are:

(a) Lift-curve-slope, C_{L_α}, for flight at 40 000 ft was in good agreement with tunnel values but results at 10 000 ft were about 20 per cent low at supersonic speeds. Corrections for elevator flexibility brought the 10 000 ft flight results to within 12 per cent of the rest.

(b) There were marked discrepancies between flight and tunnel C_{m_α} (and also dC_m/dC_L) at 40 000 ft and even more so at 10 000 ft with flight values being considerably smaller. Elevator flexibility corrections succeeded in bringing the 40 000 ft results to within 10 per cent of tunnel values but a substantial gap (30 per cent) remained with the 10 000 ft results.

As with flight values of C_{L_α} at 10 000 ft, there was some speculation that undetectable elevator oscillations could explain the low values, but this required a specific and unsubstantiated phase angle between elevator angle and normal acceleration. In the absence of firm evidence, other possible explanations were sought for the differences and, in particular, differences were found in the wing loading and centre of pressure position which may well be capable of explaining the low C_{m_α}.

Theoretical estimates for C_{L_α} and C_{m_α}, based on linear theory, were in agreement with experiment only for small incidences and/or high M. For M = 1·0 to 1·3 theoretical estimates were too low, and at subsonic speeds marked non-linearities due to leading edge vortices also made theory too low.

(c) The trim α_F was around 0·5 degrees greater in supersonic flight than in the tunnel, while substantial differences in elevator angle to trim remained for supersonic speeds even after elevator flexibility corrections. At 40 000 ft, differences in η_T were around 1 degree while at 10 000 ft they were about 2 degrees. The differences reflected differences in $C_{m_0}(\eta = 0)$, and because of the consistency of the trends with Reynolds number differences on the models and aircraft, an aerodynamic cause seemed likely. In fact, integrated wing pressures revealed lower wing loading and more rearward centre of pressure position in 40 000 ft flight than on the 1/9 tunnel model. Differences in rigged-up aileron angle were previously suggested as causing low flight C_{m_0} but it was shown that this could not be the case. Estimates of C_{m_0} were in poor agreement with tunnel measurements even at supersonic M.

(d) The main differences in wing pressures were near the blunt leading edge of the wing, where generally lower flight pressures suggested a more slowly developing leading edge separation and subsequent vortex formation. This was confirmed by surface tuft visualisation which showed a vortex system developing more rapidly on the model. It was perhaps also the cause of differences in the aileron hinge moment derivative b_{1A}, which not only had different values for 40 000 ft and 10 000 ft flight (attributable to non-linear vortex development at different incidences) but also had considerably larger values in the tunnel than in supersonic flight. This would be expected if the vortex developments were different in flight and tunnel. In contrast, elevator hinge-moment derivatives, corrected for flexibility, showed no sign of dependence on altitude while tunnel and flight results were also in reasonable agreement.

(e) Elevator derivatives C_{L_η}, C_{m_η} and elevator 'power' $(\Delta\eta/nC_w)_{\text{Trim}}$ all showed considerable dependence on elevator angle, especially on the models. This was an area where agreement between 1/9 and 1/24 models was not particularly good. Differences between tunnel and flight showed no trends consistent with Reynolds number changes and the large differences between 1/9 and 1/24 scale models suggested that non-linearities were mainly due to the interaction of the elevator (producing a shock wave at the hinge) and the rear fuselage. Differences in rear fuselage geometry then gave different non-linear effects. This, in particular, would affect C_{m_0} at elevator angles other than zero, and/or elevator angles to trim at high n. Both have been noted. At small elevator angles, agreement between results for elevator effectiveness in flight and from 1/9 model tests was, in general, quite good, since geometric differences were small in this case.

Theoretical estimates of C_{L_η} agree well with experiment except over the range M = 0·9 to 1·1, but estimates of $(C_{m_\eta})_\alpha$ are very low at subsonic speeds indicating errors in centre of pressure location of the elevator.

(f) Flight measurements of sideslip derivatives were subject to a fairly large scatter. The tunnel results for l_v, y_v appropriate to 40 000 ft lay within the flight scatter band, but for n_v the flight band lay far below the tunnel values. Lack of flight/tunnel agreement at supersonic speeds has been noted with many other aircraft. With the Fairey Delta 2 aerodynamic or Reynolds number effects are neither consistent nor large enough to explain the differences. Accurate assessment of rudder flexibility effect was not possible because of lack of basic data but here again trends were not entirely consistent with measured differences as M increased. Further, small differences between flight at 10 000 ft and at 40 000 ft did not support the case for a strong aeroelastic influence. An explanation which was consistent with trends as M increased and also appeared capable of providing the right magnitude, was the interaction of an expanding exit jet with the base region of the aircraft. The presence of a shock at the base was supported by a few limited pressure results while geometrical differences between model and aircraft added plausibility to the explanation. A similar effect has been noted at supersonic speeds on a rocket-powered aircraft.

In conclusion then, it seems that most of the major longitudinal discrepancies between flight and tunnel can be accounted for by properly allowing for control flexibility, combined with differences in wing flow development due to scale effects. Also, the possible effect of undetected elevator oscillations at 10 000 ft has not been ruled out. For the lateral derivative n_v, the influence of the expanding exhaust jet seems paramount. The importance of small geometrical differences near the rear fuselage emerges clearly. Also, the value of detailed flow and pressure measurements, not only on the wing but also on the fin and boattail, has been brought out. It seems particularly important to explore the interaction of an expanding exhaust jet with the rear region of a yawing aircraft.

b_{1E}	Elevator hinge-moment derivative due to incidence, $\delta C_{H_E}/\delta\alpha$
b_{2E}	Elevator hinge-moment derivative due to elevator angle, $\delta C_{H_E}/\delta\eta$
b_{3E}	Elevator hinge-moment derivative due to aileron angle, $\delta C_{H_E}/\delta\xi$
b_{1A}	Aileron hinge-moment derivative due to incidence, $\delta C_{H_A}/\delta\alpha$
b_{2A}	Aileron hinge-moment derivative due to aileron angle, $\delta C_{H_A}/\delta\xi$
b_{3A}	Aileron hinge-moment derivative due to elevator angle, $\delta C_{H_A}/\delta\eta$
b_{1R}	Rudder hinge-moment derivative due to sideslip angle, $\delta C_{H_A}/\delta\beta$
b_{2R}	Rudder hinge-moment derivative due to rudder angle, $\delta C_{H_A}/\delta\zeta$
$\bar{c}$	Aerodynamic mean chord
c_A	Mean aileron chord aft of hinge
c_E	Mean elevator chord aft of hinge
C_{H_A}	Aileron hinge-moment coefficient, $H_A/\frac{1}{2}\rho V^2 S_A c_A$
C_{H_E}	Elevator hinge-moment coefficient, $H_E/\frac{1}{2}\rho V^2 S_E c_E$
C_{H_R}	Rudder hinge-moment coefficient
C_L	Lift coefficient, lift/$\frac{1}{2}\rho V^2 S$
C_{L_α}	Lift due to incidence, $\delta C_L/\delta\alpha$
C_{L_η}	Lift due to elevator, $\delta C_L/\delta\eta$
C_{L_q}	Lift due to pitching velocity, $\delta C_L/\delta q$
C_{L_T}	Trimmed lift coefficient,
C_l	Rolling moment coefficient, $\dfrac{\text{Rolling moment}}{\rho V^2 S s}$
C_m	Pitching moment coefficient, moment/$\frac{1}{2}\rho V^2 S\bar{c}$
C_{m_0}	Pitching moment coefficient at zero lift
C_{m_η}	Pitching moment due to elevator, $\delta C_m/\delta\eta$
C_{m_α}	Pitching moment due to incidence, $\delta C_m/\delta\alpha$
C_{m_q}	Pitching moment due to pitching velocity, $\delta C_m/\delta q$
$C_{m_\alpha}/C_{L_\alpha}$	'Restoring margin' dC_m/dC_L
C_p	Pressure coefficient, $(p - p_\infty)/\frac{1}{2}\rho V^2$
ΔC_p	Difference in C_p between upper and lower wing surfaces
f	Frequency, cycles/sec.
G	Measure of rudder flexibility (*see* Section 6.8.2)
H_M	Manoeuvre margin
H_A	Aileron hinge moment
H_E	Elevator hinge moment
i_B	Non-dimensional moment of inertia in pitch = Inertia in pitch/$W\bar{c}^2$
J	Non-dimensional frequency of short period oscillation, frequency $x\hat{t}$ (rads/sec.)
L	Rolling moment

l_p	Rolling moment due to rolling velocity $(\delta L/S_p)/eVSs^2$
l_v	Rolling moment due to sideslip, $(\delta L/\delta\beta)/\rho V^2 Ss$
l_r	Rolling moment due to yawing velocity, $(\delta L/\delta r)/\rho VSs^2$
l_ζ	Rolling moment due to rudder, $L_\zeta/\rho V^2 Ss$
l_ξ	Rolling moment due to aileron, $L_\xi/\rho V^2 Ss$
m	Mass of aircraft
M	Mach number
M_a	Ambient Mach number (at jet exit)
m_q	Damping in pitch derivatives, $(V/\bar{c})\delta C_m/\delta q$
$m_{\dot{w}}$	Pitching moment derivative due to $\dot{w}$, $(V/\bar{c})\partial C_m/\partial\dot{\alpha}$
$m_{\dot{\theta}}$	Full rotary damping derivative $= m_q + m_{\dot{w}}$
N	Yawing moment
n	Normal acceleration, g units
n_r	Yawing moment due to yawing velocity derivative, $N_r/\rho VSs^2$
n_v	Yawing moment due to sideslip derivative, $N_\beta/\rho V^2 Ss$
n_ζ	Yawing moment due to rudder derivative, $N_\zeta/\rho V^2 Ss$
p	Static pressure, rolling velocity (rads/sec)
P_0	Total pressure
p_∞	Free-stream static pressure
p_j	Static pressure at exit jet
p_a	Ambient pressure (at jet exit)
$\dot{p}$	Time rate of change of rolling velocity
q	Pitching velocity (rads/sec)
Q	Mass flow rate/sec.
$\dot{q}$	Time rate of change of pitching velocity
r	Yawing velocity
R	Non-dimensional damping of short period oscillation, damping $\times\, \hat{t}$
Re_x	Reynolds number based on x, $\rho Vx/\mu$
s	Wing semi-span
S	Gross wing area
S_A	Aileron area
S_E	Elevator area
$\hat{t}$	Aerodynamic time $= m/\rho VS$
T_0	Total temperature
V	Velocity
W	Weight of aircraft $= mg$
x	Chordwise distance, measured from leading edge

LIST OF SYMBOLS (continued)

Y	Sideforce
y_p	Sideforce due to rolling velocity derivative, $Y_p/\rho VSs$
y_r	Sideforce due to yawing velocity derivative, $Y_r/\rho VSs$
y_v	Sideforce due to sideslip derivative, $Y_\beta/\rho V^2 S$
y_ζ	Sideforce due to rudder derivative, $Y_\zeta/\rho V^2 S$
y_ξ	Sideforce due to aileron derivative, $Y_\xi/\rho V^2 S$
z_q	Lift due to pitching velocity derivative, $-(V/\bar{c})C_{L_q}$
α	Incidence
$\dot{\alpha}$	Time rate of change of incidence
α_F	Incidence of fuselage datum line
β	Sideslip angle
δ	Boundary layer thickness
δ^*	Boundary layer displacement thickness
Δ	Small increment
ζ	Rudder angle
η	Elevator angle, +ve trailing edge down
η	Elevator angle to trim
μ	Coefficient of viscosity
μ_1	Relative aircraft density $= 2m/\rho S\bar{c}$
ξ	Aileron angle; also damping factor $= R/2\pi f\hat{t}$
ρ	Density
ϕ	Phase angle between pitching velocity and normal acceleration in short period oscillation.
$\phi_{\eta n}$	Phase angle by which elevator angle leads normal acceleration.

REFERENCES

No.	*Author(s)*	*Title, etc.*
1	R. L. Lickley and L. P. Twiss ..	The Fairey Delta 2. *J. R. Ae. Soc.*, Vol. 61, No. 559, July 1957.
2	R. L. Lickley and L. P. Twiss ..	F.D.2 Faireys Delta 2—Over 1000 m.p.h. on Rolls-Royce power. *Flight*, 25th April, (1958).
3	T. A. Holbeche	A preliminary data report on ground pressure disturbances produced by the Fairey Delta 2 in level supersonic flight. A.R.C. R. & M. No. 3296 (1958).
4	T. A. Holbeche	B.A.C. 221 slender-delta research aircraft. *Flight*, Vol. 86, No. 2889, 23rd July, 1964.
5	A. Spence and D. Lean	Some low-speed problems of high-speed aircraft. A.G.A.R.D. Rept. 357, April 1961.
6	W. G. A. Port and J. C. Morrall	Low-speed tests on a tailless delta wing aircraft (Avro 707B). A.R.C. C.P. No. 1105 (1967).
7	P. L. Bisgood	Results of flight tests on a slender wing low speed research aircraft (H.P. 115). A.G.A.R.D. Rept. No. 535, May 1966.
8	K. J. Staples	Flight tests on the short S.B.5 with 60° sweepback and low tailplane. A.R.C. R. & M. No. 3558 (1967).
9	F. J. Drinkwater III and L. S. Rolls	Flight experience with the Ogee wing at low speeds. A.G.A.R.D. Rept. 538, May 1966.
10	C. S. Barnes and O. P. Nicholas ..	Preliminary flight assessment of low speed handling of the B.A.C. 221 Ogee-wing research aircraft. A.R.C. C.P. 1102 (1967).
11	D. E. Shaw	Some comparisons of wind tunnel measurements and flight test data. B.A.C. Report Ae. 207, March 1967.
12	R. B. Yancey, H. A. Rediess and G. H. Robinson	Aerodynamic-derivative characteristics of the X-15 airplane as determined from flight tests for M from 0·6 to 3·4. N.A.S.A. TN D-1060, 1962.
13	C. H. Wolowicz, L. R. Strutz, G. B. Gilyard and N. W. Matheny	Preliminary flight evaluation of the stability and control derivatives and dynamic characteristics of the unaugmented XB-70-1 airplane including comparisons with predictions. NASA TN D-4578, May 1968.
14	C. S. Barnes and A. A. Woodfield	Measurements of the moments and products of inertia of the F.D.2 aircraft. A.R.C. R. & M. No. 3620 (1968).

REFERENCES

No.	Author(s)	Title, etc.
15	R. Rose, C. S. Barnes and A. A. Woodfield	Flight measurements of lift, longitudinal trim and drag of the Fairey Delta 2 at M up to 1·65 and comparison with wind tunnel results. A.R.C. R. & M. No. 3577 (1967).
16	D. Kuchemann	Types of flow on swept wings. *J. Ae. Soc.*, Vol. 57, No. 515 (Nov. 1953).
17	C. W. Harper and R. L. Maki ..	A review of the stall characteristics of swept wings. NASA TN D-2373 (July 1964).
18	D. R. Andrews	Measurements in flight of the longitudinal stability derivatives of a 60° delta wing aircraft (F.D.2). A.R.C. C.P. No. 639 (1959).
19	R. Rose	Flight measurements of the Dutch roll characteristics of a 60° delta wing aircraft (F.D.2) at M from 0·4 to 1·5 with stability derivatives extracted by vector analysis. A.R.C. C.P. No. 653 (1961).
20	F. W. Dee	Investigation of the position of boundary layer transition on the fin of the F.D.2. Unpublished M.O.D. (P.E.) material.
21	E. W. E. Rogers and I. M. Hall ..	An investigation at transonic speeds of the performance of various distributed roughness bands used to cause boundary layer transition near the leading edge of a cropped delta half-wing. A.R.C. C.P. 481 (1959).
22	M. D. Dobson	Wind tunnel tests at supersonic speeds on a model of the Fairey Delta 2. A.R.C. C.P. No. 672 (1962).
23	T. A. Cook and R. Hayward ..	Force and moment measurements on a 1/9 scale model F.D.2 aircraft. R.A.E. T.R. 68294, A.R.C. 31 236 (1968).
24	P. G. Hutton and D. Morton ..	Results of pressure plotting and control hinge moment tests on 1/9 scale model of F.D.2 in the A.R.A. transonic tunnel. A.R.A. Model Test Note J.12/1, May 1961.
25	D. Morton..	Force and moment tests on a 1/9 scale model F.D.2 aircraft. A.R.A. Model Test Note M.6/2, Nov. 1964.
26	H. Schlichting	*Boundary Layer Theory.* McGraw-Hill Co. Inc., 40th Edition, 1960.
27	A. A. Woodfield, Ann Cromin and Glynis Vorley	Measurements of the performance of a turbo-jet engine with reheat (R-R RA28R Avon) in high speed flight and under simulated conditions in test beds. A.R.C. R. & M. No. 3538 (1966).

REFERENCES

No.	Author(s)	Title, etc.
28	G. Lee	An investigation of transonic flow fields surrounding hot and cold sonic jets. NASA TN D-853, April 1961.
29	R. Rose, O. P. Nicholas and Glynis Vorley	Flight measurements of the elevator and aileron hinge moment derivatives of the F.D.2 aircraft up to a Mach number of 1·6, and comparisons with wind tunnel results. A.R.C. R. & M. No. 3485 (1965).
30	R. Rose	Flight measurement of the low speed drag in the approach configuration of a 60° delta wing research aircraft (Fairey E.R. 103). R.A.E. T.N. Aero 2599, A.R.C. 21 183 (1959).
31	F. W. Dee and D. C. Mabey ..	Wind tunnel calibration of incidence vanes for use on the Fairey E.R. 103. R.A.E. T.N. 2785, A.R.C. 23 611 (1961). *J. R. Ae. Soc.*, Vol. 67, No. 628, D 267 (April 1963).
32	S. Neumark	Analysis of short period longitudinal oscillations of an aircraft: Interpretation of flight tests. A.R.C. R. & M. No. 2940 (1952).
33	C. H. Wolowicz and E. C. Holleman	Stability-derivative determination from flight data. A.G.A.R.D. Rept. 224, Oct. 1958.
34	W. E. A. Acum	Aerodynamic forces on a rectangular wing oscillating in a supersonic air stream. A.R.C. R. & M. No. 2763 (1950).
35	F. W. Dee	Flight measurements at subsonic speeds of the aileron rolling power and lateral stability derivatives l_v and y_v on a 60° delta wing aircraft. A.R.C. C.P. 739 (1963).
36	D. J. Kettle	8 ft × 6 ft transonic tunnel tests on 1/24 scale model of the F.D.2 (E.R. 103). A.R.C. C.P. 656 (1962).
37	H. H. B. M. Thomas and S. Neumark	Interim note on stability and response characteristics of supersonic aircraft (linear theory). R.A.E. T.N. Aero 2412, A.R.C. 18 263 (1955).
38	F. W. Dee and O. P. Nicholas ..	Flight determination of the wing flow patterns and buffet boundaries for the F.D.2 aircraft at M between 0·4 and 1·3, and comparisons with wind tunnel results. A.R.C. R. & M. No. 3482.
39	E. W. E. Rogers, I. M. Hall and C. J. Berry	An investigation of the flow about a plane half-wing of cropped-delta planform and 6 per cent symmetrical section at stream M between 0·8 and 1·41. A.R.C. R. & M. No. 3286 (1960).

REFERENCES

No.	Author(s)	Title, etc.
40	E. P. Sutton	Some observations of the flow over a delta-winged model with 55° leading edge sweep at Mach nos. between 0·4 and 1·8. A.R.C. R. & M. No. 3190 (1955).
41	J. S. Roper	The F.D.2—Measurement of leading edge pressures in supersonic flight. Fairey Aviation Co. Ltd., Aerodynamic Dept., Rept. V.1., April 1958.
42	O. P. Nicholas and F. W. Dee ..	Flight measurements of the wing pressure distribution of the F.D.2 aircraft at M up to 1·7. R.A.E. T.R. (To be issued). Unpublished M.O.D. (P.E.) material.
43	R. Rose, F. W. Dee and A. E. Acethorpe	The test bed calibration of an Avon RA28 engine under both non-reheat and reheat conditions with comparison of thrust measurements by a swinging probe and various conventional methods. A.R.C. C.P. No. 729 (1962).
44	J. E. Nethaway and O. P. Nicholas	Measurements of aerodynamic heating on the nose of a delta aircraft at speeds up to M = 1·65. A.R.C. R. & M. No. 3280 (1960).
45	D. R. B. Webb, A. R. Keeler and G. R. Allen	Surface pressures and structural strains resulting from fluctuations in the turbulent boundary layer of a Fairey Delta 2 aircraft. A.R.C. C.P. No. 638 (1962).
46	P. F. Ashwood	Flight tests of N.G.T.E. ventilated propelling nozzle using Fairey E.R. 103 aircraft. Unpublished M.O.D. (P.E.) material.
47	T. H. Kerr	A preliminary review of the low level supersonic tests on the Fairey E.R. 103. R.E.A. T.N. Aero 2565 (1958). A.R.C. 20 797.
48	G. F. Moss and R. W. Hayward	Wind tunnel measurements of aileron and elevator hinge moments on a 1/9 scale model of the F.D.2. Unpublished M.O.D. (P.E.) material.
49	R. W. Hayward	Pressure measurements on a 1/9 scale model of the F.D.2. Unpublished M.O.D. (P.E.) material.
50	K. J. Turner	Free flight model measurements of the zero lift drag, longitudinal stability and rolling characteristics of a supersonic research aircraft (E.R. 103) over the Mach number range 0·4–1·4. R.A.E. Rept. 2615, A.R.C. 21 062 (1959).
51	M. M. Shaw and R. Rose ..	Wing flow measurements of lift and pitching moment at transonic speeds on a 60° Delta (E.R. 103). R.A.E. Tech. Memo. Aero 323.

REFERENCES

No.	*Author(s)*	*Title, etc.*
52	R. Rose	Wing flow measurements of the damping in pitch and stiffness deviations of a 60° delta wing-body combination. R.A.E. Tech. Note Aero 2480, A.R.C. 20 035 (1957).
53	W. B. McCarter	Longitudinal stability characteristics and damping in pitch of delta wings. College of Aeronautics Note No. 11, A.R.C. 18 131 (1954).
54	W. D. Manison, Jr.	Model F-101 flight test data summary analysis and comparison with estimates. McDonnell Aircraft Corp. Rept. 5018, Serial No. 19, 2nd Feb., 1957.
55	G. J. Hancock	Aerodynamic loading induced on a two-dimensional wing by a free vortex in incompressible flow. *Aeronautical Journal*, Vol. 75, No. 726, June 1971.
55	I. McGregor	Wind tunnel investigation at transonic and supersonic speeds of the static lateral stability of a 60° swept wing fighter aircraft (English Electric P.1A). R.A.E. T.N. Aero 2567, A.R.C. 23 254, April 1961.
56	H. Ashley and M. T. Landahl ..	*Aerodynamics of Wings and Bodies* Addison-Wesley (1965).

TABLE 1

Leading Particulars of Aircraft

Wing	
Gross area	360 ft^2
Span	26·83 ft
Aspect ratio	2
Centre line chord (nominal)	25 ft
Tip chord	1·83 ft
Mean aerodynamic chord	16·75 ft
Wing section	4% Symmetrical, maximum t/c at 29·5%C
Leading edge sweep	59·9°
Trailing edge sweep	0°
L.e. radius/local chord (nominal)	0·00189
Twist	0°
Dihedral	0°
Setting to fuselage datum	+1·5°
Elevators	
Net area (each)	20·22 ft^2
Angular movement	20° Down, 33° Up
Mean chord	3·69 ft
Sweep of hinge line	9·7°
Ailerons	
Net area (each)	16·01 ft^2
Angular movement	±25°
Mean chord	2·70 ft
Weights	
A.U.W. at take off	14 109 lb
Fuel content	2464 lb
Mean weight at test conditions	12 800 lb
Mean C.G. position at test, undercarriage up	163·1″ aft of l.e. of C_L ch. = 0·544 C_L chord = 0·317 $\bar{c}$
Variation of C.G. position due to fuel usage	±0·5 inches
Moments and products of inertia	*See* Ref. 14

TABLE 2

Model Jet Pressure Ratio Assuming Choked Exit Flow

M_a	p_a/p_0	p_j/p_a
1·1	0·468	1·12
1·2	0·412	1·27
1·3	0·361	1·46
1·4	0·314	1·67
1·5	0·272	1·94
1·6	0·235	2·24
1·7	0·203	2·60

TABLE 3

Jet Exit Pressure Ratio on Aircraft

	Non-Reheat		Reheat	
Ma	(p_j/p_a)40 000 ft	(p_j/p_a)10 000 ft	(p_j/p_a)40 000 ft	(p_j/p_a)10 000 ft
0·9	2·08	1·72	2·10	1·68
1·0	2·20	1·84	2·31	1·82
1·2	2·61	2·14	2·65	2·10
1·4	3·20	2·49	3·22	2·52
1·6	3·56	2·61	3·57	2·66

TABLE 4

	Ref. 15	Ref. 29	Ref. 18	Ref. 19	Ref. 35
M	0·55–1·15 (10 000 ft) 0·7–1·65 (40 000 ft)	0·55–1·2 (10 000 ft) 0·85–1·6 (40 000 ft)	0·5–1·15 (10 000 ft) 0·65–1·6 (38 000 ft)	0·4–1·0 (10 000 ft) 0·7–1·5 (40 000 ft)	0·3–0·35 (20 000 ft) 0·6–0·85 (40 000 ft)
Altitude/$Re_{\bar{c}}$	$4{\cdot}3 \times 10^7$ at M = 1·35 $1{\cdot}9 \times 10^7$ at M = 0·6 (40 000 ft) $5{\cdot}4 \times 10^7$ at M = 0·6 (10 000 ft)	As in Ref. 15	As in Ref. 15	As in Ref. 15	As in Ref. 15
$\alpha_F/C_L/n$	α_F less than 10° n less than 4 (turns)	$\alpha_F = -1°$ to 5° (Short period oscills. and turns)	$\alpha_F = -0{\cdot}5°$ to 2° (10 000 ft) $\alpha_F = 1°$ to 6° (40 000 ft) (S.P. oscills.)	$n = 1$ (10 000 ft, 40 000 ft) $n = 2$ (40 000 ft) (Dutch roll oscills.)	$n = 1$ (30 000 ft, 40 000 ft) (Sideslips)
Aileron rigged-up angle	3·2° nom. to 3·8/4·2° in flight (t.e. up)	As in Ref. 15	—	—	As in Ref. 15
Moment Ref.	C.G. at 0·544 ℄ Chord ±0·3%	As in Ref. 15	As in Ref. 15	As in Ref. 15	As in Ref. 15
η range	$\eta_T = 0$ to $-15°$	$\eta_T = 1°$ to $-7°$	$\eta_T = -0{\cdot}6°$ to $-1{\cdot}65°$ (10 000 ft) $\eta_T = 0$ to $-3{\cdot}3°$ (40 000 ft)	$\eta_T = -0{\cdot}6°$ to $-1{\cdot}65°$ (10 000 ft) $\eta_T = 0$ to $-3{\cdot}3°$ (40 000 ft)	Sideslip trim
β range	–	–	–	Typically $-2° \leqslant \beta \leqslant 2°$ (Dutch roll)	$\beta = \pm 5°$
ξ range	Turns	$\xi = 2°$ to $-8°$ (w.r.t. wing plane)	–	–	$\xi = 0$ to $-10°$ (w.r.t. wing plane)
ζ range	Turns	Turns	–	–	$\zeta = \pm 6°$
Results	Lift, drag, longitudinal trim	$b_{1A}, b_{2A}, b_{3A}, b_{1E}, b_{2E}, b_{3E}$	$C_{L_\alpha}, H_M, m_w, m_{\dot{w}}, (m_\eta)c_L$	n_v, y_v, l_v, n_r, l_p	l_v, y_v, l_ζ

TABLE 4 (Continued)

	Ref. 38	Ref. 41	Ref. 42	Ref. 20
M	M = 0·40–1·3	M = 0·57–1·53	M = 0·5–1·6	M = 1·0–1·5
Altitude/$Re_{\bar{c}}$	35 000 ft to 40 000 ft $Re_{\bar{c}}$ = 1·6 to 4·5 × 10^7	5000 ft to 50 000 ft	10 000 ft and 40 000 ft (M = 0·5) 40 000 ft (M = 0·85 to 1·6)	40 000 ft
$\alpha_F/C_L/n$	n = 1 to 3	α_F = 0·5 to 6·7° n = 0·9 to 3·75 (max)	α_F = 1·9 to 6·3° (M = 0·5) α_F = 1° to 8° (M = 0·85 to 1·6) n = 1 to 3·7	Level trimmed flight
Aileron rigged-up angle	3·2° nom. up to 3·8/4·2° in flight (t.e. up)	As in Ref. 38	As in Ref. 38	–
η range	η_T = 0·9° to 12·4° (turns)	η_T = 0 to −15° (turns and pull-ups)	η_T = −1° to −15°	Level trimmed flight
ξ range	Turns	Turns	Turns	—
ζ range	Turns	Turns	Turns	—
Results	Tuft visualisation Wing pressures Buffet onset	Leading edge pressures at 58% Semi-span	Wing pressures including pressures on Elevators and Ailerons	Position of B.L. Transition on fin

TABLE 5

	Ref. 22	Ref. 23	Ref. 25	Ref. 36	Ref. 38	Ref. 24	Ref. 49
Model	1/24 Scale	1/9 Scale	1/9 Scale	1/24 Scale	1/9 Scale	1/9 Scale	1/9 Scale
Tunnel	3 ft × 3 ft Bedford	8 ft × 8 ft Bedford	8 ft × 9 ft ARA	8 ft × 6 ft Farnborough	8 ft × 8 ft Bedford	9 ft × 8 ft ARA	8 ft × 8 ft Bedford
M	1·42 to 2·00	0·60, 0·85, 1·35, 1·50, 1·65, 1·80	0·85 to 1·35	0·85 to 1·25	0·5, 0·9, 1·3, 1·5, 1·8	0·7 to 1·30	0·5, 0·7, 0·9, 1·3, 1·5, 1·8, 2·0
Re_c	$1·9 \times 10^6$ at M = 1·42 $2·7 \times 10^6$ at other M	$7·4 \times 10^6$ (2×10^6 to 2×10^7 for drag measurements)	$6·8 \times 10^6$ at M = 0·7 to 8×10^6 at M = 1·4	$1·48 \times 10^6$	$1·3 \times 10^7$ at M < 1 $8·4 \times 10^6$ at M > 1	As in Ref. 23	As in Ref. 23
α_F/C_L	$\alpha_F = -2°$ to 18° (M = 1·42) $\alpha_F = -2°$ to 14° (other M) $C_L = -0·1$ to 0·5	$\alpha_F = -3°$ to 8° $C_L = -0·2$ to 0·35	$\alpha_F = 0°$ to 10° $C_L = 0$ to 0·5	$\alpha_F = -2·5°$ to 13·5° $C_L = -0·2$ to 0·8	$\alpha_F = 5·1°$ to 16·1° (M = 0·5) $\alpha_F = 3°$ to 8° (M = 0·9, 1·3) $\alpha_F = 0$ to 6° (M = 1·5, 1·8)	$\alpha_F = -2°$ to 10°	$\alpha_F = 0$ to 20° max.
Aileron rigged-up angle	3° t.e. up	2·9° t.e. up except for drag tests	2·93° t.e. up	3° t.e. up	2·9° t.e. up	2·93° t.e. up	2.9° t.e. up
Moment Ref.	0·544℄ chord	As in Ref. 22	As in Ref. 22	As in Ref. 22	As in Ref. 22	As in Ref. 22	As in Ref. 22
Elevator settings	0°, −4°, −10°	0°, 2·4° M < 1 0°, −4·8°, −9·8°, −14·8° $M > 1$	0°, −2·4°, −4·8°, −9·8°, −14·8°	0°, −4°	−2·5°	0°, −5°, −10°	−2·47° to −15·15°

TABLE 5 (Continued)

	Ref. 22	Ref. 23	Ref. 25	Ref. 36	Ref. 38	Ref. 24	Ref. 49
Model	1/24 Scale	1/9 Scale	1/9 Scale	1/24 Scale	1/9 Scale	1/8 Scale	1/9 Scale
β range	$-2°$ to $+8°$	$-2° \leqslant \beta \leqslant +2°$	$-1°$ to $3°$	$\pm 1°$, $\pm 3°$	—	—	—
ξ range	$0°$, $\pm 5°$ w.r.t. rigged-up angle	$\pm 9{\cdot}7°$ w.r.t. wing plane	$\pm 2°$, $\pm 4{\cdot}8°$ w.r.t. wing plane	$-2°$ port, $-8°$ starb. w.r.t. wing plane	—	—	—
ζ range	—	$0°$, $3{\cdot}2°$, $6{\cdot}6°$	$0°$, $1{\cdot}3°$, $3{\cdot}2°$	$0°$, $\pm 3°$	—	—	—
Results presented	Lift, drag, trim, y_v, l_v, n_v, y_ξ, l_ξ, n_ξ	Lift, drag, trim, y_v, l_v, n_v, l_ξ, n_ξ, y_ζ, l_ζ, n_ζ,	Lift, drag, trim, y_v, l_v, n_v, l_ξ, n_ξ, l_ζ, n_ζ	Lift, drag, trim, y_v, l_v, n_v, y_ξ, l_ξ, n_ξ, y_ζ, l_ζ, n_ζ	Surface tuft observations	Wing pressure hinge moments	Wing pressure measurements

TABLE 6

Quantities Measured in Flight and/or Wind Tunnel

Quantity	Flight reference	Wind tunnel reference
Lift	15, 18	22, 23, 25, 36
η_T	15	22, 23, 25, 36
$\Delta\eta/nC_w$	15, 18	22, 23, 25, 36
C_{m_α}, dC_m/dC_L, H_M	15, 18	22, 23, 25, 36
C_{m_η}	15, 18 (derived)	22, 23, 25, 36
C_{L_η}	15 (derived)	22, 23
b_{1E}	29	24, 48
b_{2E}	29	24, 48
b_{3E}	29	—
b_{1A}	29	24, 48
b_{2A}	29	—
b_{3A}	29	24, 48
C_{m_0}	Derived from 15, 18	22, 23, 25, 36
Drag	15	23, 25, 36
n_v	19	22, 23, 25, 36
y_v	19, 35	22, 23, 25, 36
l_v	19, 35	22, 23, 25, 36
$m_{\dot\theta}$	18	—
l_p	19	—
n_r	19	—
n_ξ	—	22, 23, 25, 36
y_ξ	—	22, 36
l_ξ	35	22, 23, 25, 36
n_ζ	—	23, 25, 36
y_ζ	—	23, 36
l_ζ	—	23, 25, 36

TABLE 7

Corrections to n_v

M	Correction
0·7	0·0035
0·8	0·0039
0·9	0·021
1·0	0·024
1·1	0·0235
1·2	0·022
1·3	0·018
1·4	0·016
1·5	0·0155
1·6	0·014

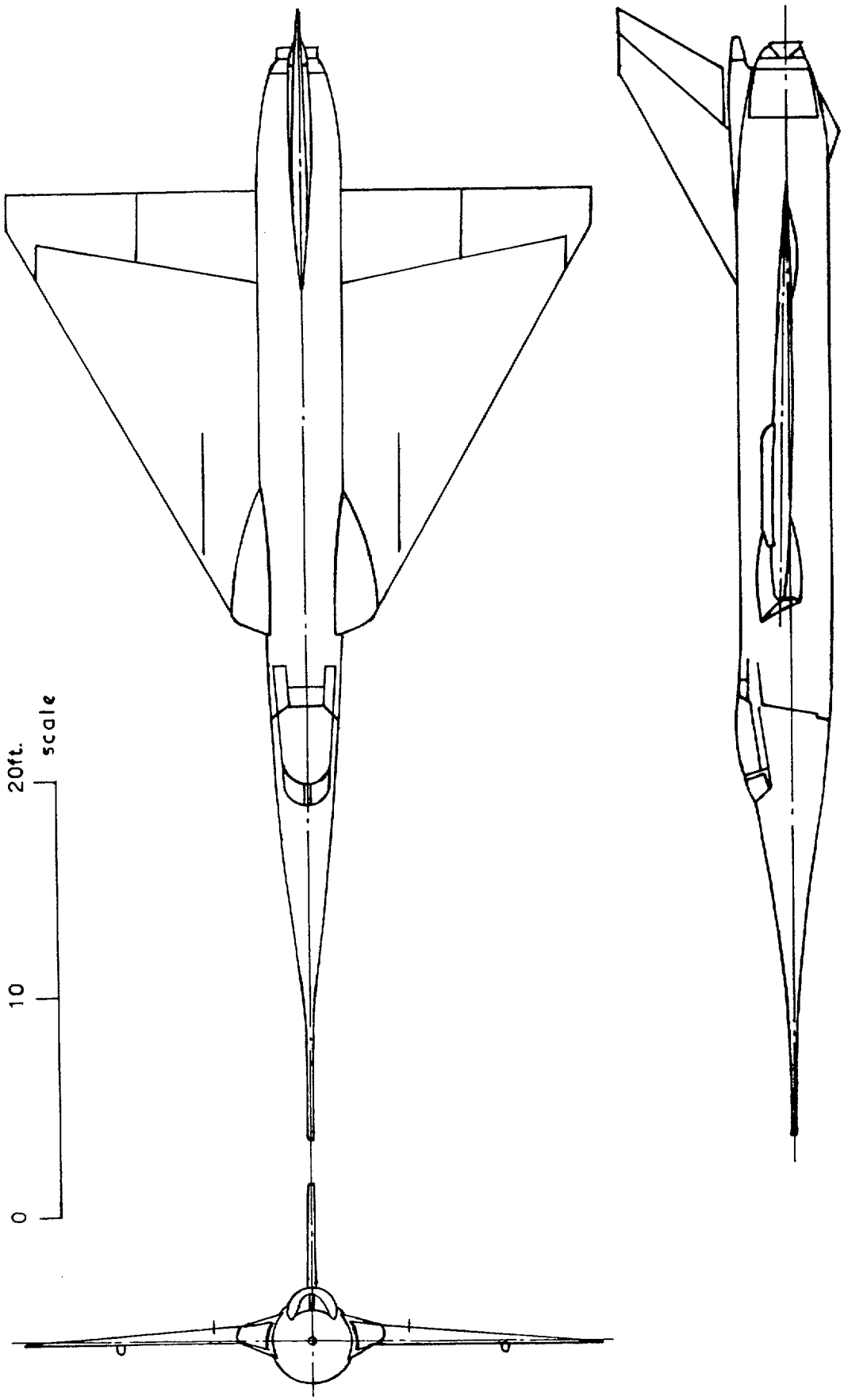

FIG. 1. General arrangement of the Fairey Delta 2.

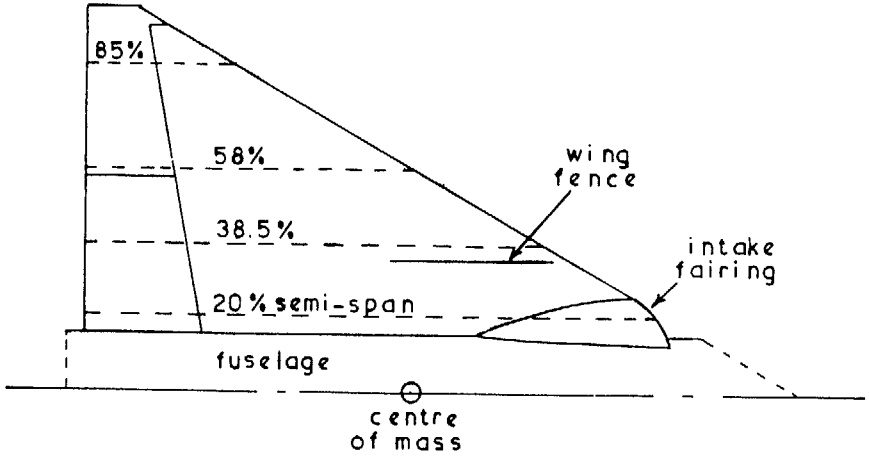

FIG. 1a. Upper wing surface.

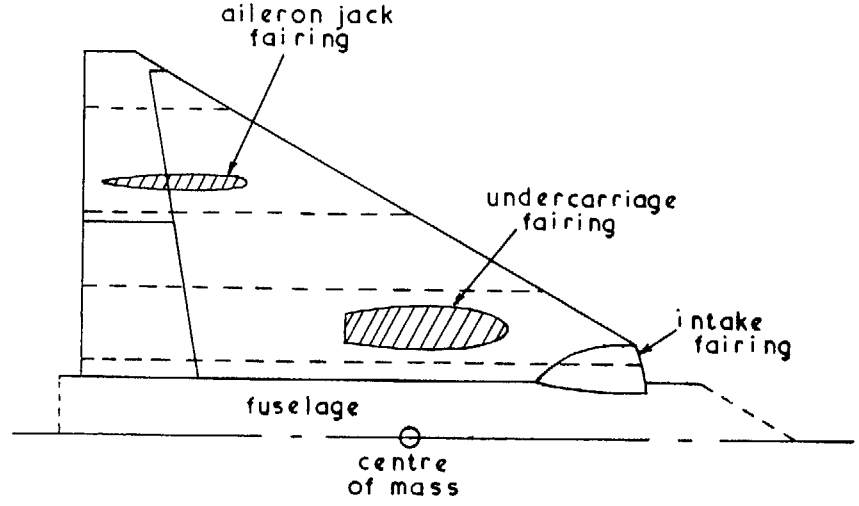

FIG. 1b. Lower wing surface

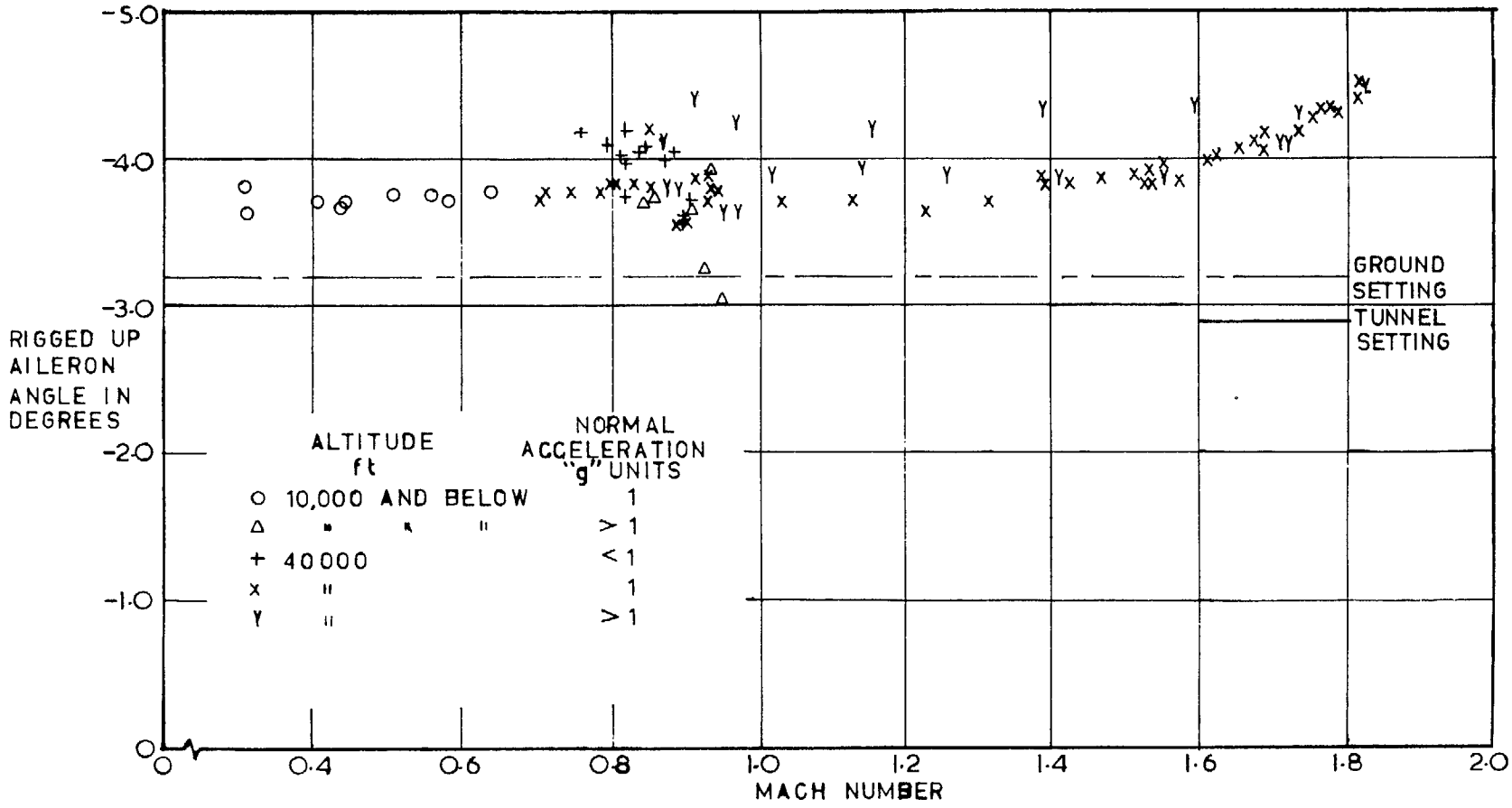

FIG. 2. Measured aileron rigged-up angle in flight.

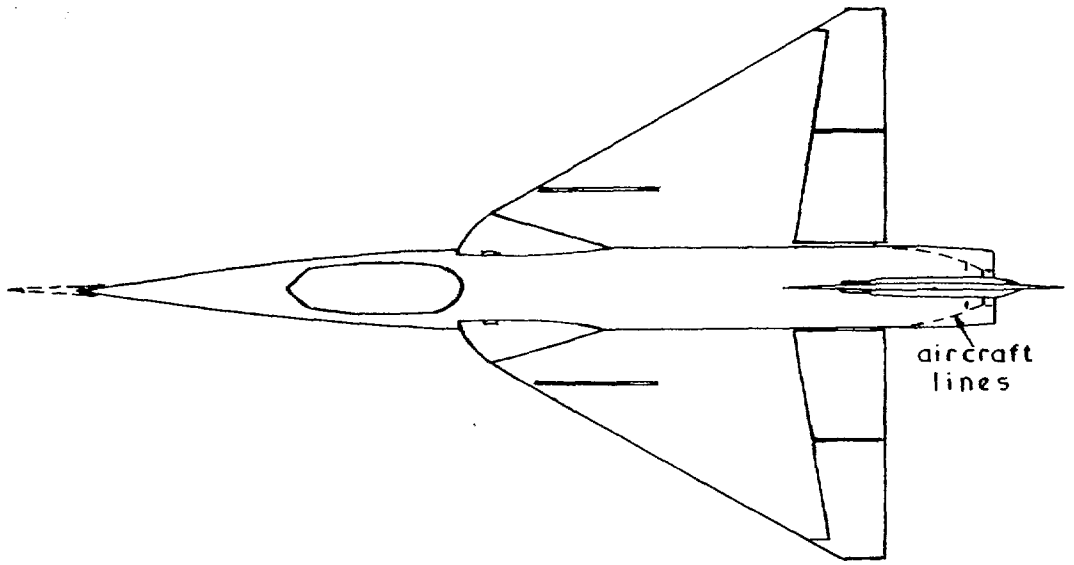

FIG. 3a. Plan view of distorted nose and rear fuselage on 1/24 model.

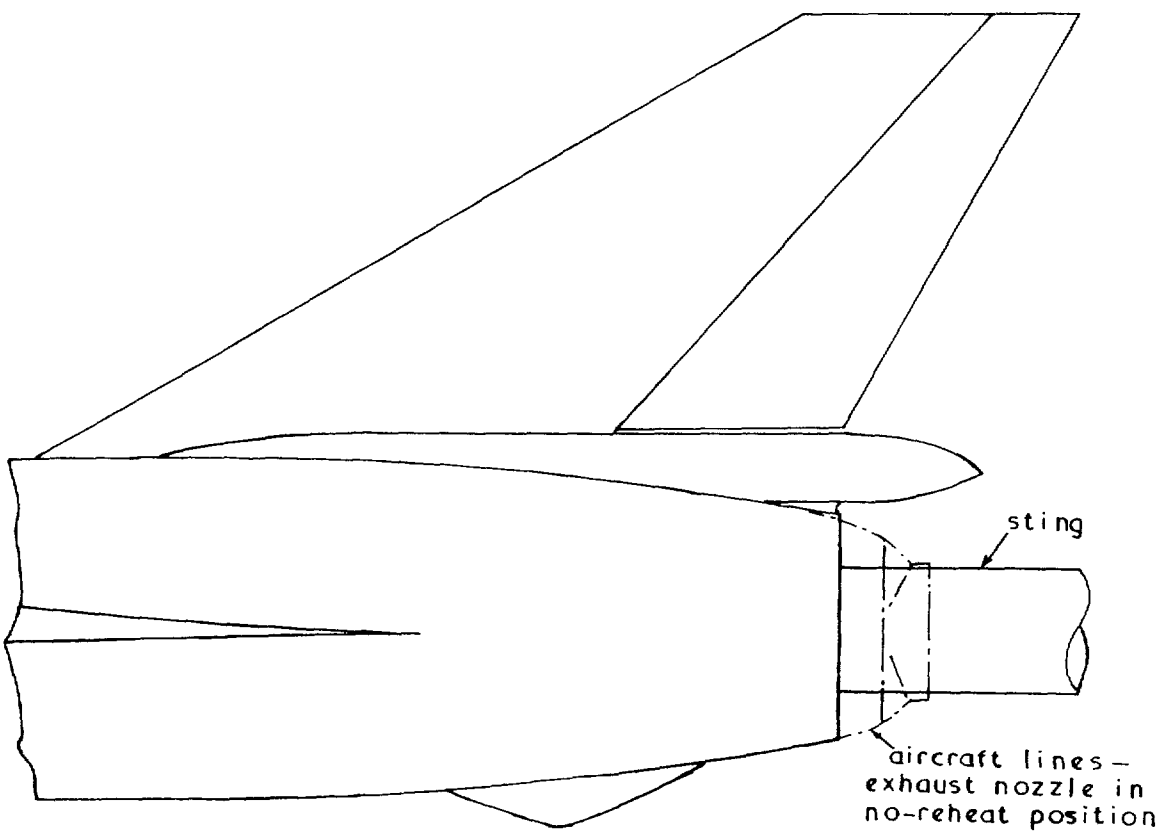

FIG. 3b. Distortion of rear fuselage on 1/9 model.

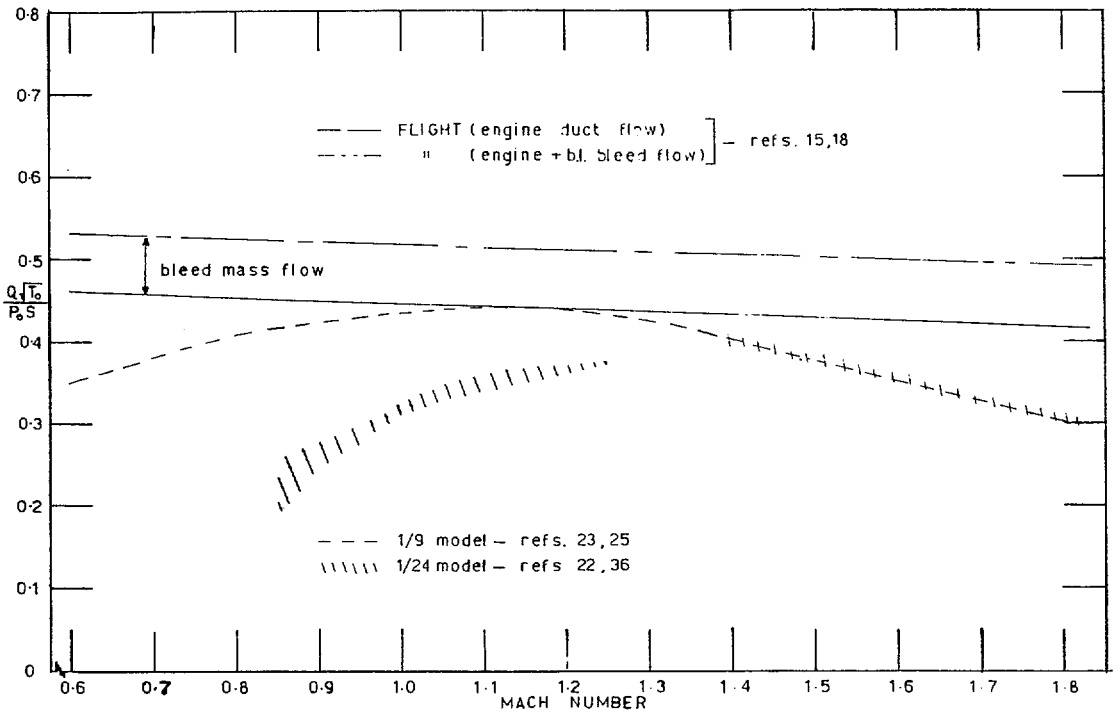

FIG. 4. Intake mass flow.

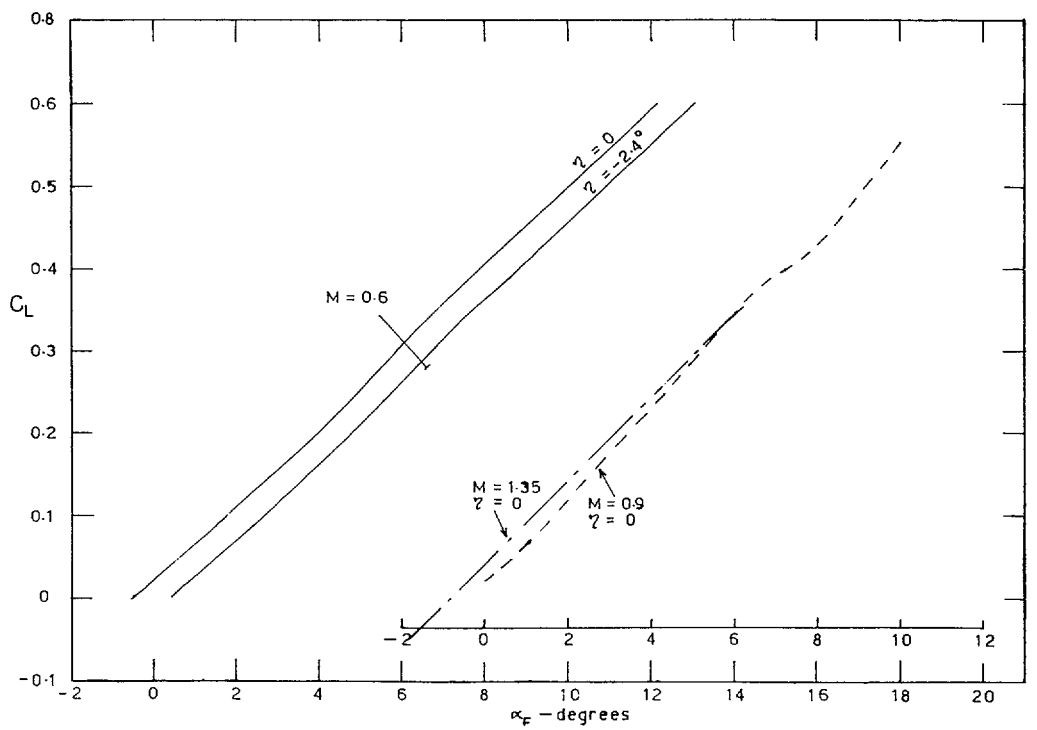

FIG. 5. Variation of lift with incidence.

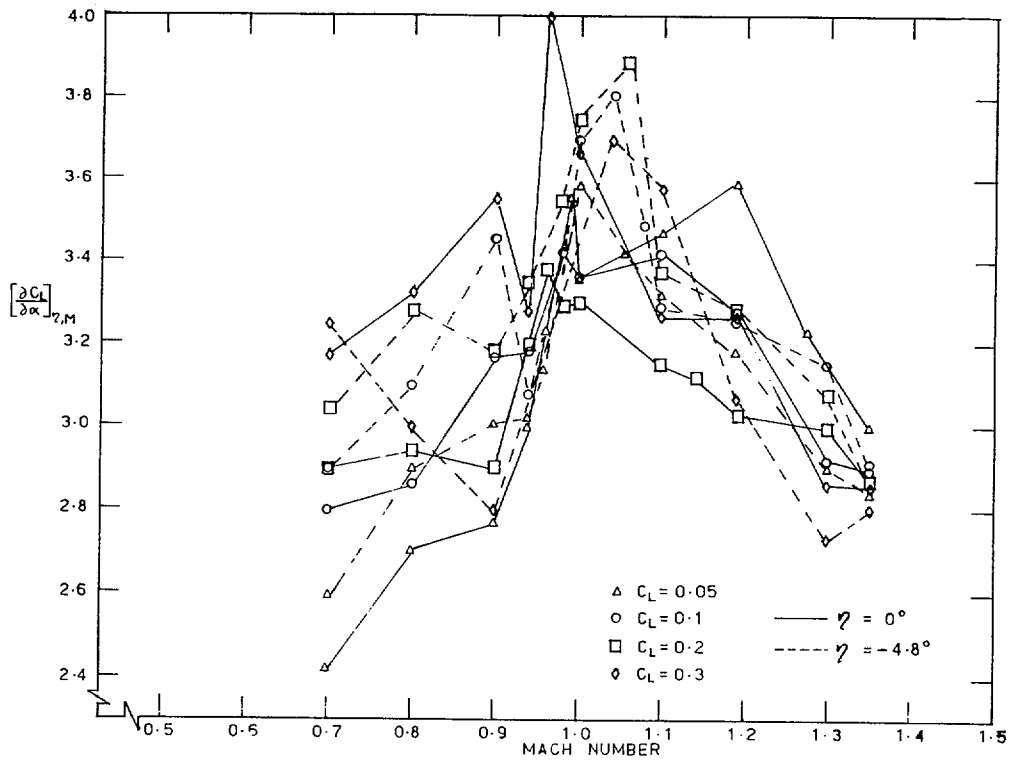

FIG. 6. Variation of lift curve slope with C_L and/or elevator setting.

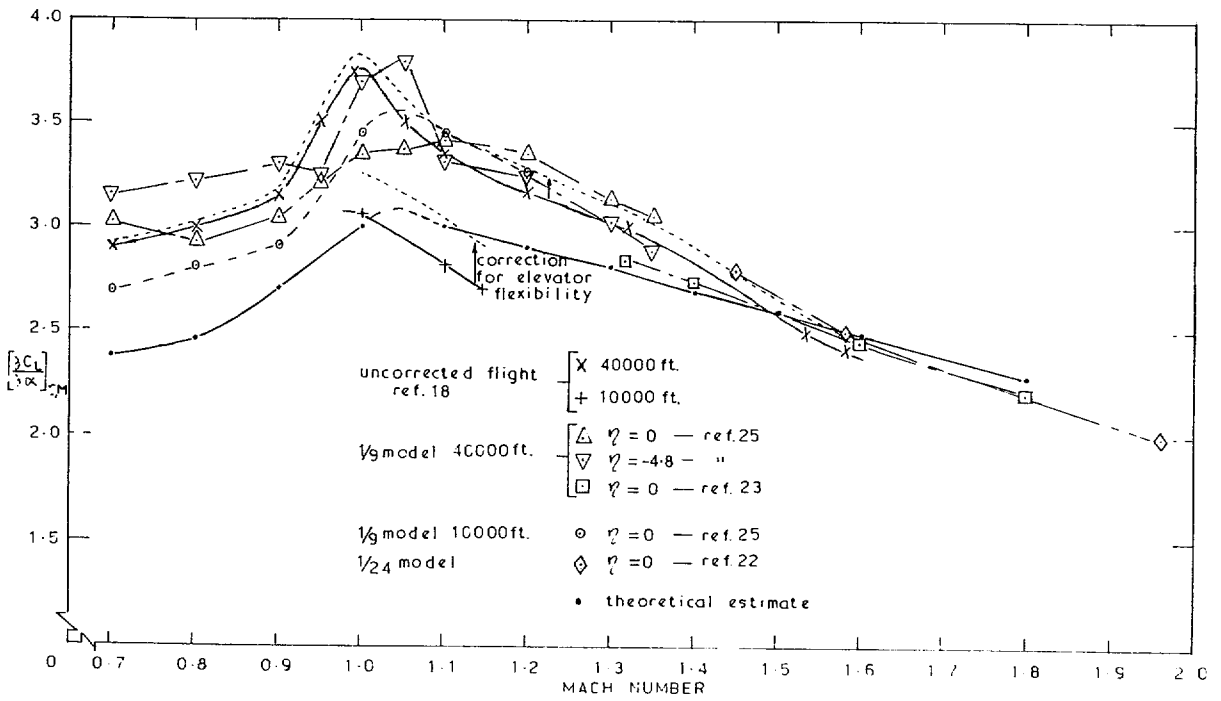

FIG. 7. Comparison of flight and tunnel values of lift curve slope at level flight C_L.

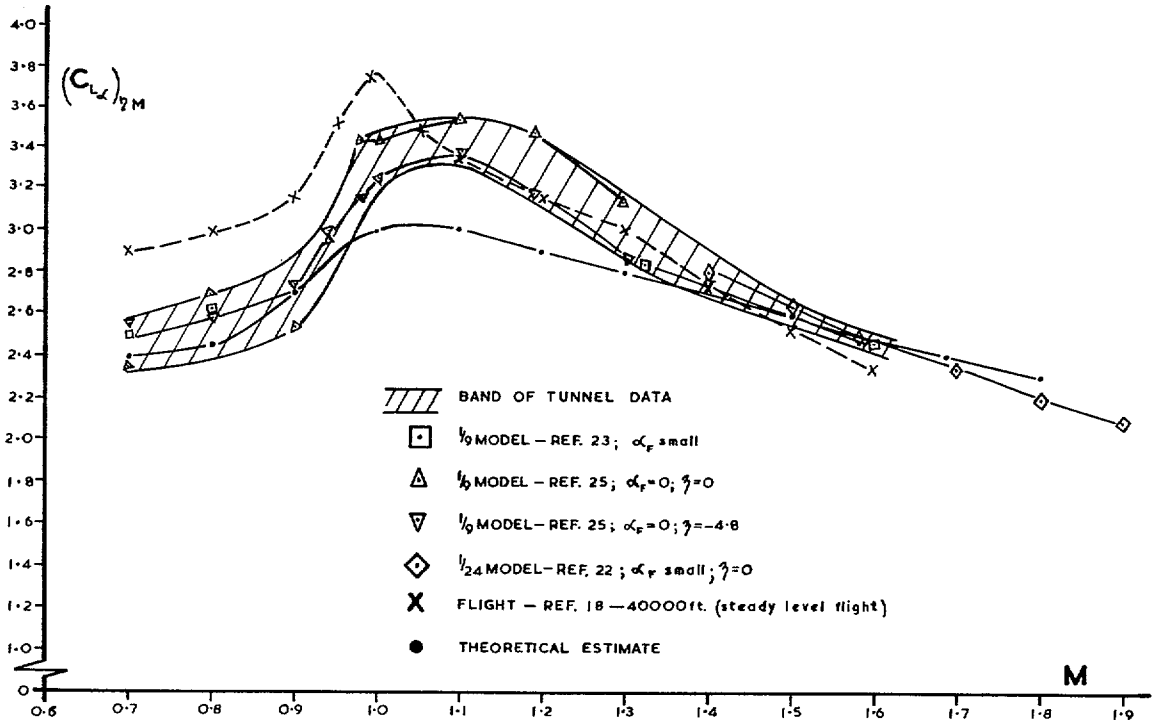

FIG. 8. Comparison of theoretical estimate and experimental data at small angles of incidence.

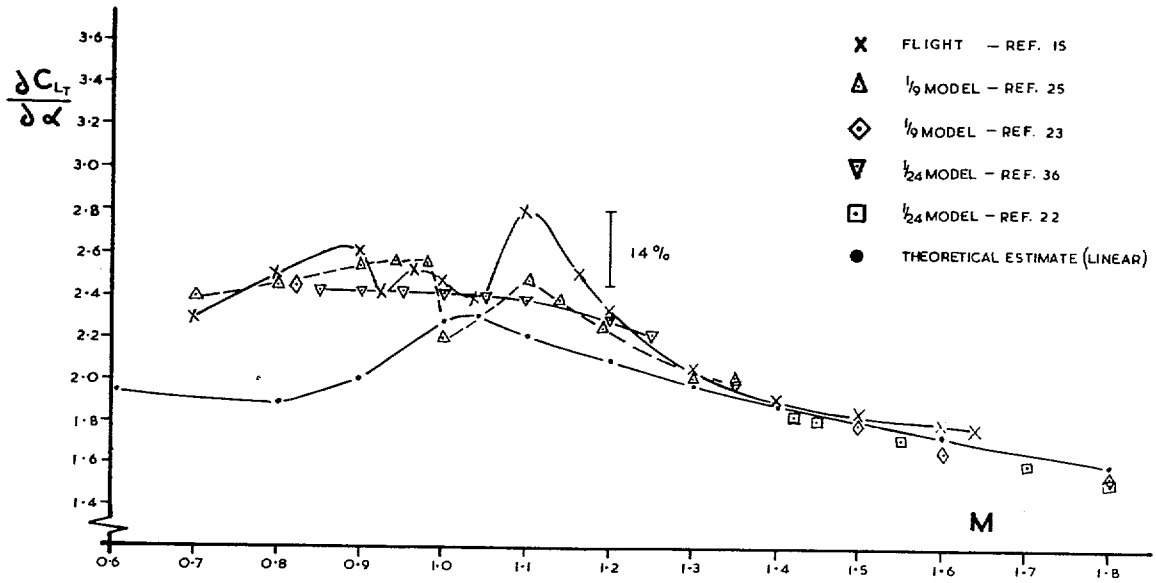

FIG. 9. Trimmed lift curve–slope.

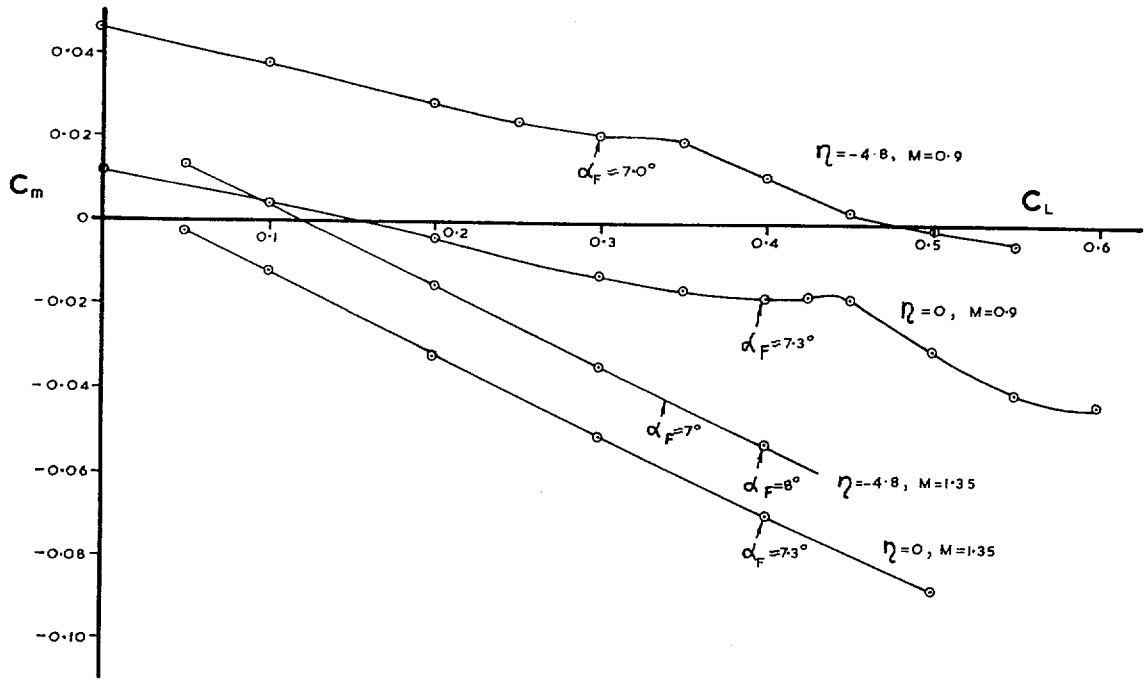

FIG. 10. Variation of pitching moment with C_L.

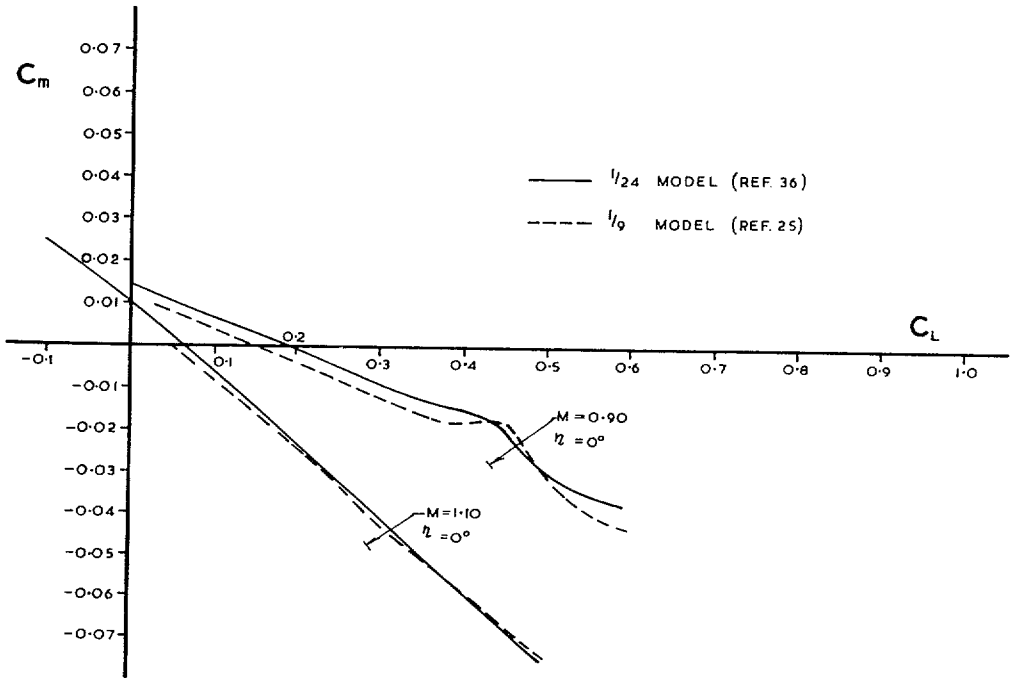

FIG. 10a. Effect of Reynolds Number on C_m *vs.* C_L curves.

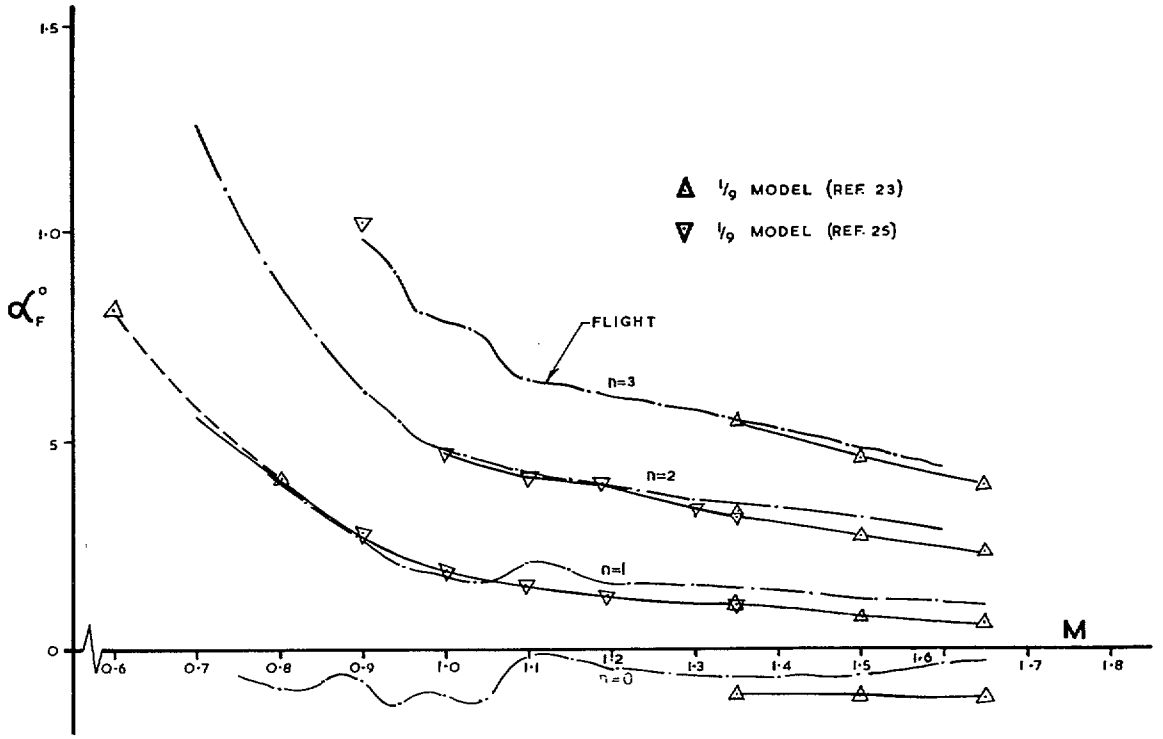

FIG. 11a. Incidence in trimmed flight—Flight and model at 40 000 ft.

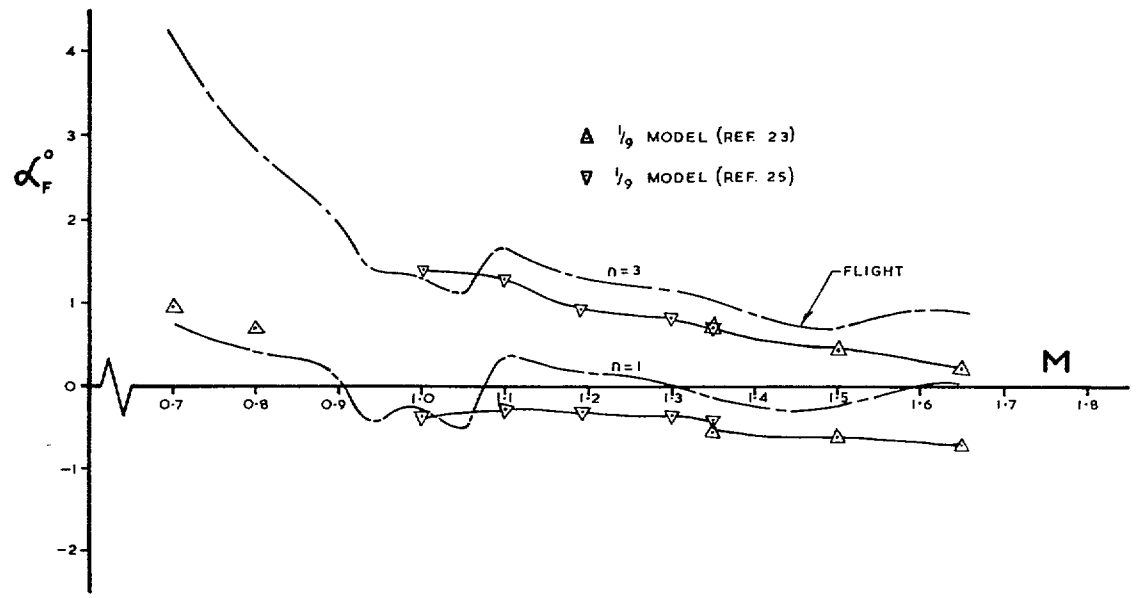

FIG. 11b. Incidence in trimmed flight—Flight and model at 10 000 ft.

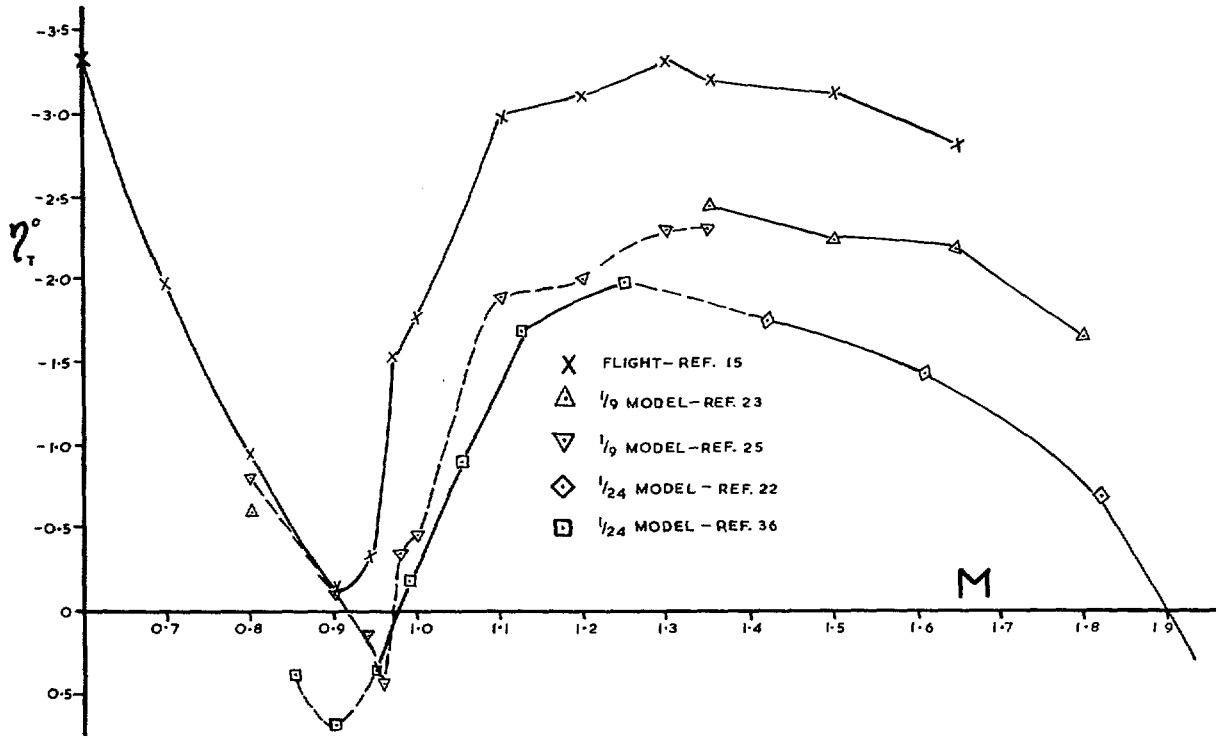

FIG. 12a. Elevator angle to trim in steady level flight at 40 000 ft.

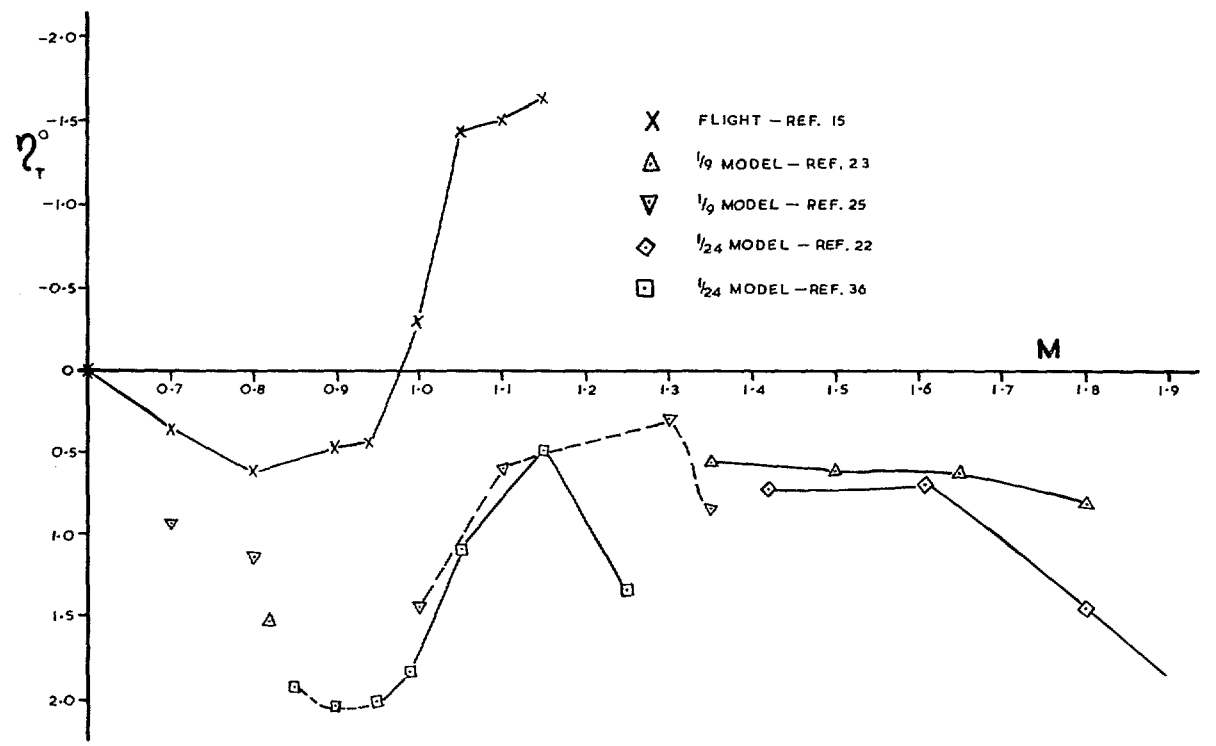

FIG. 12b. Elevator angle to trim in steady level flight at 10 000 ft.

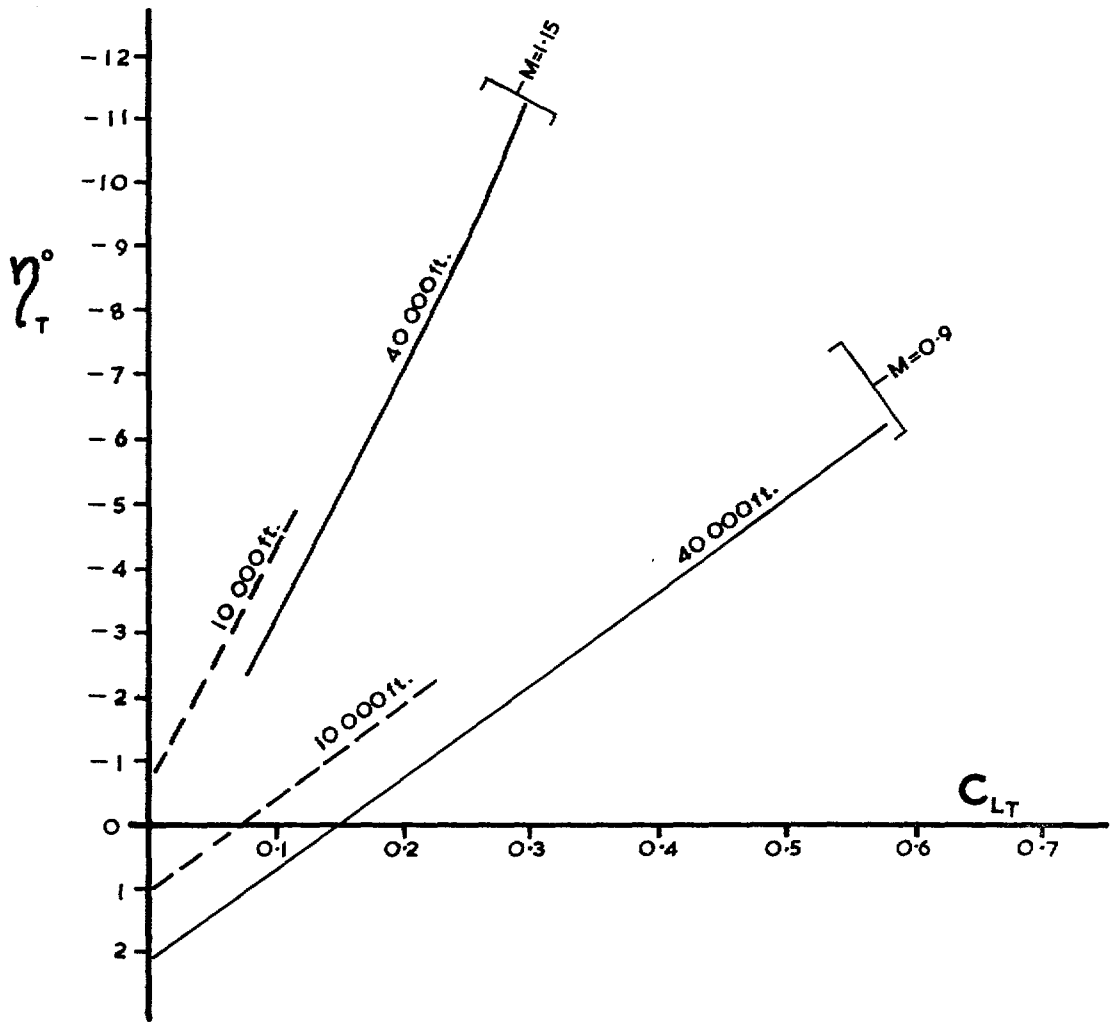

FIG. 13. Variation of elevator angle to trim with C_{L_T}.

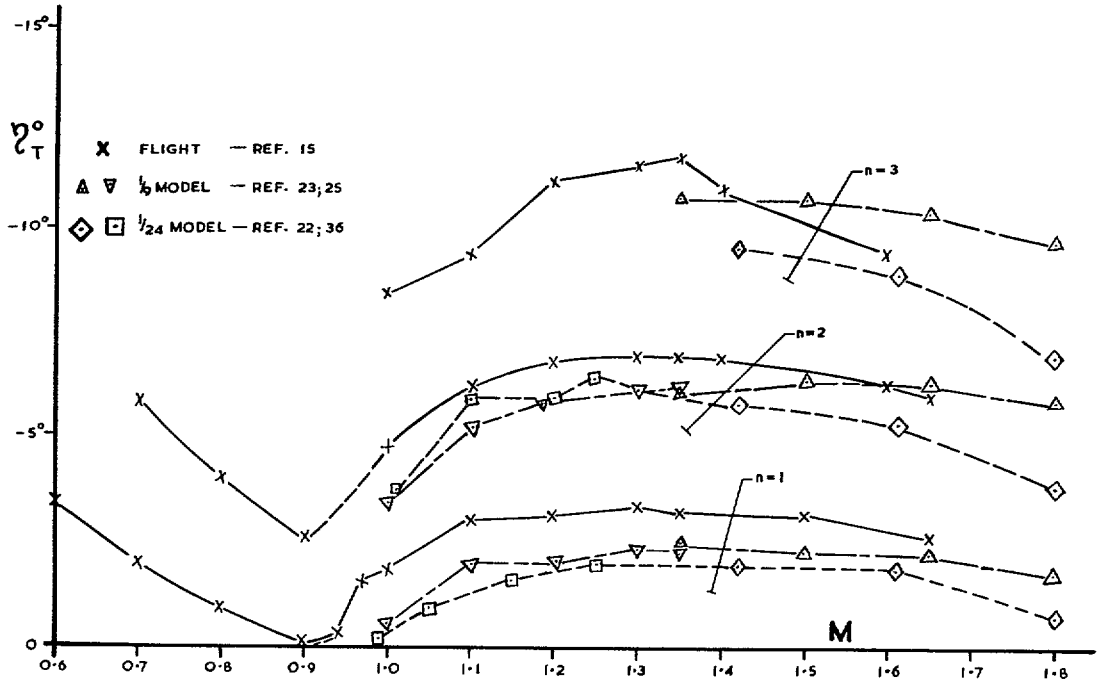

FIG. 14a. Variation of elevator angle to trim with normal acceleration—40 000 ft.

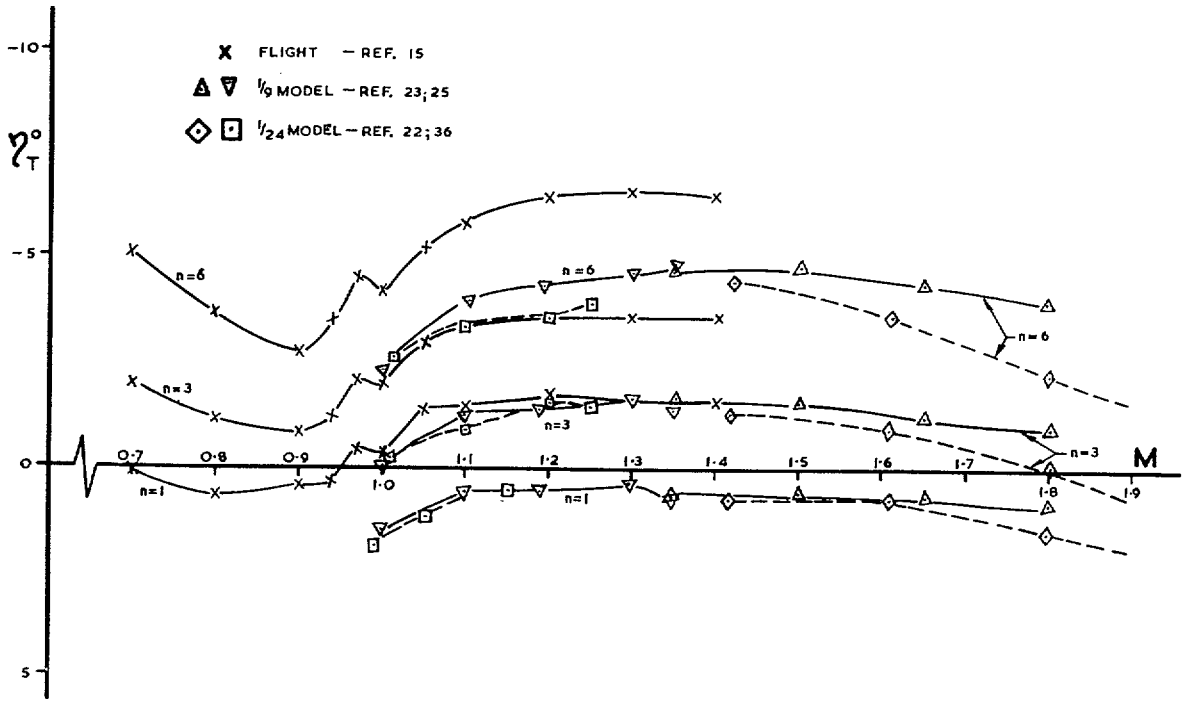

FIG. 14b. Variation of elevator angle to trim with normal acceleration—10 000 ft.

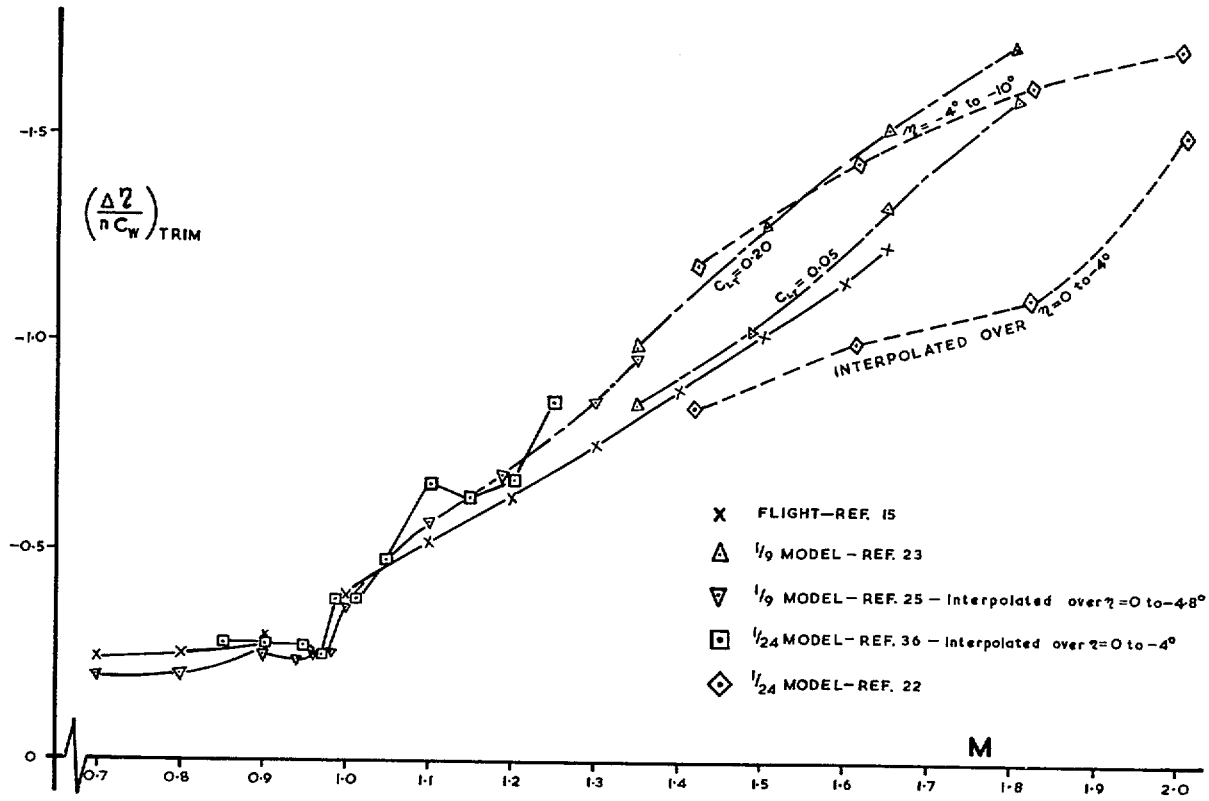

FIG. 15. Variation of elevator power with Mach No.

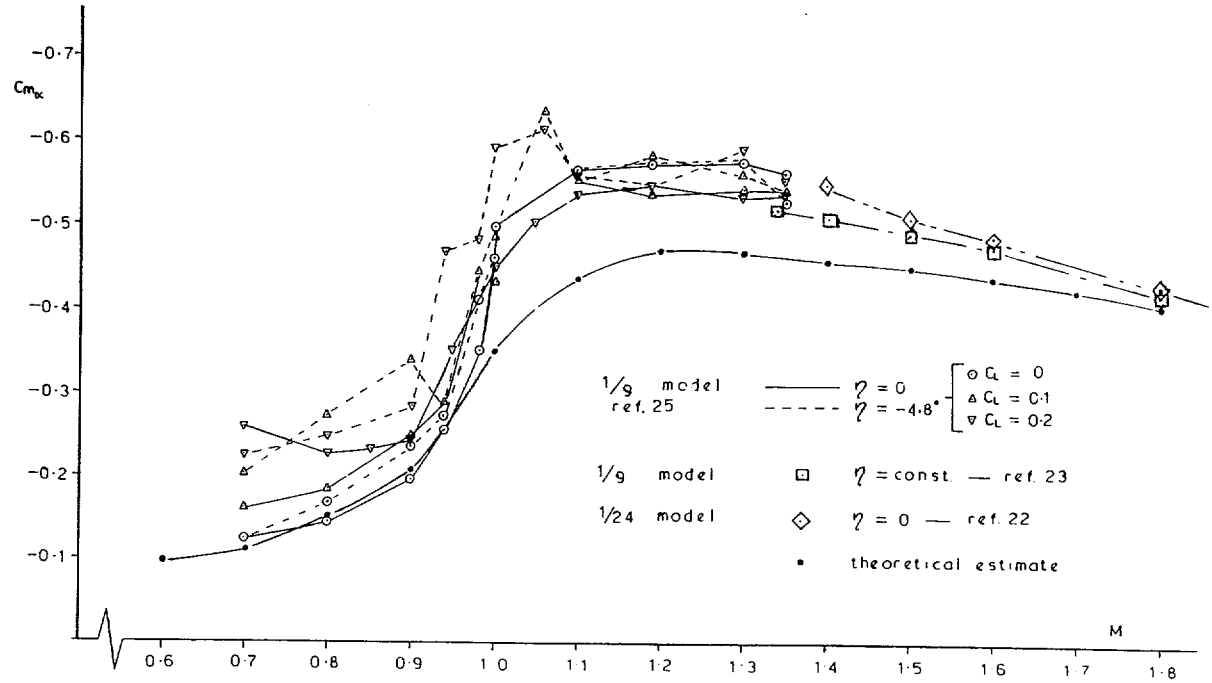

FIG. 16. Variation of C_{m_α} with incidence—Tunnel results.

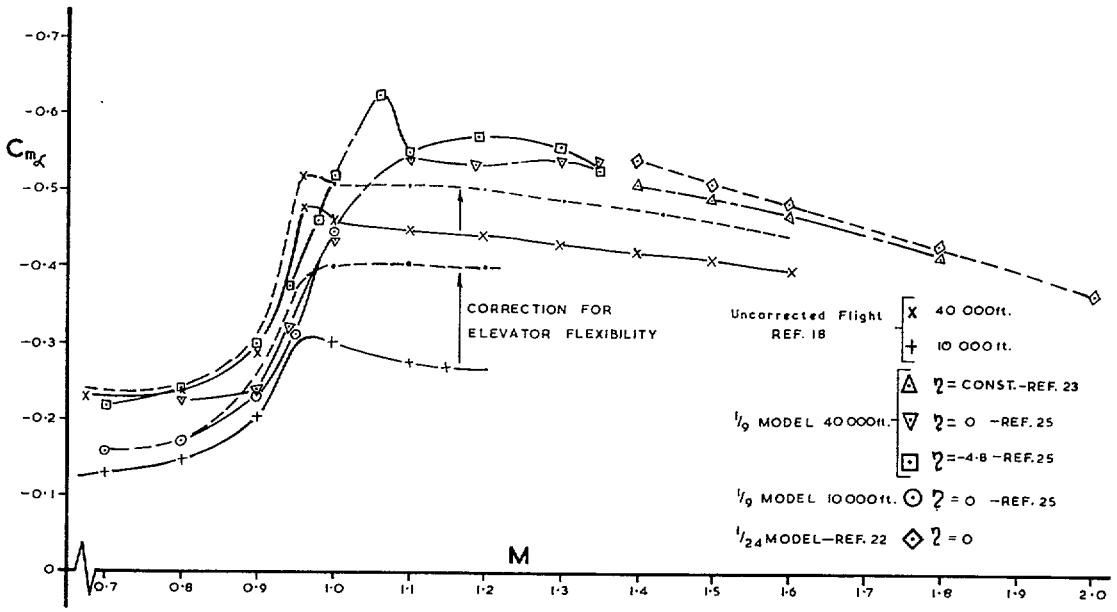

FIG. 17. Comparison of flight and tunnel results for C_{m_α} at 40 000 ft. and 10 000 ft.

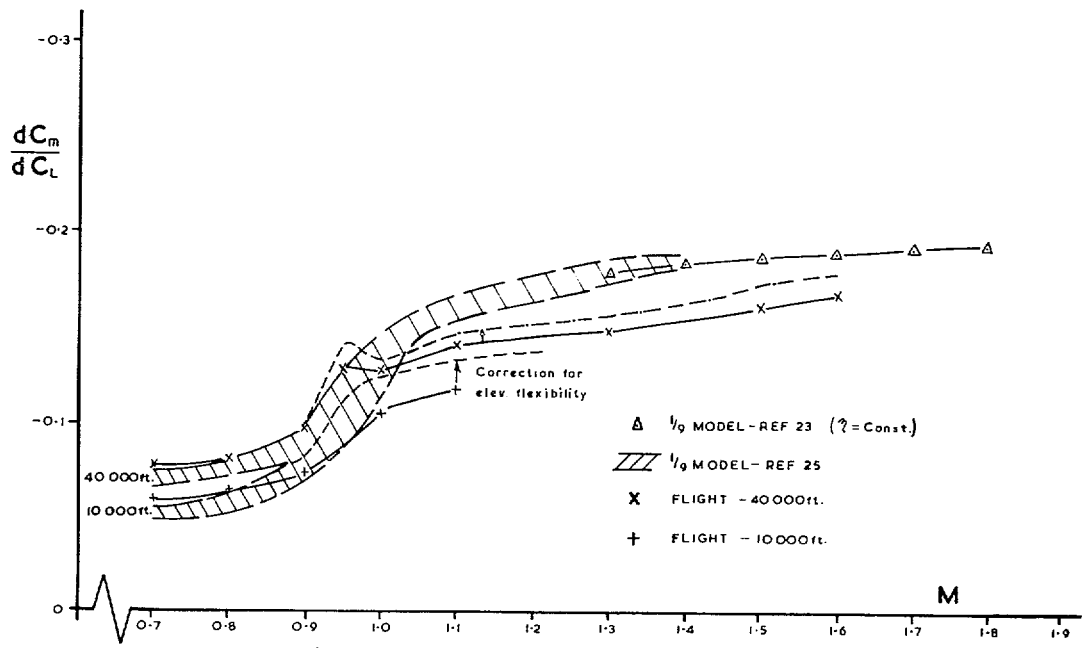

FIG. 18. Comparison of flight and tunnel results for dC_m/dC_L.

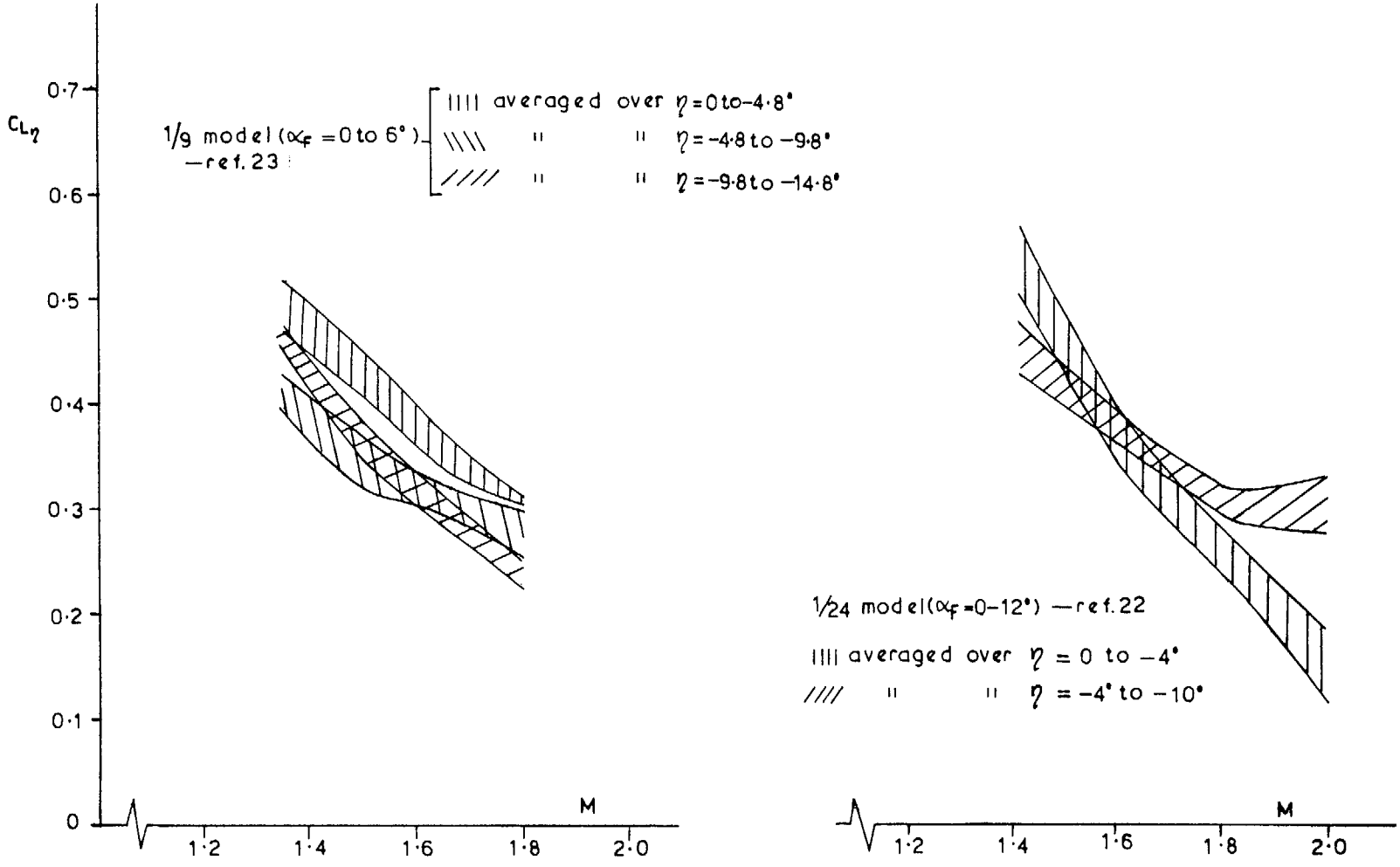

FIG. 19. Variation of C_{L_η} with elevator angle—Tunnel results.

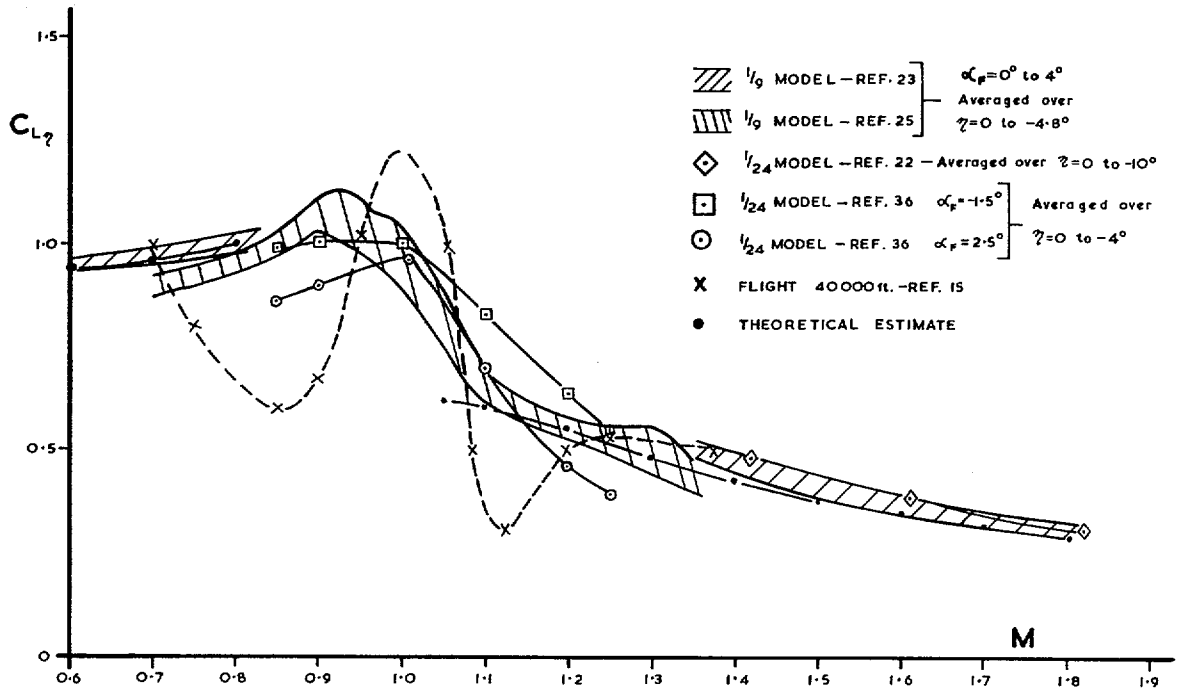

FIG. 20. Comparison of flight and tunnel data for C_{L_η}.

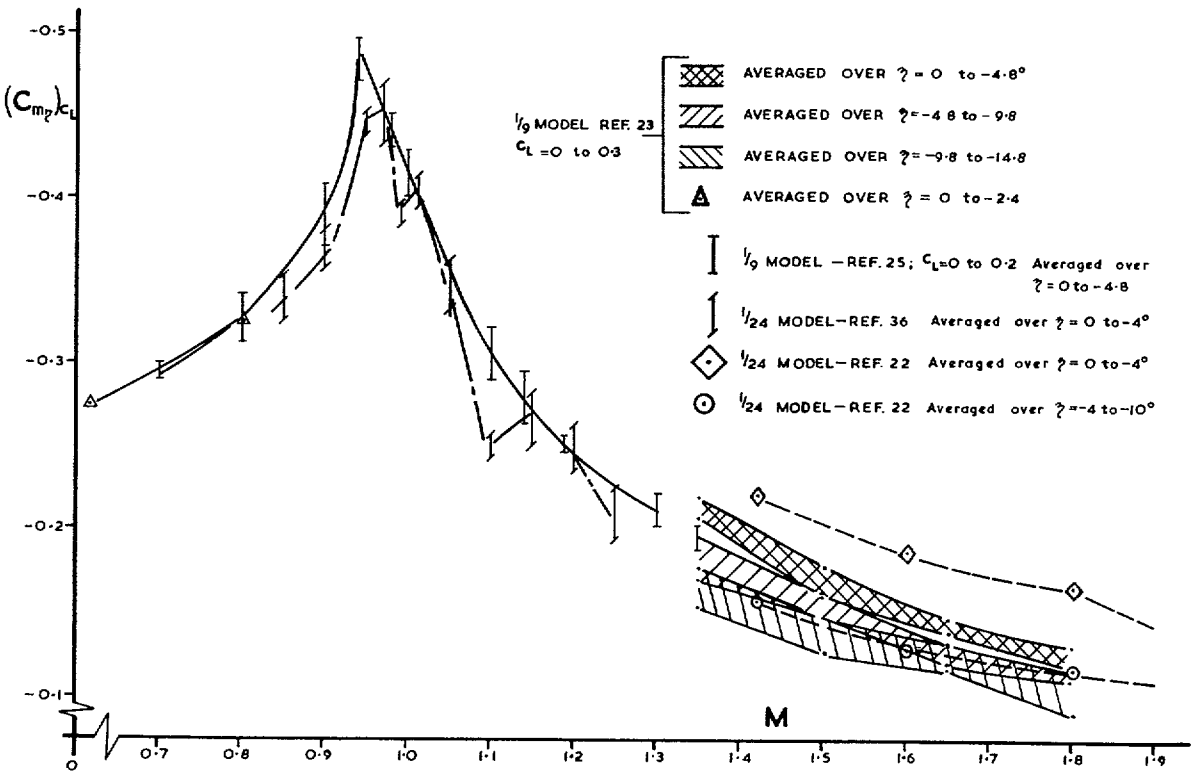

FIG. 21. Variation of $(C_{m_\eta})_{C_L}$ with elevator angle and incidence—Tunnel.

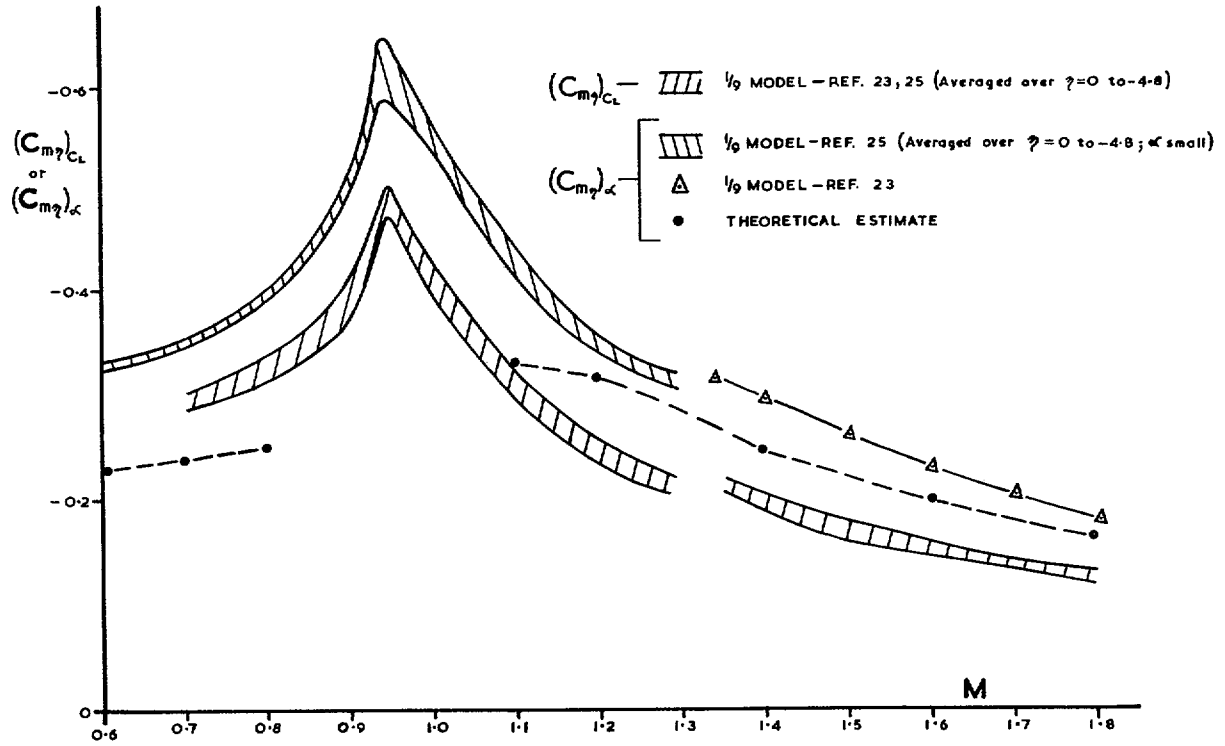

FIG. 22. Comparison of flight and tunnel results for $(C_{m_\eta})_{C_L}$.

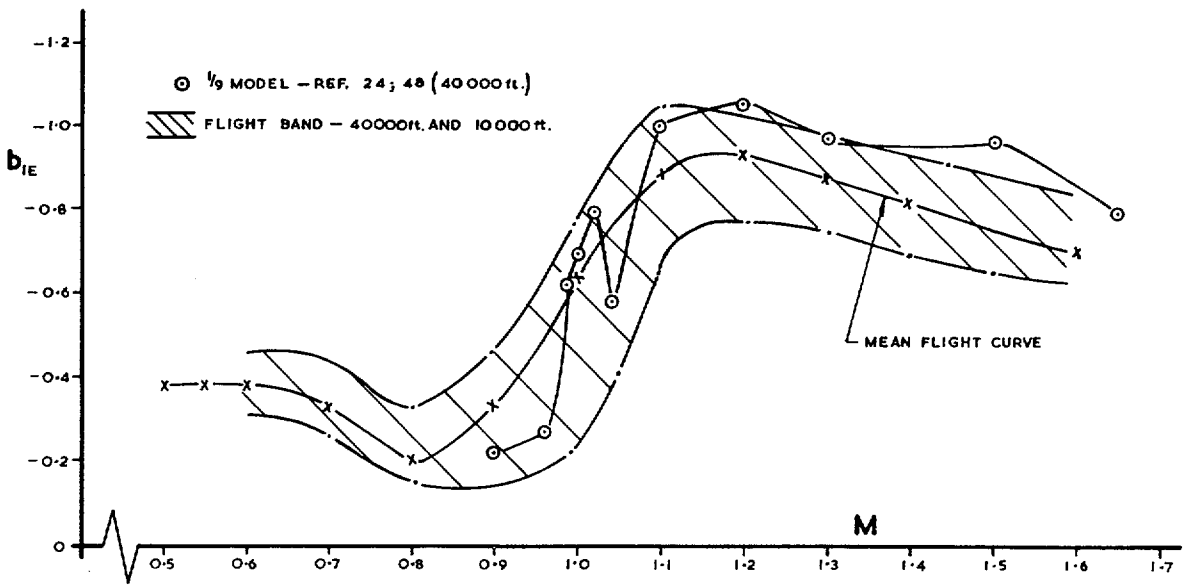

FIG. 23. Comparison of b_{1E} results from flight and tunnel.

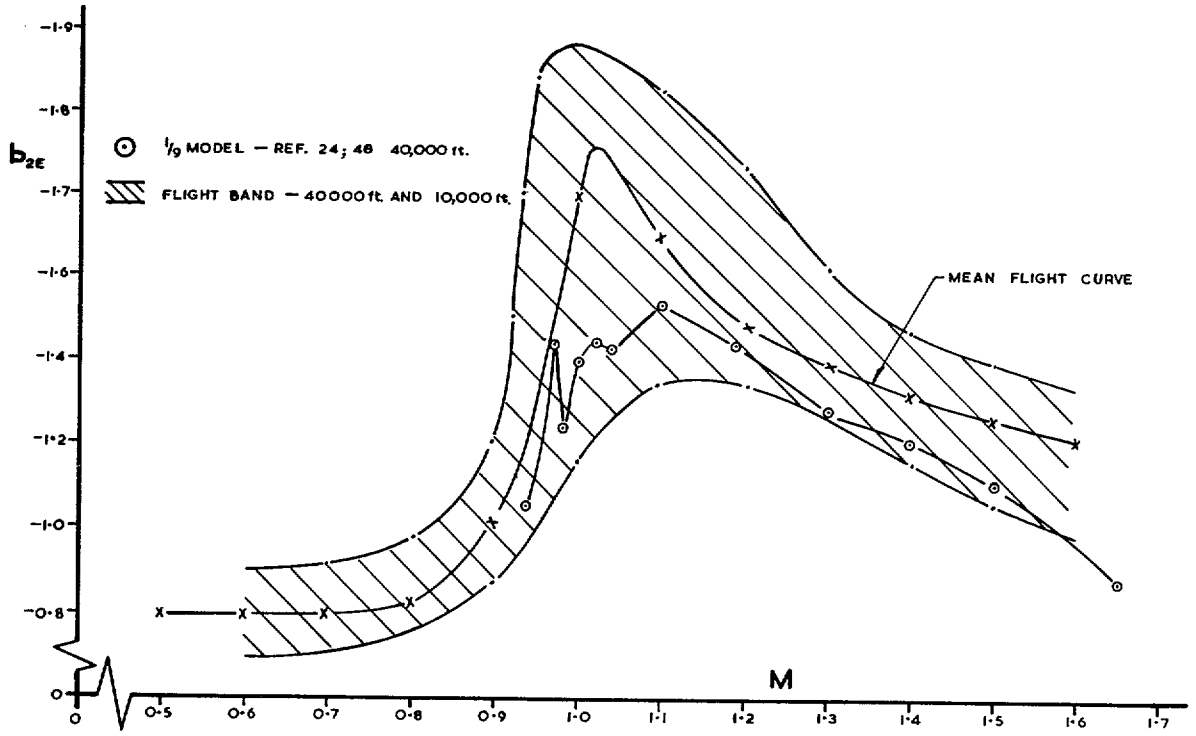

FIG. 24. Comparison of b_{2E} results from flight and tunnel.

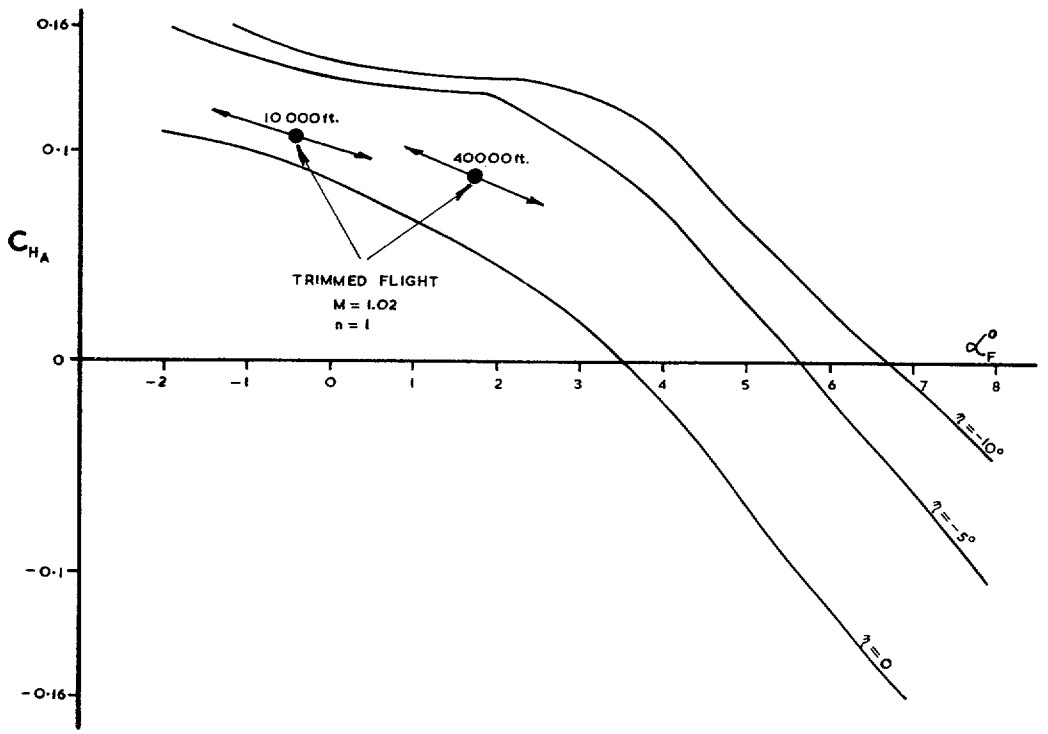

FIG. 25. Variation of aileron hinge moment with incidence and elevator angle—Tunnel.

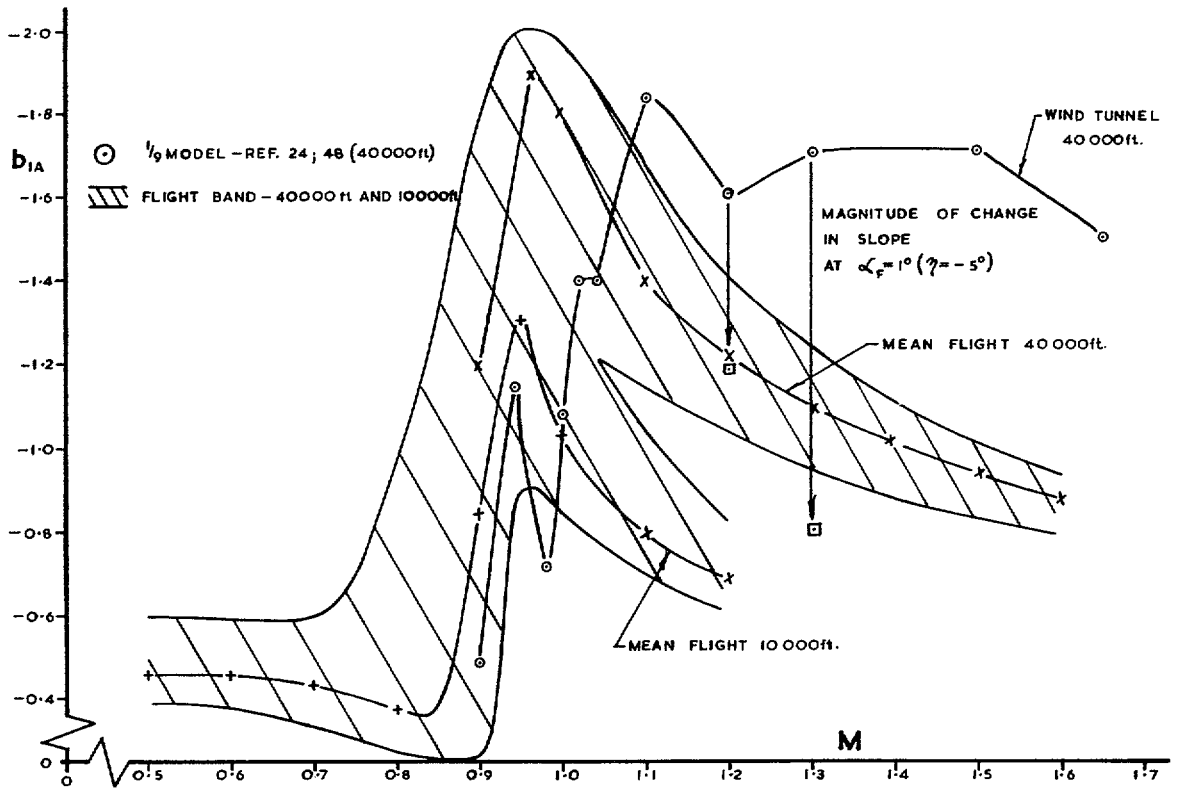

FIG. 26. Comparison of b_{1A} results from flight and tunnel.

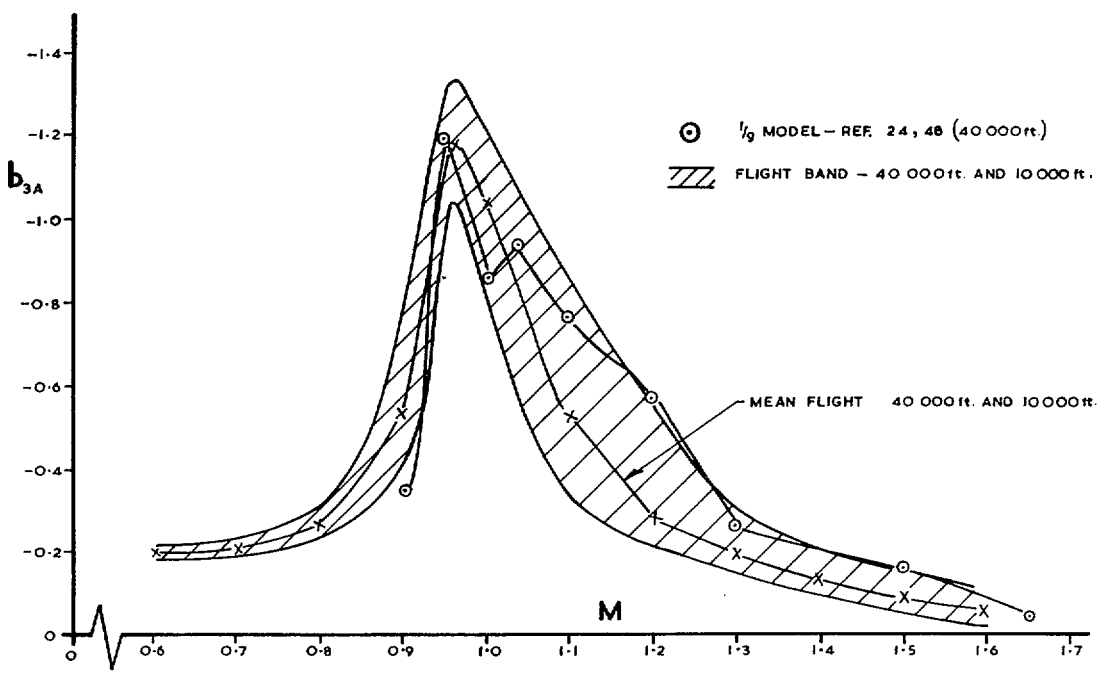

FIG. 27. Comparison of b_{3A} results from flight and tunnel.

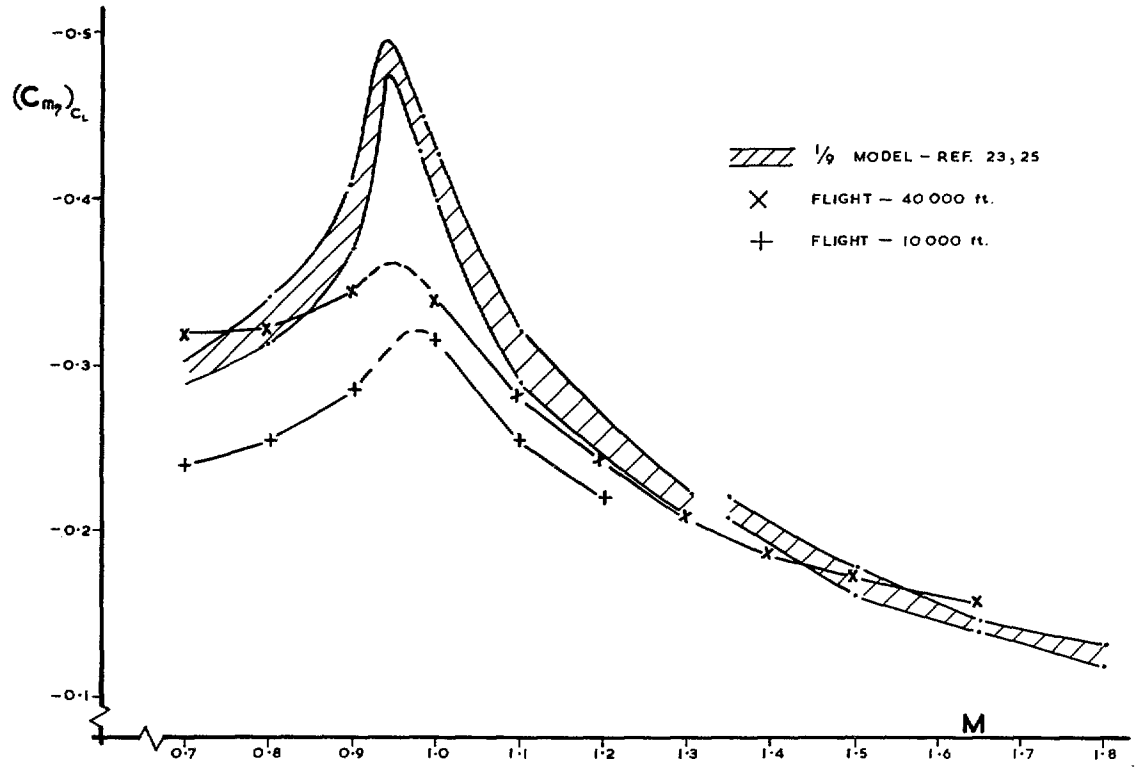

FIG. 28. Flight values of $(C_{m_\eta})_{C_L}$ corrected for elevator flexibility and comparison with tunnel.

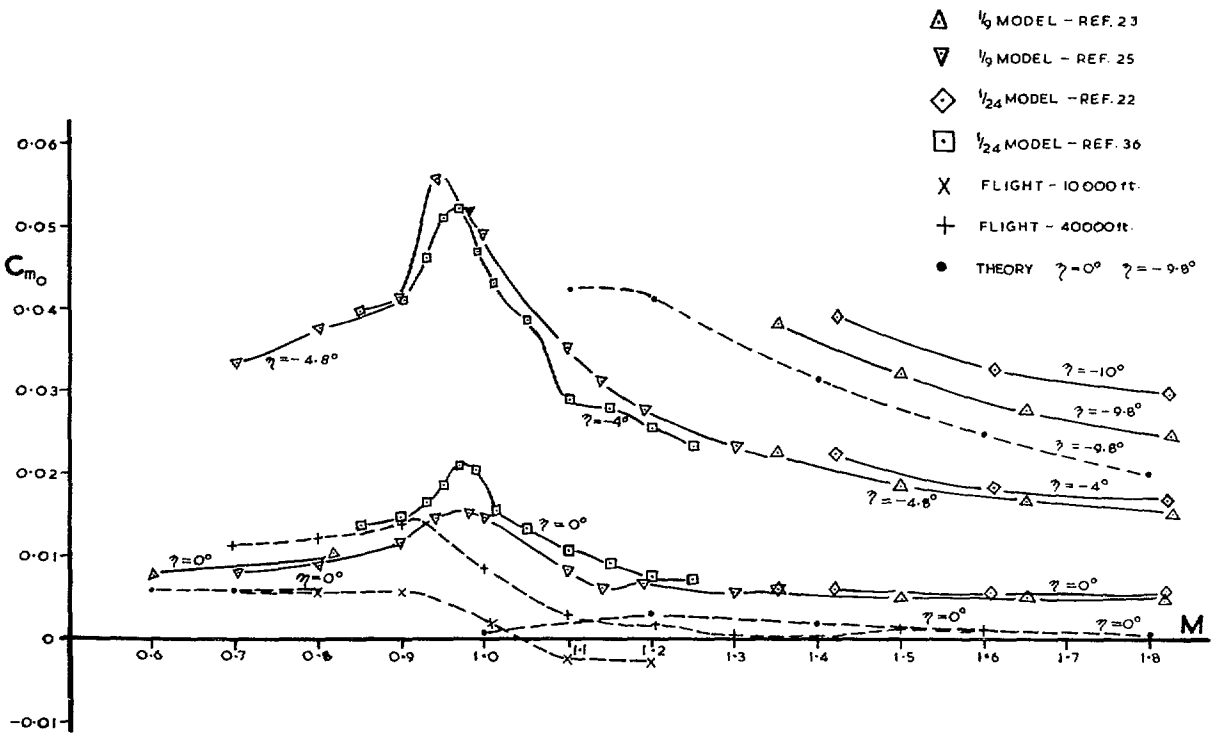

FIG. 29. Comparison of flight and tunnel values of C_{m_0}.

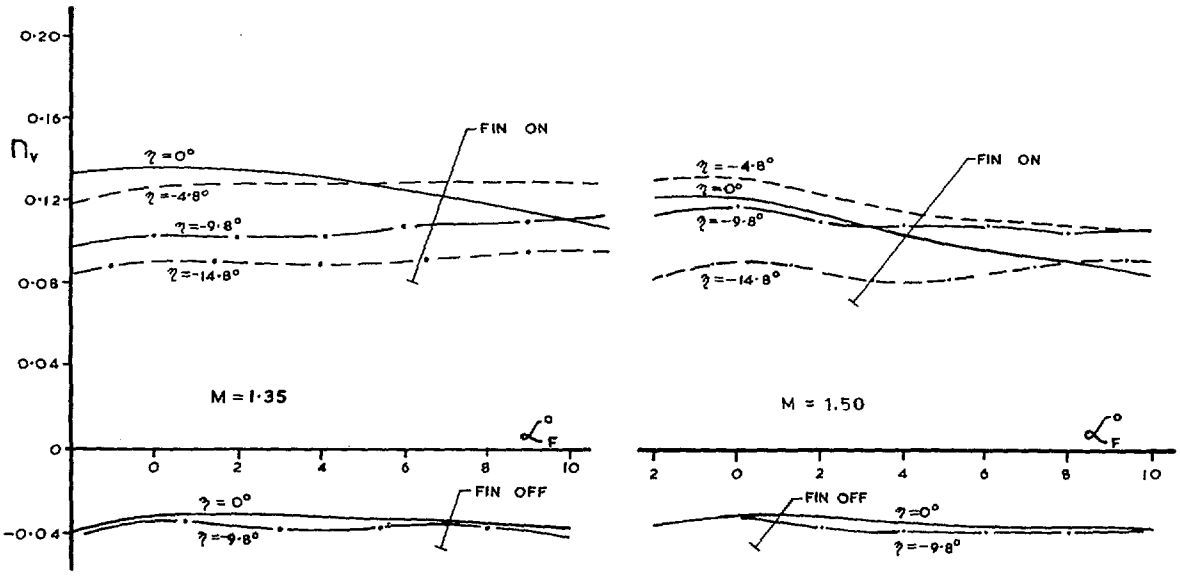

FIG. 30. Variation of n_v with incidence and elevator angle—Tunnel.

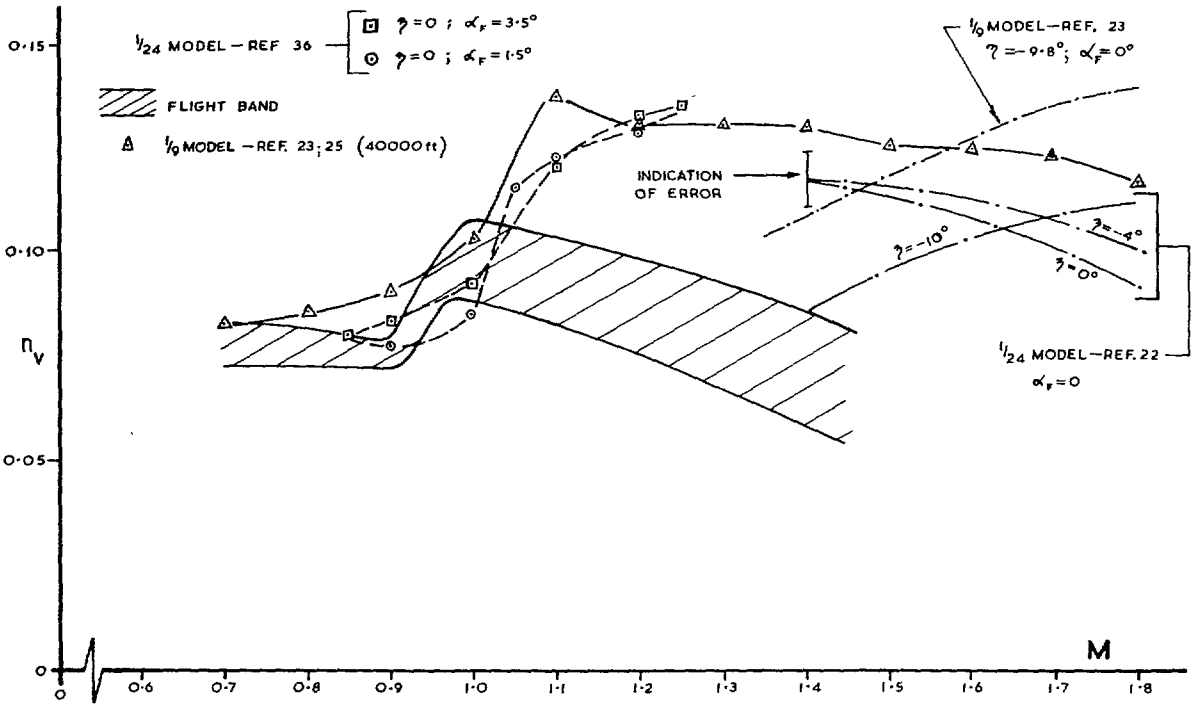

FIG. 31. Comparison of flight and tunnel results for n_v.

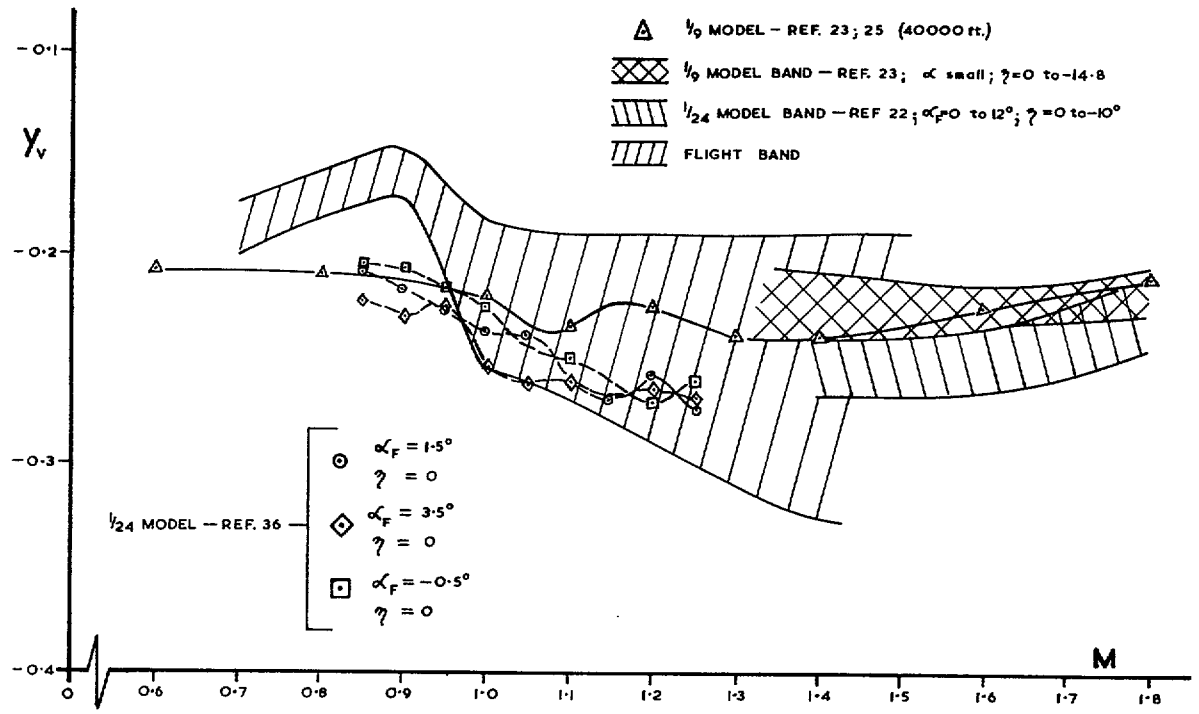

FIG. 32. Comparison of flight and tunnel results for y_v.

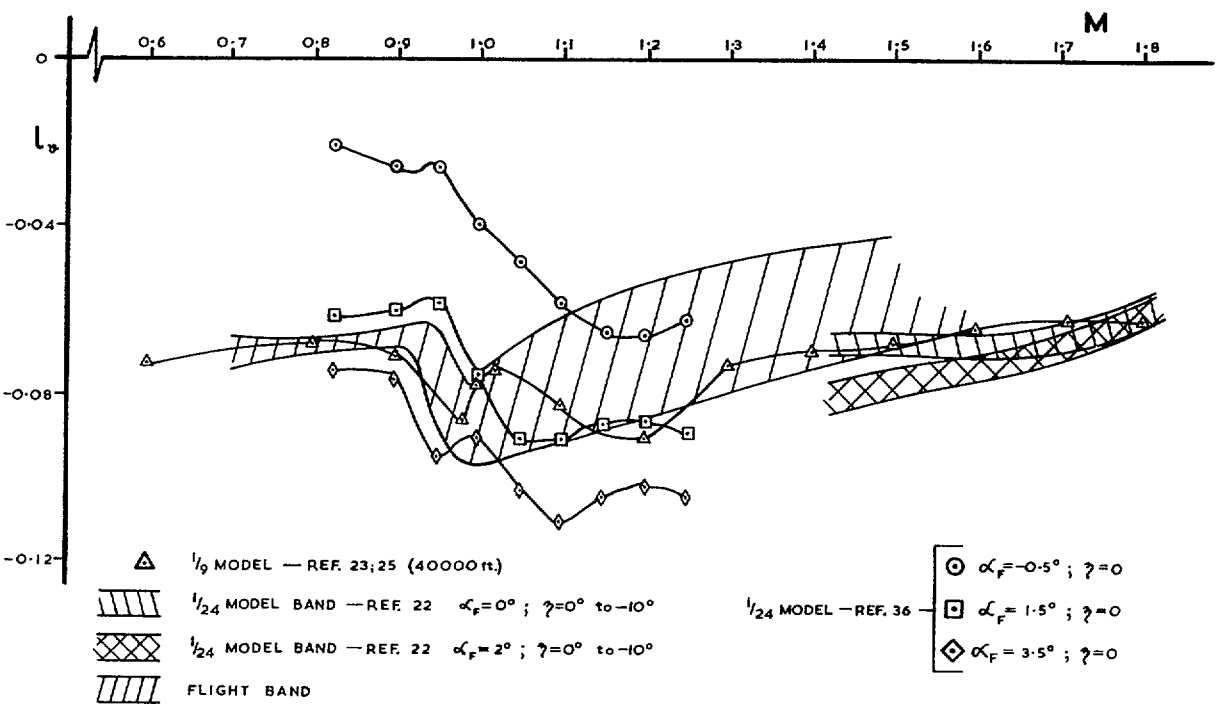

FIG. 33. Comparison of flight and tunnel results for l_v.

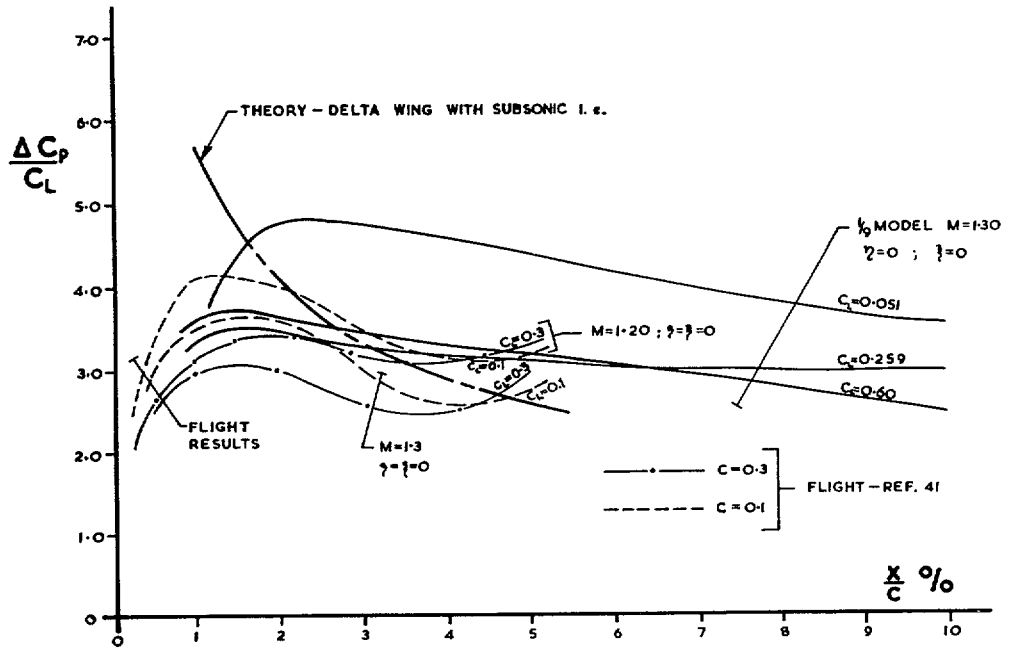

FIG. 34. Non-dimensional loading near the leading edge at 58% semi-span, flight and tunnel.

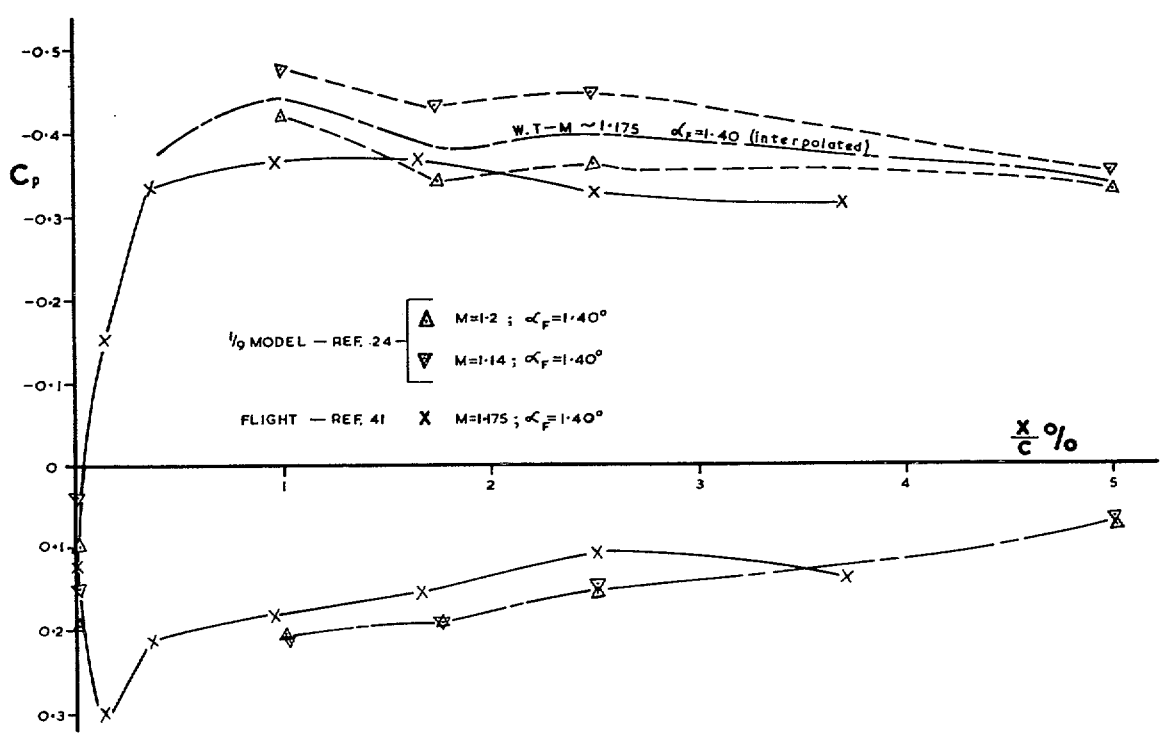

FIG. 34a. Comparison of flight and tunnel leading edge pressures M ≑ 1·2; 58% semi-span.

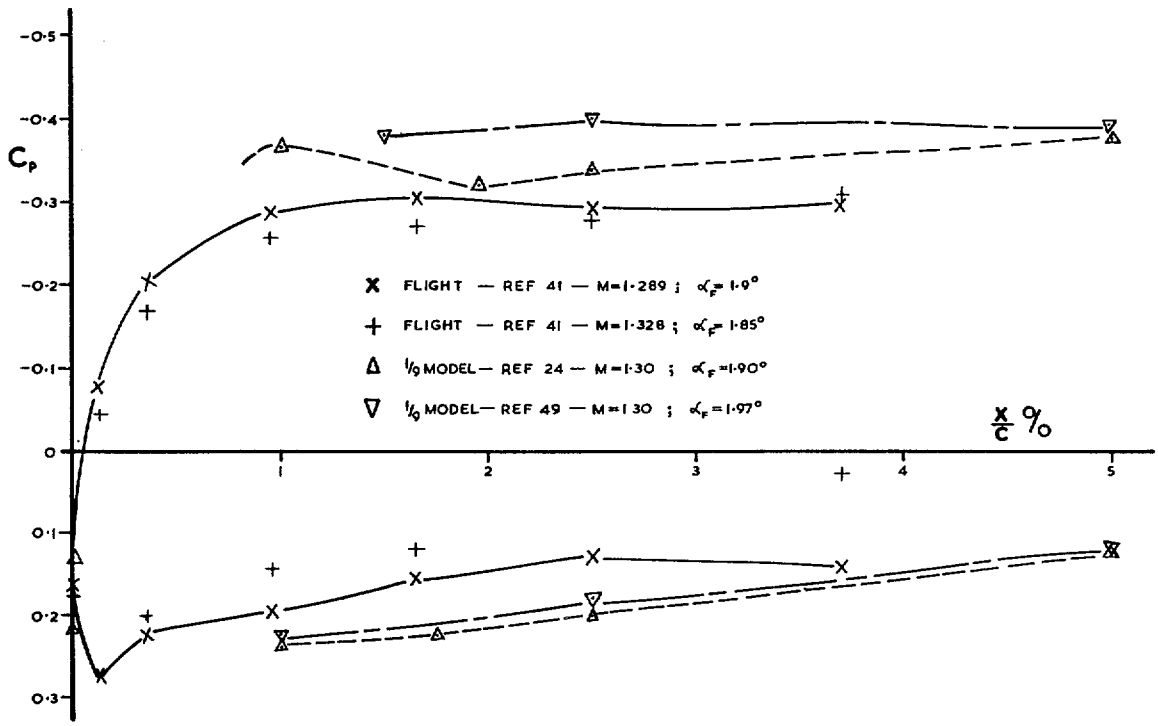

FIG. 34b. Comparison of flight and tunnel loading edge pressures—M ≒ 1·3; 58% semi-span.

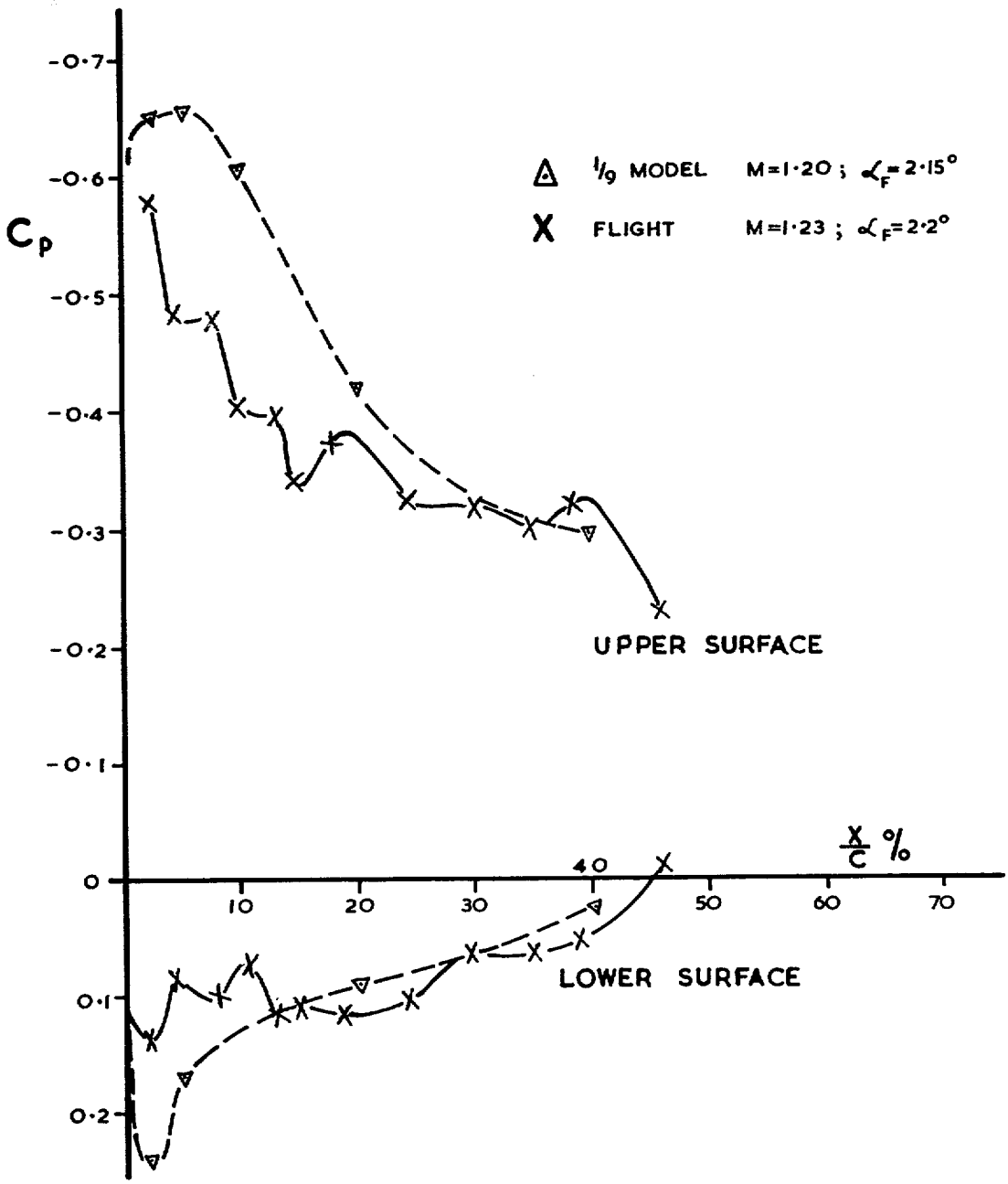

FIG. 35a. Chordwise pressure distributions—85% semi-span.

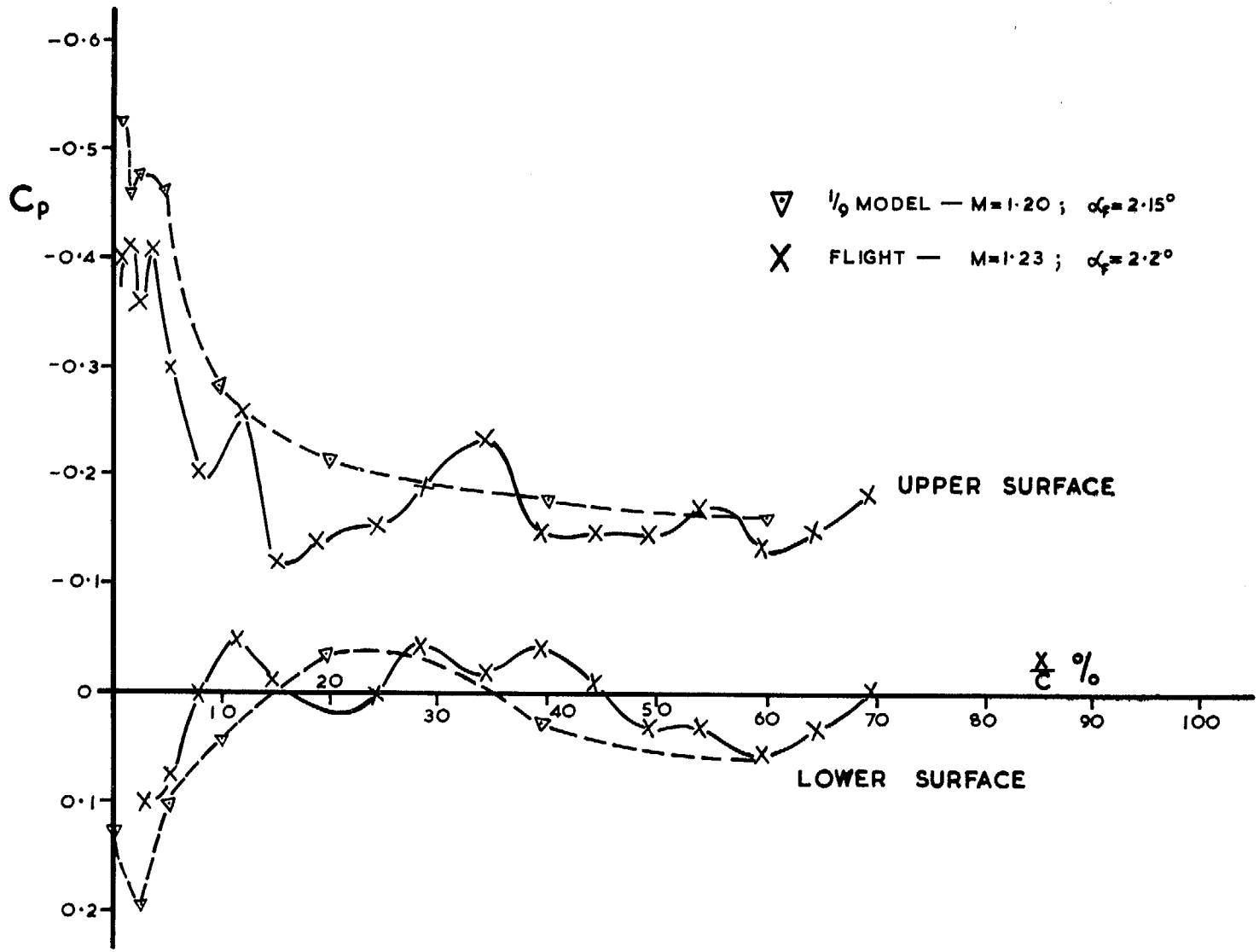

FIG. 35b. Chordwise pressure distributions—58 % semi-span.

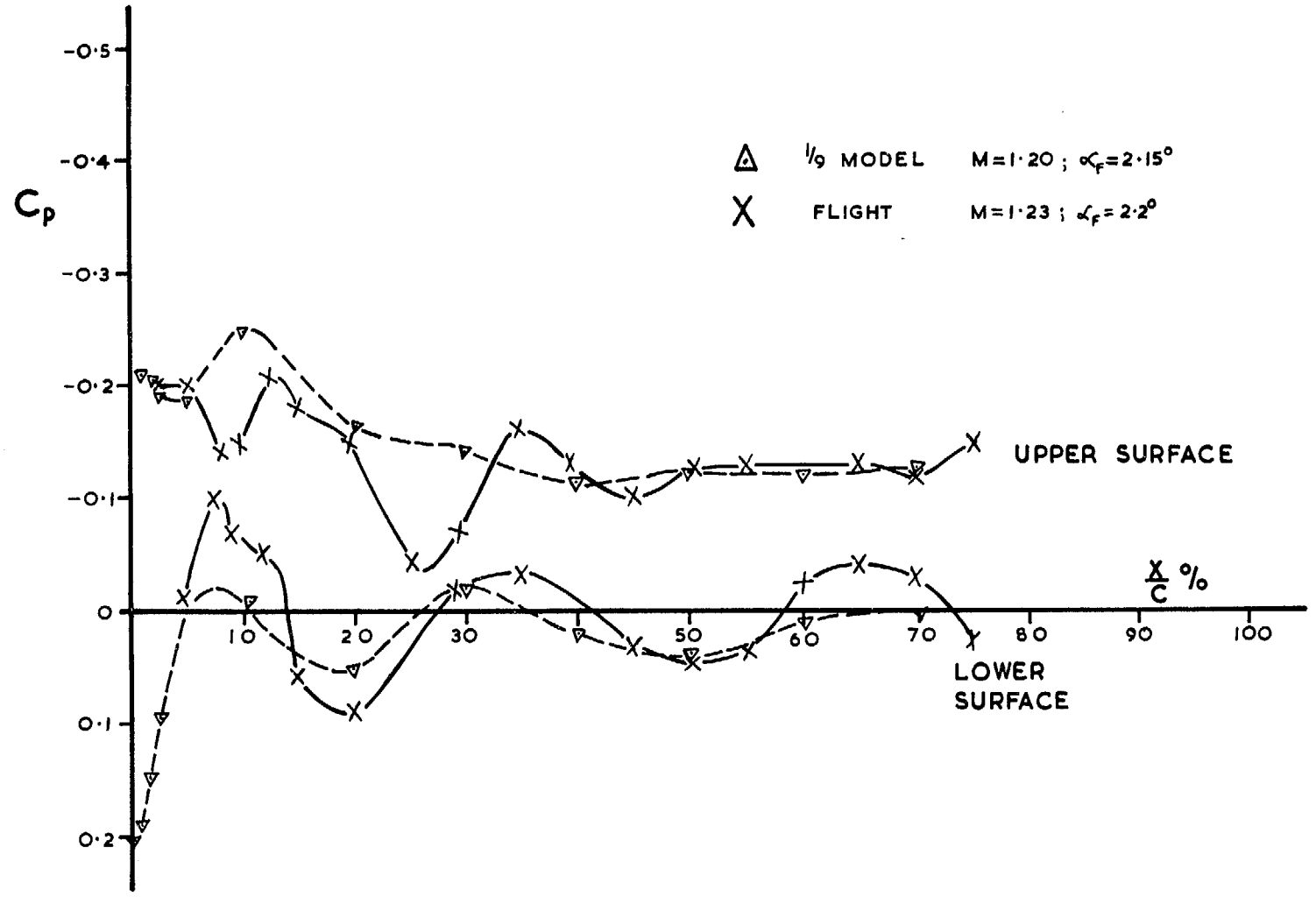

FIG. 35c. Chordwise pressure distributions—35·5% semi-span.

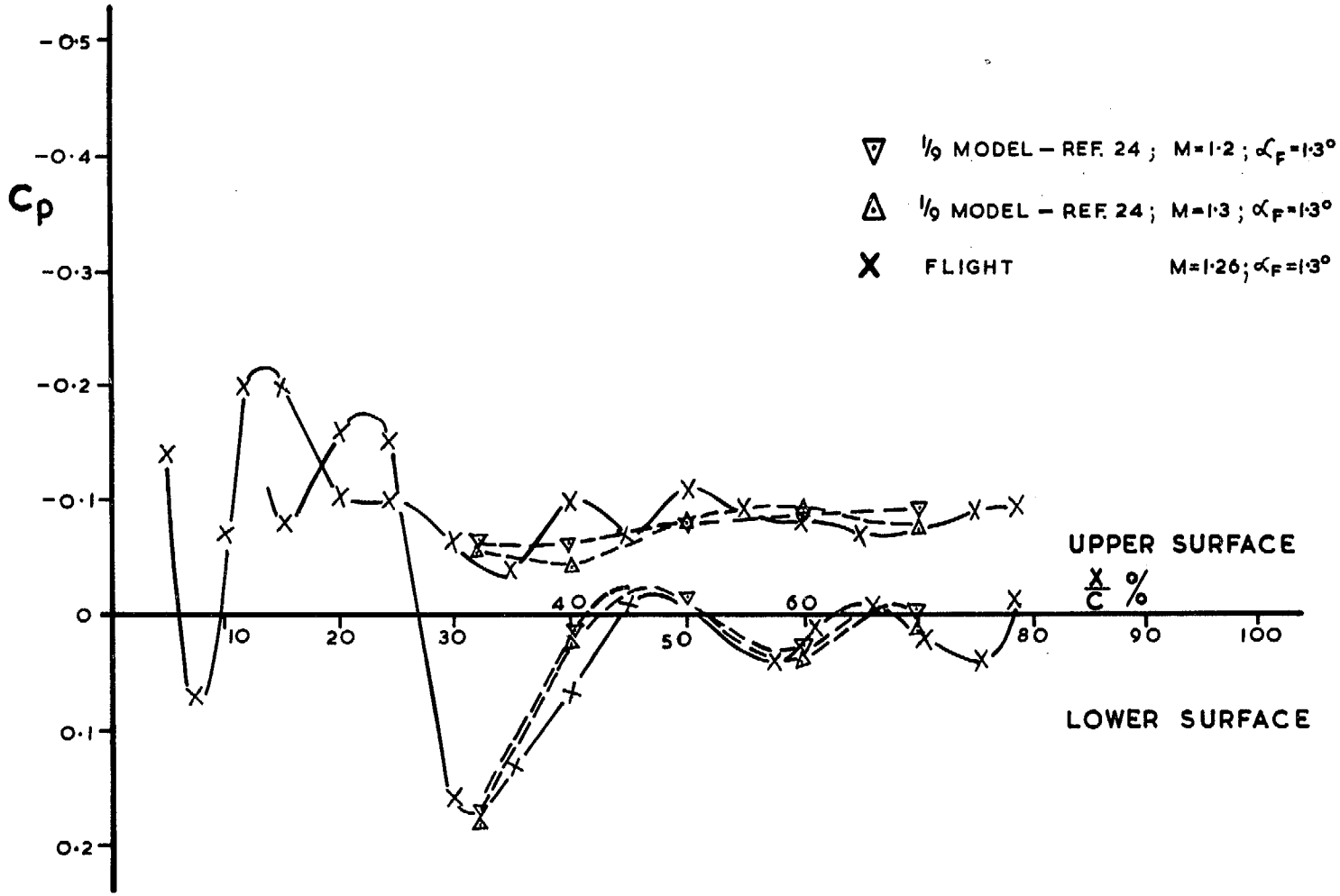

FIG. 35d. Chordwise pressure distributions—20% semi-span.

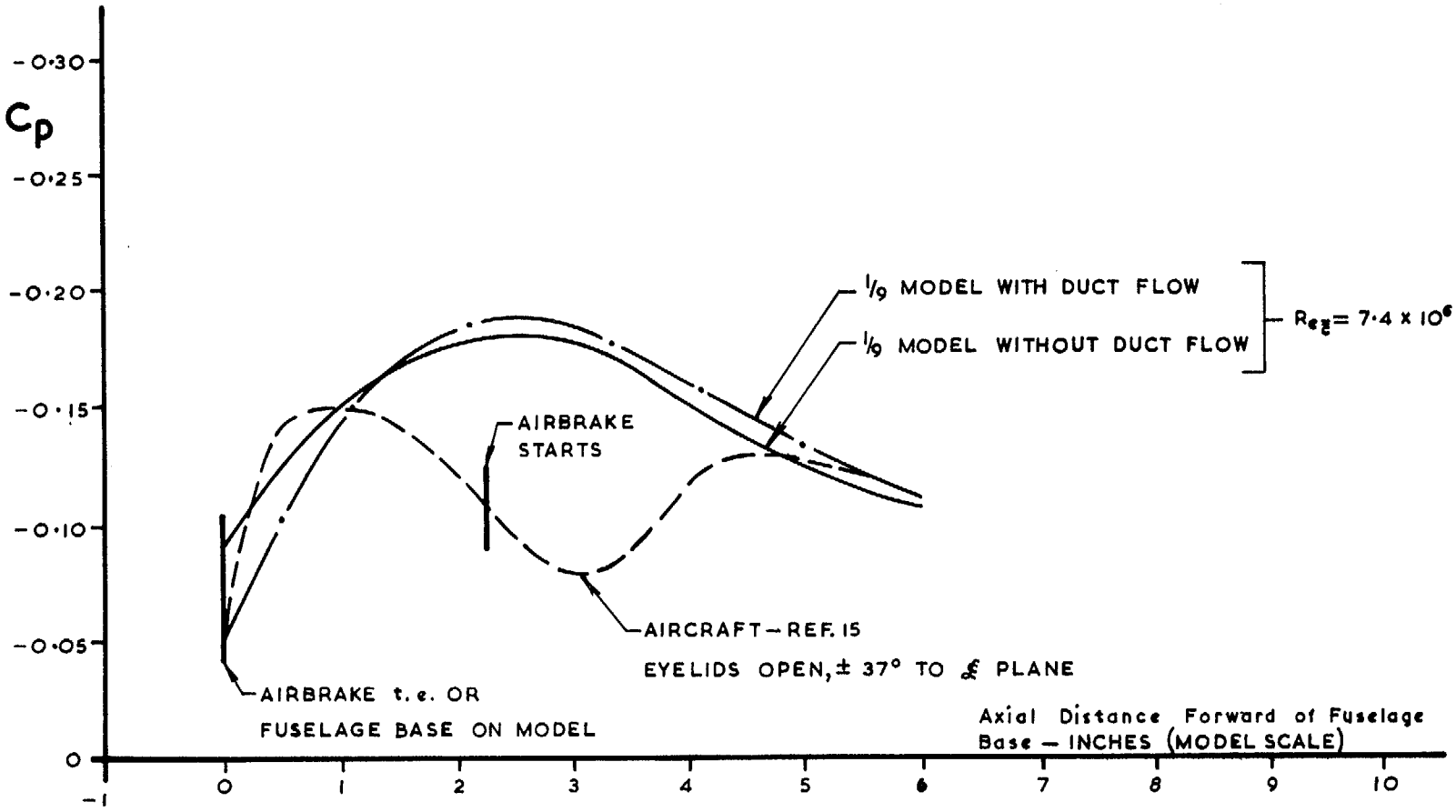

FIG. 36. Flight and tunnel pressures on rear fuselage—M = 1·35.

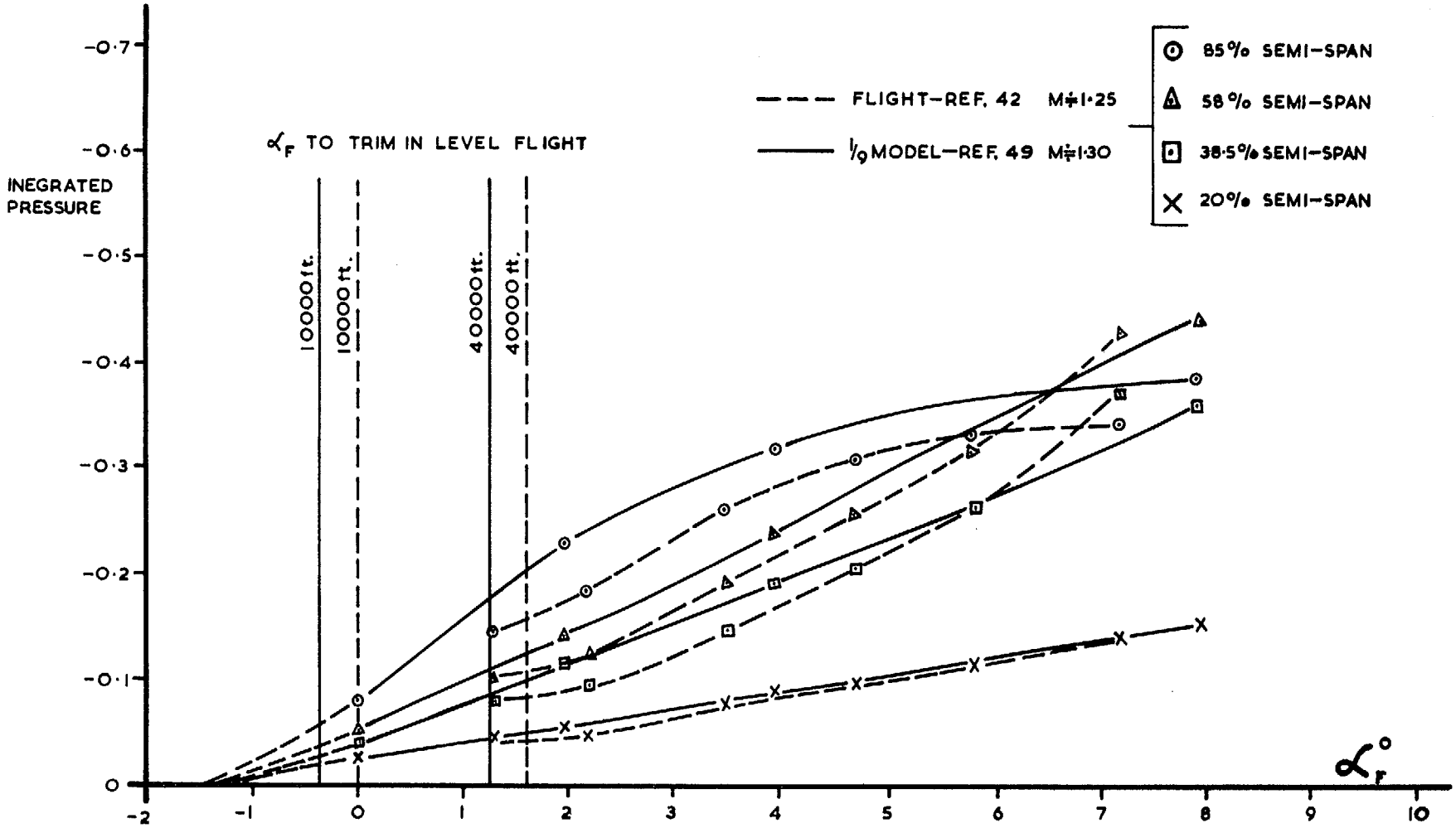

FIG. 37a. Integrated pressure distribution versus incidence—M ≒ 1·3.

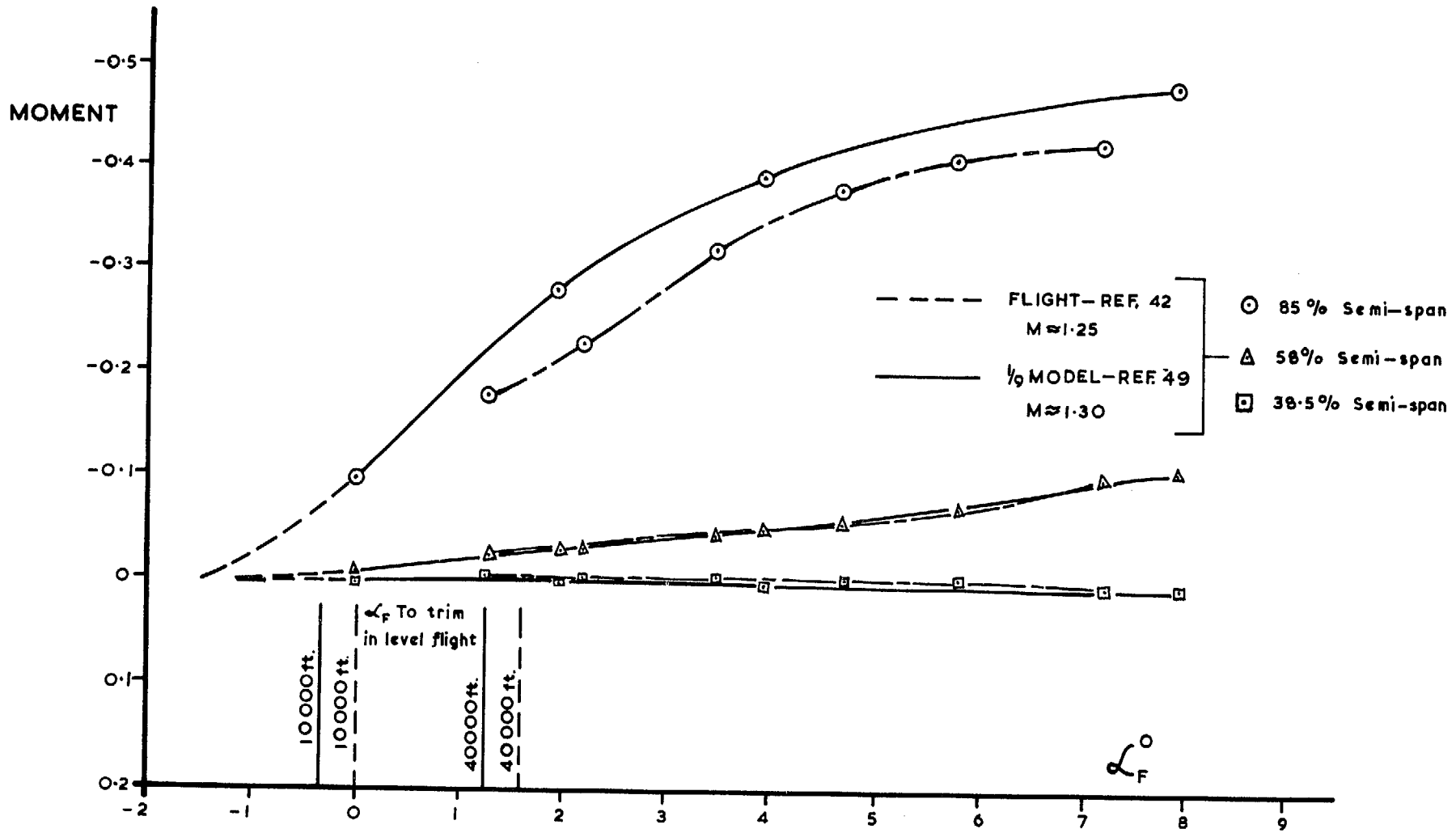

FIG. 37b. Integrated moment about C.G. versus incidence—M ≒ 1·3.

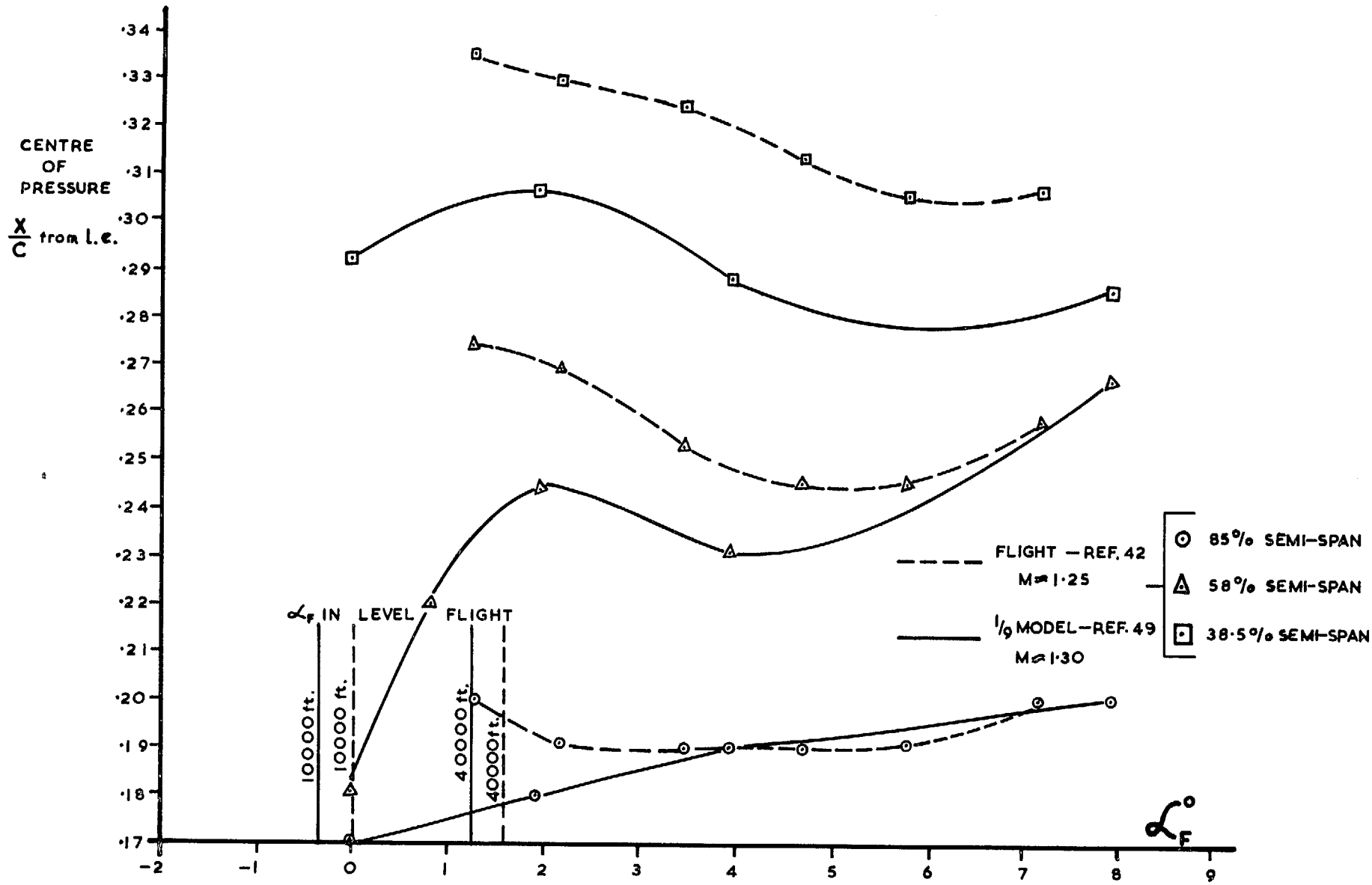

FIG. 37c. Centre of pressure location versus incidence—M ≒ 1·3.

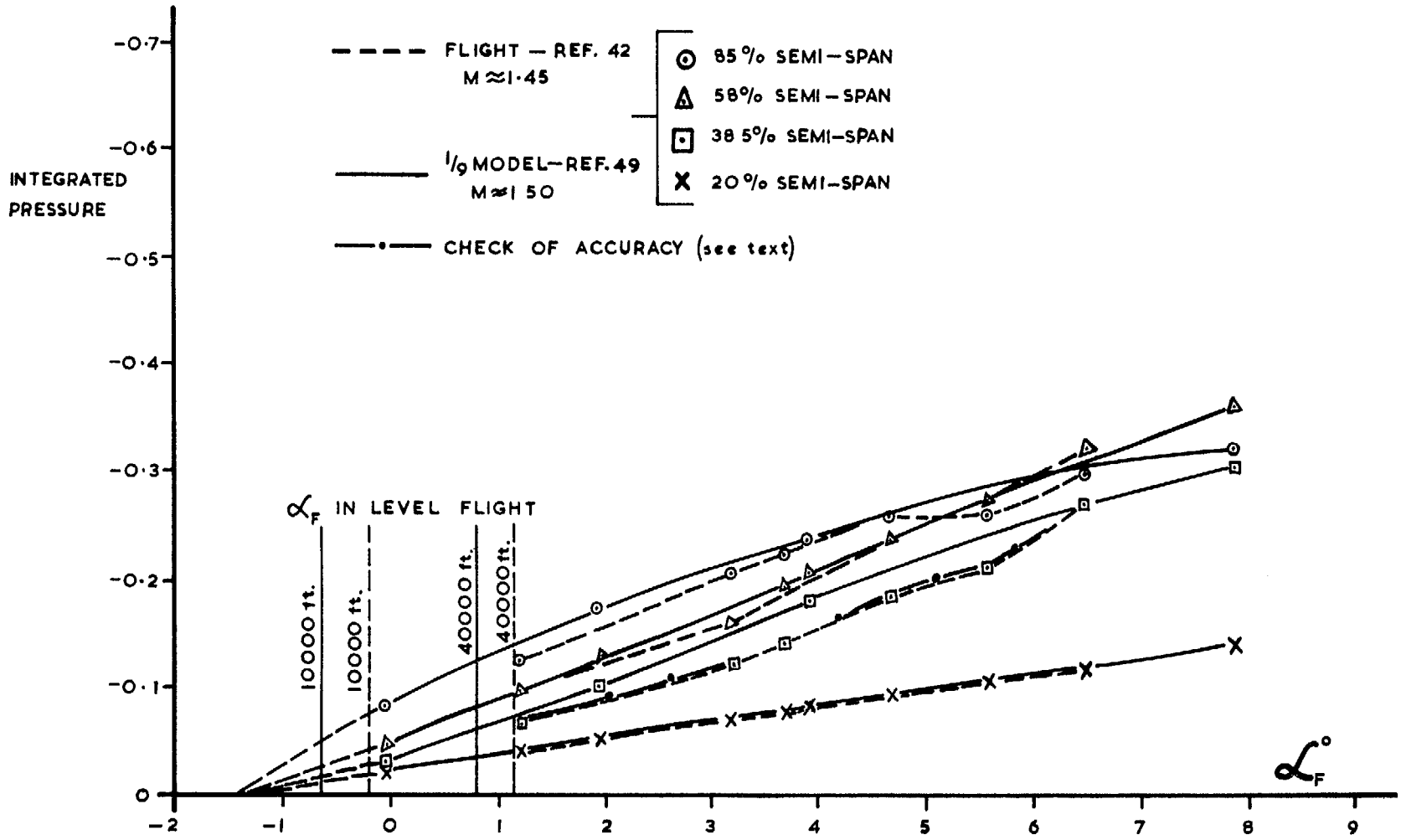

FIG. 38a. Integrated pressure distribution versus incidence—M ≒ 1·5.

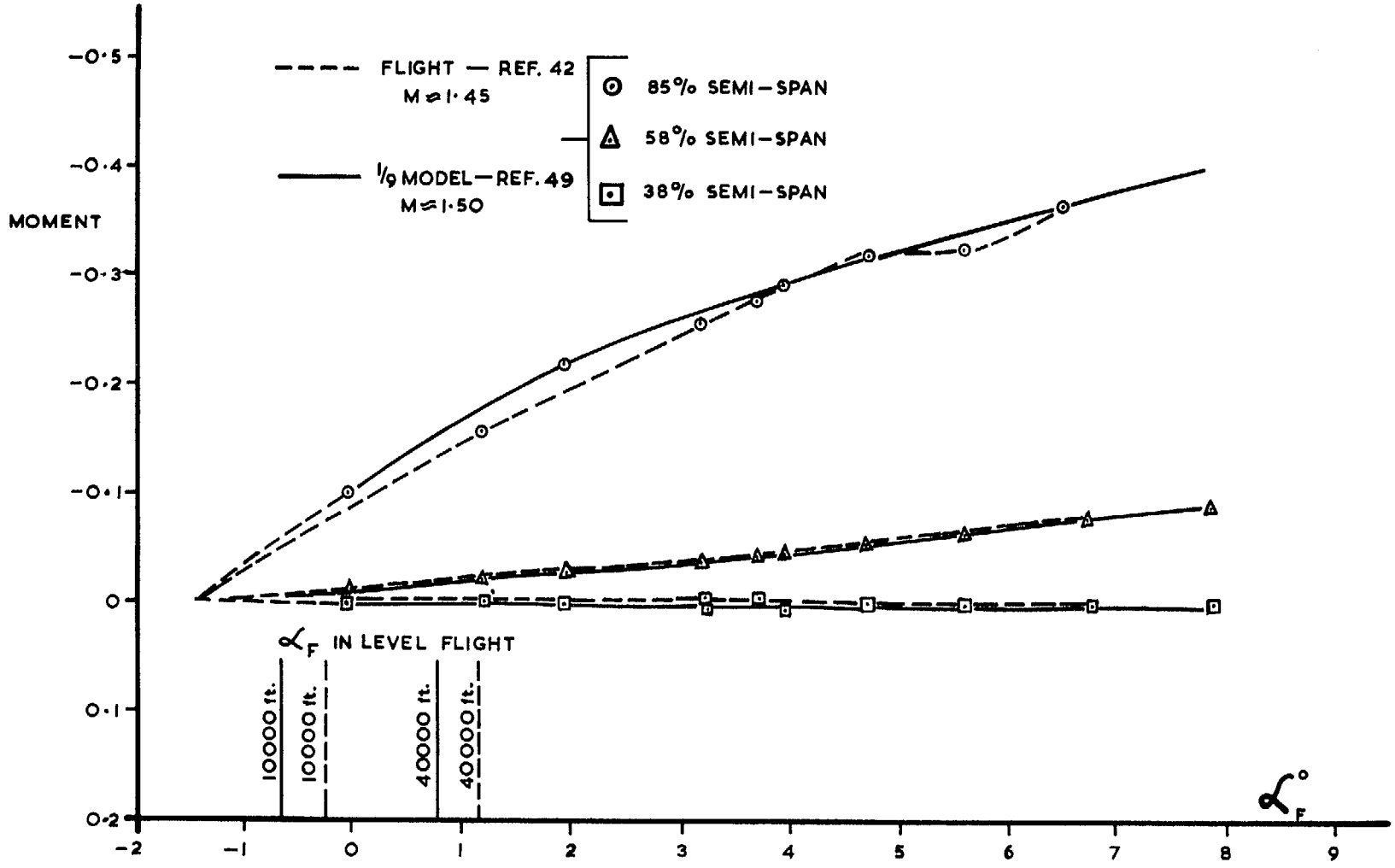

FIG. 38b. Integrated moment about C.G. versus incidence—M ≒ 1·5.

Printed in England for Her Majesty's Stationery Office by J. W. Arrowsmith Ltd., Bristol BS3 2NT
Dd 505715 K5 6 74

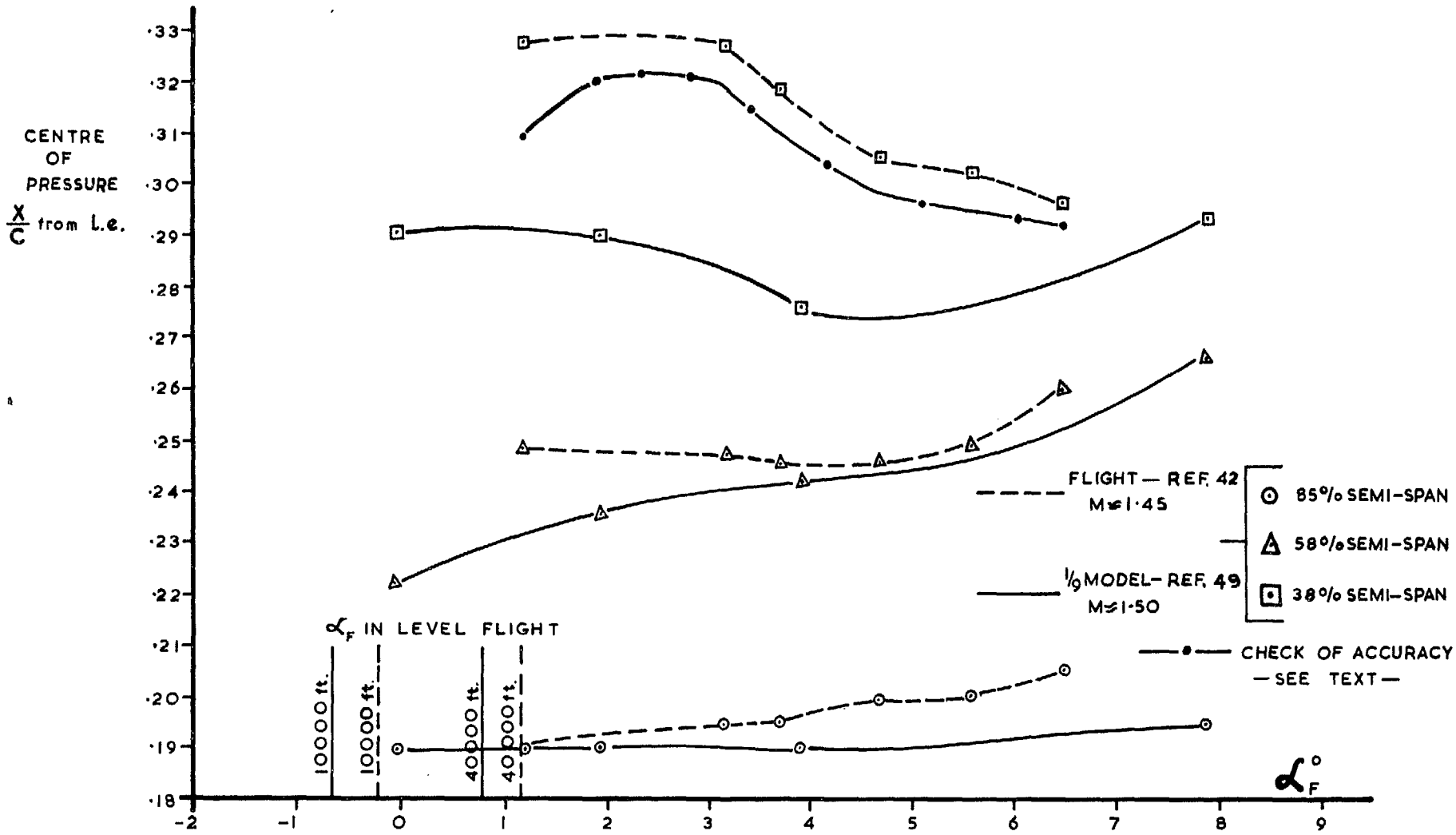

FIG. 38c. Centre of pressure location versus incidence—M ≒ 1·5.

HER MAJESTY'S STATIONERY OFFICE

Government Bookshops

49 High Holborn, London WC1V 6HB
13a Castle Street, Edinburgh EH2 3AR
41 The Hayes, Cardiff CF1 1JW
Brazennose Street, Manchester M60 8AS
Southey House, Wine Street, Bristol BS1 2BQ
258 Broad Street, Birmingham B1 2HE
80 Chichester Street, Belfast BT1 4JY

Government publications are also available through booksellers

R. & M. No. 3738

ISBN 0 11 470831 2*